Master Thesis

Modelling Approach for Special Properties of Magnetic Materials Applied in Actuators

Jie Zhang

Master of Science

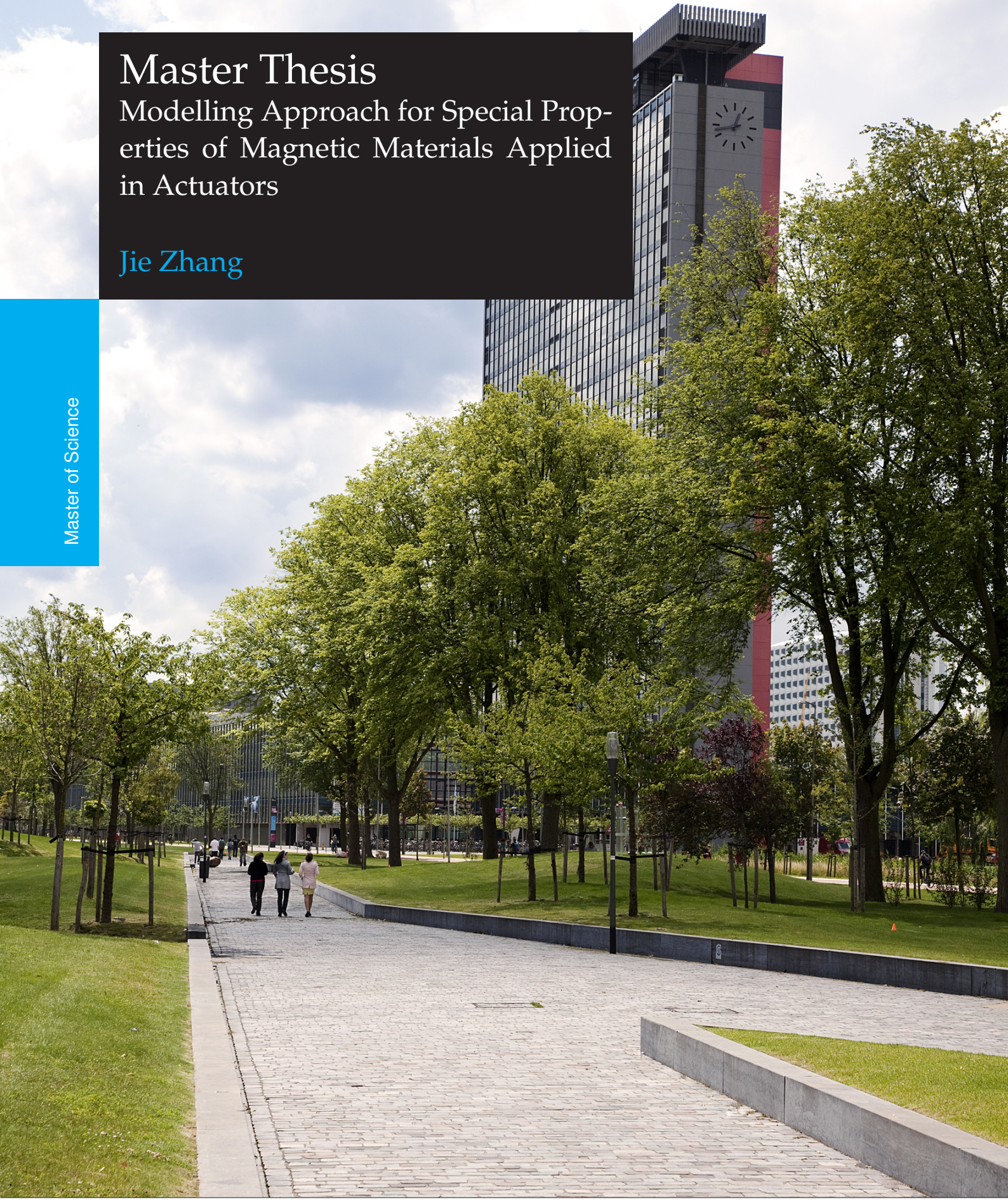

TU Delft Delft University of Technology

Challenge the future

Master Thesis

Modelling Approach for Special Properties of Magnetic Materials Applied in Actuators

by

Jie Zhang

in partial fulfillment of the requirements for the degree of

Master of Science
in Electrical Sustainable Engergy

at the Delft University of Technology,
to be defended publicly on Thursday September 21, 2017 at 2:00 PM.

Supervisor:	Dr. ir. P. J. Bax	
	Prof. dr. ir. H. Polinder	
Thesis committee:	Prof. dr. H. Polinder,	TU Delft
	Dr. J. Dong,	TU Delft
	Dr. D. J. P. Lahaye,	TU Delft
	Dr. ir. P. J. Bax,	Philips

This thesis is confidential and cannot be made public until September 21, 2017.

An electronic version of this thesis is available at http://repository.tudelft.nl/.

TU Delft Delft University of Technology

This is the first book in my life

Dedicated to my parents

Thank you for supporting my dream

Dedicated to my supervisors

Thank you for all your efforts

Dedicated to my boyfriend

Thank you for putting up with all my bad temper

Dedicated to everyone who reads it

Thank you for your attention and trust

Wish your dream come true

Acknowledgements

First, I would like to express my thanks for the continuous guidance from Dr. P.J Bax. Without him this thesis would not have been finished. He has always been supportive and patient. He helps me to become a better student and an engineer. I am very lucky to meet Peter. More fortunately, he has been my supervisor for this thesis during 9 months. I would say: Peter, you are a good teacher and also my best friend in the Netherlands.

Next, I would like to thank Prof. Henk Polinder. He always gives me valuable suggestions on the thesis as well as the presentation. I also want to thank Jianning Dong. You always answer my questions on time. Thank you for your advice on the report.

Also, I want to express my gratefulness to my friendly and helpful colleagues from Philips. Jan and Job, we shared the office together. Job is very warmhearted in giving me a lot of useful tips of the life in the Netherlands. My gratefulness is extended to Mahesh, Douwe, and Menno. We spent good time together during our internships.

Many thanks to all my friends in the Netherlands. These 2 years in TU Delft is wonderful, and I will always cherish the memories here.

My last, and most heartfelt words are to my parents and my boyfriend. I am really grateful that my parents could support my every decision and dream. Donghao, it is so nice to meet you in the Netherlands; it is nicer to graduate with you together. Thank you !

Jie Zhang
Drachten, September 2017

ABSTRACT

Eddy currents are loops of electrical currents induced within conductors by varying magnetic field in the conductor. Eddy currents flow in the closed loops in the conductor, in planes perpendicular to the magnetic field. The eddy current effect plays an important role in the transformer or an actuator system.

If there is a coil wound around a cylindrical iron core, system, the AC coil can induce eddy currents in the solid core. The eddy current can change the flux in the core, and further influence the impedance of the system. If such a system is applied to an electromagnetic actuator, a proper modeling approach for the eddy current effect can help the researchers to determine the impedance change and predict the output power of the actuator. This thesis deals with the eddy current modeling improvement problem. A concept of the transformer ring topology is proposed to simplify the actuator model. A brass ring and an iron material ring are studied, in the purpose of realizing modeling optimization and test functions respectively. By using analytical calculation and modeling analysis, the eddy current modeling method is improved and optimized. The practical impedance of the model becomes closer to the simulation results. This research can help the researcher to compute the actuator model, and better simulates it.

CONTENTS

List of Figures

LIST OF TABLES

1

INTRODUCTION

1.1. BACKGROUND

With the focus on delivering meaningful innovation, Philips serves both professional and consumer markets throughout the world in the areas of healthcare, consumer lifestyle and lighting. Launched in the 80's, the Philips toothbrush is one of the most famous healthcare products of the company. Power electric toothbrushes can be classified into two categories according to the type of that action that they employ: vibration or rotation-oscillation [2]. In order to have vibrations used for electrical power toothbrushes, a resonant actuator is used. A large variety of actuators exist, but for the toothbrush actuator, in the first place, it should be thin, suiting the shape of a toothbrush handle.

Fig. 1.1 gives an overview of different toothbrush actuators. An actuator is an interface between the electrical and the mechanical domain. It has components of housing, coils, spindle, springs or magnets. Here the spindle is used to transfer the motion and vibration to the toothbrush.

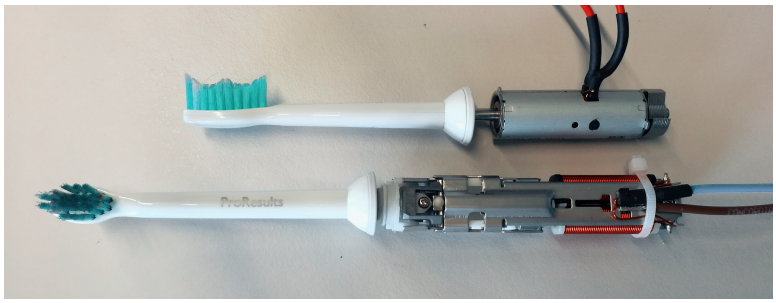

Figure 1.1: Toothbrush actuators in Philips

The old Philips toothbrush actuator contains vulnerable springs; these springs can break. The new actuators with longer life time are invented to solve this problem. With the new actuator, no springs are used. The mechanical spring should be replaced by magnetic attraction. In this case, the actuator has a long life time.

The Philips present actuator uses a resonant magnetic circuit. Fig. 1.2 shows the cross section of the present actuator with five pairs of poles. This new toothbrush actuator shows attractive properties, because it can be very well adapted to the particular requirements of the application. The actuator has a natural thin shape, and the actuator strength can easily be maximized to a stroke range. Also the magnetic cogging can provide the spring function. Therefore, the actuator offers very good opportunities to obtain a device with minimal

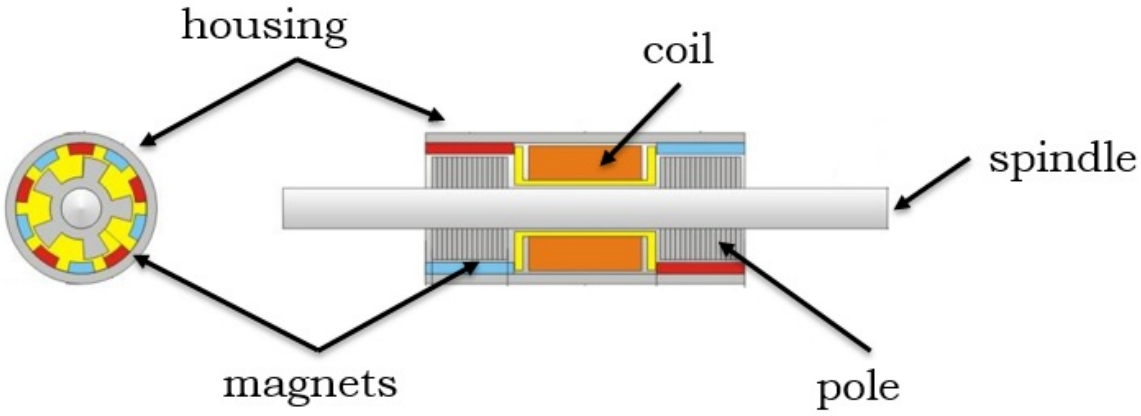

Figure 1.2: Diagram of the new actuator

vibrations in the handle [3]. In a word, the new actuator significantly improved the user's experience.

1.2. PROBLEM DEFINITION

In the development of this new actuator, a variety of simulation models is applied. Not only finite element models have been developed, but also several analytical and circuit models are available. Many models make use of a combination of different simulation approaches.

At the moment, a circuit model for the toothbrush actuator is available, in which some modeling techniques have been applied for describing the nonlinear effect and the eddy current effect. The eddy current is a linear effect. But how the eddy current flows in the fixed plane is not clear on beforehand. Current densities in the spindle vary with frequency, which makes the effect harder to describe. In this case, the circuit model lacks accuracy and needs to be checked and assessed. There is a need for the improvement on these models. The objectives of the thesis are:

- to explain why the eddy currents in actuators are studied
- to investigate a new way of modelling eddy currents and to optimize this method
- to apply this method to an actuator and evaluate this results

This report is based on these issues. The answers to the the objectives are discussed in the following chapters.

1.3. RESEARCH METHOD

The actuator model is a complex model. It not only includes the eddy current effect model, but also includes nonlinear effect such as saturation and hysteresis loss. In this case, it is very difficult to directly use the actuator prototype to measure the eddy current effect. Therefore, a simpler and more practical electrical circuit model is to be made, with only the eddy current effect included. With this practical circuit design, the researcher can do practical experiments and build a simulation circuit in Ltspice. Next, the measurements and simulation results can be compared and analyzed. Further, the optimization methods can be tested.

The simpler circuit model is the transformer ring. The transformer ring has toroidal shape and rectangular cross section. The primary winding and secondary winding are uniformly wound around the core. Depending on the purpose of the study, the core material of the transformer ring can be very different. In this report, the rings are named according to the

core material; for instance, the ring core made of brass is named as brass ring, and the ring core made of the spindle material is named as spindle ring.

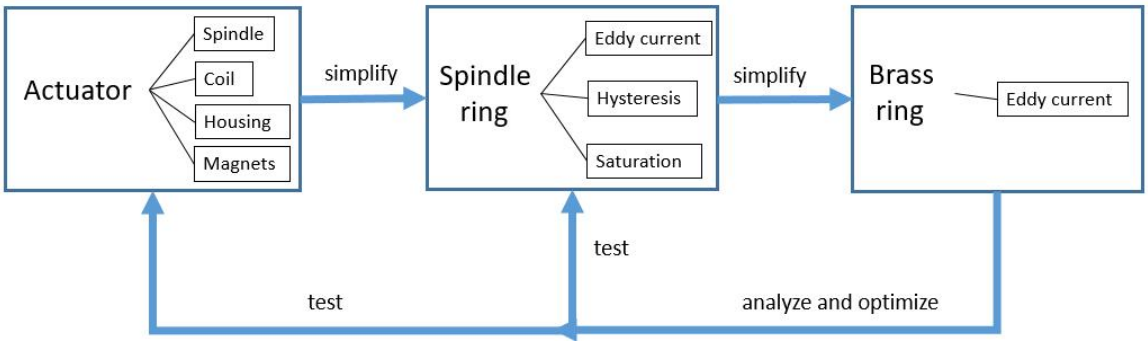

Figure 1.3: The research methodology diagram

Fig. 1.3 shows the flow chart of the research methodology. The actuator contains components of spindle, coil, housing, and magnets. In this case, it is hard to only study on the eddy current effects of the spindle. Next, the spindle transformer ring is proposed. The spindle material is iron, and there is not only the eddy current effect but also hysteresis and saturation effects included. So the spindle ring is still a complicated model. To get rid of hysteresis effects, brass material is chosen as ring material. Brass has diamagnetism property, and it contains no hysteresis or saturation effects. The relative magnetic permeability μ_r of brass is 1, and it is constant. Therefore, in the brass ring, only the eddy current effect is considered. Now, the researcher can study the eddy current effect properly. If the modeling method is feasible for the brass ring, then this approach can be tested into spindle ring, and further in the actuator.

Normally, numerical methods such as the finite element method (FEM) or boundary element method are often employed, and recent increase of computer power have enabled three-dimensional eddy current analysis [4][5][6]. Recently, eddy current distribution imaging has also been developed by several research groups [7][8][9]. Although the FEM is a potential for solving eddy current problems, it is hardly applied to improving the eddy current model. Therefore, in this paper, 1-dimensional mathematical analysis is used to study on the eddy current model.

1.4. THESIS LAYOUT

To accomplish the thesis objectives, in this report, the individual steps are divided into five chapters, which are described subsequently:

- Chapter 2 first gives a general concept for the toothbrush circuit model and the actuator model from Philips. The basic working principle of the actuator is introduced. Second, a background information is presented about the eddy current effect. Third, the eddy current effect in the actuator is described, especially how much the eddy current influences the actuator, which helps to understand the meaning of the thesis.

- Chapter 3 mostly concentrates on the research methodology for the eddy current effect. The transformer ring is introduced, and the geometry, conductivity measurement method, as well as the choice of the effective length are described in detail. The reasons for using the transformer ring are explained. In this chapter, the eddy current distribution and magnetic flux density distribution based on 1-dimensional case are analyzed.

- Chapter 4 is the most critical part of this thesis. It introduces each step for the improvement of the eddy current model. First, the Present Model is illustrated. However, it has two problems, and there is an obvious deviation from the measurement results. Thus the improvement steps of the the eddy current model are proposed. The idea of improvement is about finding a more accurate way to describe how the eddy current is distributed and how the magnetic flux is enclosed by the eddy current. Three improving steps are conducted, and they are advanced step by step. Finally, from the observation of the transfer impedance, the eddy current model has been improved in a big progress. But there are still some unknown results, for example, the eddy current effect in the simulation model shifts compared to the measurement.

- Chapter 5 is about the test for the optimized eddy current model, by using the spindle ring, which is made of the same material used for the toothbrush actuator. This step is a preparation for applying eddy current model into toothbrush actuator. Because the nonlinear effect is in the ring, the BH curve is first measured. Then the Philips model for the description of nonlinear effect is presented. By finding the fitting curve parameters the BH curve model is applied to the ring model to represents for the nonlinear effect. Based on this, the eddy current model is tested with the same process and approach in Chapter 4.

- In Chapter 6, the eddy current model is tested in the toothbrush actuator model. The permeances and mutual permeances are derived from ANSYS simulation. Two occasions are defined in ANSYS: equal eddy current distribution and linear eddy current distribution. The output power of the actuator is compared between the measured result and the modeling result.

- Chapter 7 summarizes this report, and it is the conclusion part. The conclusions for the present work are presented first. Also, the limitations and the further work are proposed.

1.5. CONTRIBUTION

The contribution of this thesis to toothbrush model in Philips, to technology, and to science is explained as follows:

- Contribution to toothbrush model: If the eddy current can be known well, it helps to improve the behavior of the toothbrush actuator. If the eddy current effect can be studied and modelling properly, then it helps the designers to choose the materials of the spindle in the actuator.

- Contribution to technology: In this thesis, the transformer ring is used for modeling. Both one dimensional model and two dimensional model of eddy current are analyzed in the report. How the eddy current density distributes in the solid iron material is studied. Also, in the solid ring, the distribution of magnetic flux generated by eddy current is discussed. It helps to better simulate the eddy current effect.

- Contribution to science: Eddy current analysis is widely used in solving the problems on magnetic interaction between an electricity conductive material and an excitation coil that carries an AC current[10]. This paper uses a combination of physical and mathematical analysis method. Also, a lot of theoretical research and calculation are carried out.

2

ACTUATOR MODEL

This chapter first gives a review for the toothbrush circuit model and the actuator model from Philips. Second, a literature review about skin effect and induced eddy current is given. Third, the eddy current effect in the actuator is introduced, and in the spindle, this effect is more emphasized. Finally, it is shown that how the actuator is influenced by the eddy currents.

2.1. MULTI-DOMAIN TOOTHBRUSH MODEL

In the toothbrush circuit model, blocks with different functions are defined. How the power input and transferred should be described in the blocks. See the Fig. 2.1, there are several domains in the total model including electrical domain, mechanical domain, magnetic domain (actuator) and chemical domain[3]. In this thesis, we concentrate on the actuator model.

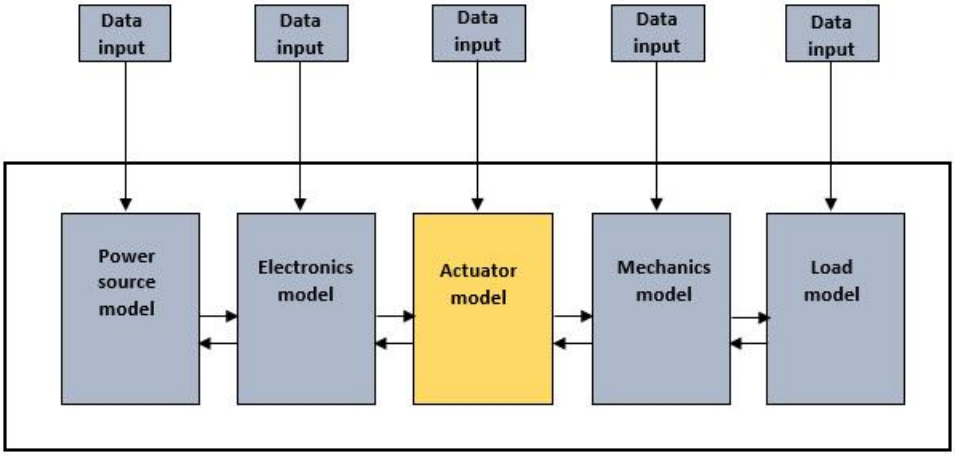

Figure 2.1: Block diagram of the toothbrush circuit model[3]

Every block in this model contains specific sub models to describe the different physical effects of interest. These models show the certain effect takes place, but do not define to what extent the effect would be. Therefore, for the input data of the models, it can be the result of analytical solutions, pre-simulation, measurement or by estimation [3]. Next, the actuator is introduced in detail.

2.2. ACTUATOR MODEL

Used as the toothbrush motor, the actuator needs to meet some design requirements such as volume and shape requirements. From Fig. 1.2, the magnets are placed on the outside housing used as stator while the spindle and iron poles are used as rotor.

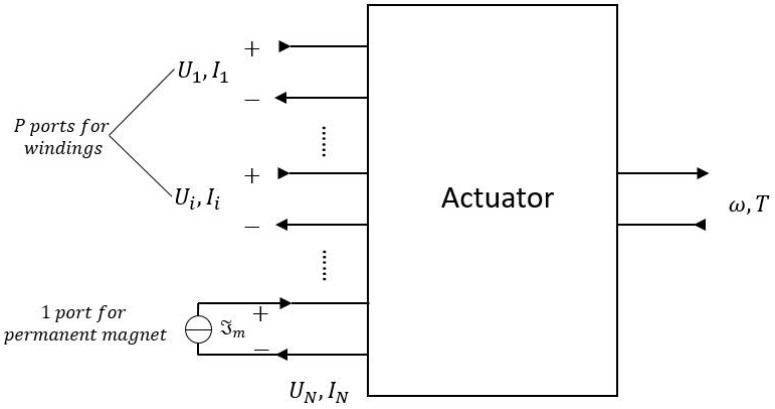

Figure 2.2: The actuator with N electrical ports, and one mechanical port

In Fig. 2.2 a general description of an actuator is given. The system is assumed to be linear, which means that no saturation or hysteresis effects occur. The actuator has N electrical ports, and one mechanical port. The actuator provides the power from the electrical domain to the mechanical domain. Every electrical port is connected to a winding, also it can be used to represent for a permanent magnet [11]. In the new actuator in Philips, the torque given by the actuator provided with permanent magnets can be written as [11]:

$$T = \sum_{i=1}^{P}\sum_{j=1}^{P}\frac{1}{2}I_i I_j\frac{dL_{ij}(\alpha)}{d\alpha} + \sum_{i=1}^{P} I_i I_m\frac{dL_{im}(\alpha)}{d\alpha} + \frac{1}{2}I_m^2\frac{dL_{mm}(\alpha)}{d\alpha} \tag{2.1}$$

It can seen that a torque can be generated by the interaction between the mutual windings, by windings and the permanent magnets, and by the permanent magnets only. In (2.1), the mechanical domain is described with rotational parameters. The first term is the torque only dependent on the currents in the winding, and L_{ij} represents for the mutual inductance between winding i and j; the second term is the torque which is generated by the interaction of current-carrying windings and the magnets; the third term is the torque caused by the permanent magnets only. In the first term, the winding self-inductance will not vary with the angular position(applicable in the new actuator). The actuator shows a strong preference position; the poles are magnetically coupling a north segment to the neighboring south pole segment. This cogging effect gives the desired spring function. For the resonant toothbrush this effect can be used for the realization of the spring function. Therefore this term should be increased so that the desired spring constant is reached.

In the actuator model, 4 windings have been implemented. Only winding 1 is a real winding representing the coil around the spindle. Winding 2 and 3 are added for the calculation of eddy current and nonlinear effect respectively. Winding 4 represents the permanent magnet system.

For the new Philips actuators, a completed actuator model consists of:

- A winding part. It contains the number of turns and resistance of winding.
- A flux generation part. This block calculates the total flux effectively enclosed by the winding. It contains the permeances and mutual permeances.

- A torque generation part which calculates the torque contribution of this winding. It contains the permeances and mutual permeances.

Not every winding is simulated completely. The winding 4, which represents the permanent magnet only has a block for the torque generation. Also the hysteresis winding is different: instead of a "winding" block it has a sub circuit that contains a BH curve for the spindle material.

In this thesis, the research objective is to study on the eddy current effect and find a new modelling approach to simulate it. Therefore only winding part and flux generation part, and winding 1, 2, 3 are considered for the research purpose. The permanent magnet system and torque generation and mechanical domain will not be discussed in next contents. This section gives some information about the electromagnetic actuator and the working principle of this new PM actuator.

2.3. BACKGROUND INFORMATION

This section gives background information about the skin effect and induced eddy current in the conductors. It is divided into 3 parts. In the first part, Maxwell's equations and Bessel functions are adapted to the calculation of the current distribution in the cylindrical conductor. The second part shows the electrical field distribution in a lamination when magnetic field with frequency f is driven, which helps the researcher to know the skin depth in the conductor. The (2.4) derived in the second part is adapted to this thesis. The third part gives an example of a COMSOL result, which helps the researcher to know the distribution and direction of the induced eddy current in the cylindrical conductor.

- The book Power Electromagnetics, Chapter 6 talks about the diffusive fields and eddy currents in the cylindrical conductors. One consider the current distribution through a circular cross section of a conductor characterized by a conductivity σ. The reference is chosen that the current is running in the positive x-direction. The current density distribution in the cross section is analyzed by starting from Maxwell's equations. It concludes that as the frequency is increased, the current is concentrated near to the surface the conductor. This is phenomenon is called the skin effect [1].

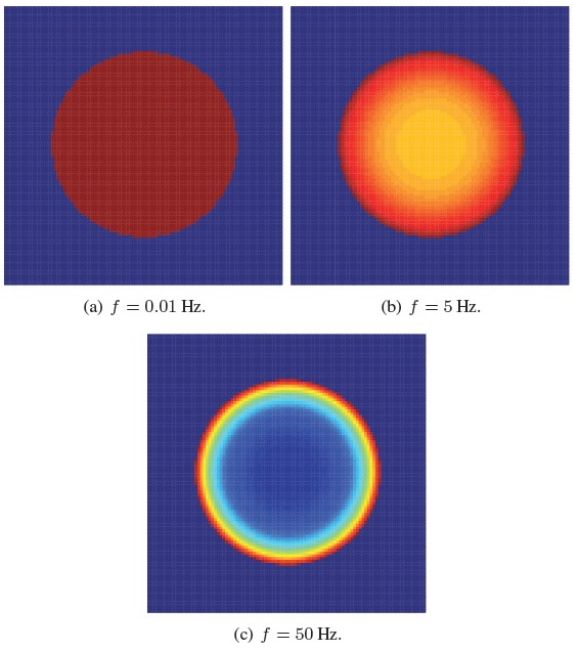

(a) $f = 0.01$ Hz. (b) $f = 5$ Hz.

(c) $f = 50$ Hz.

Figure 2.3: The normalized current distribution at a frequency of 0.01Hz, 5Hz, 50Hz [1]

In Fig. 2.3, the radius of the cross section is considered to be 5 cm. The conductivity of the conductor is $5.8 \cdot 10^7 S/m$ and its permeability equals $\mu = \mu_0 \mu_r$. Fig. 2.3(a) shows the normalized absolute value of the current density under steady state conditions at frequency f=0.001Hz. One can observe that the current density is uniform in the cross section. In (b) and (c), using a frequency of 5Hz and 50Hz respectively. From this figure it is concluded that as the frequency increases, the current is very concentrated close to the surface of the conductor. This is applicable to the induced eddy current.

- Ferromagnetic metals usually have good electrical conductivity and induced eddy currents are generated if solid magnetic cores are excited with an AC flux. If an AC magnetic field B_x with frequency f is applied to a lamination in x-direction, the induced eddy current distributes in the thickness of the lamination h (see Fig. 2.4). The electrical field distribution as function of depth is given by [1]:

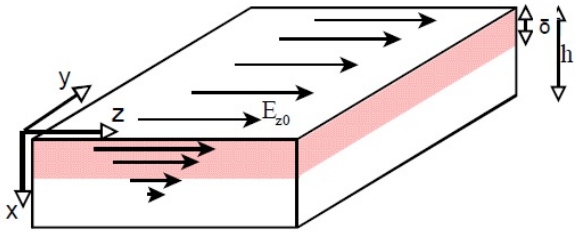

Figure 2.4: The electrical field distribution in a lamination [1]

$$E_z(x,t) = E_{z0} e^{-x/\delta} cos(\omega t - x/\delta) \tag{2.2}$$

The current density becomes:

$$J_z(x,t) = J_{z0} e^{-x/\delta} cos(\omega t - x/\delta) \tag{2.3}$$

where

$$\delta = \frac{1}{\sqrt{\pi f \mu \sigma}} \tag{2.4}$$

E_{z0} is the electrical field in the surface

J_{z0} is the current density in the surface

f=frequency

μ=permeability

σ=electrical conductivity

δ is the depth where the eddy current reduced to 1/e of the surface current [1], which is called skin depth. The skin depth equation is adapted to do the analytical computation for eddy current in this thesis.

- An example in COMSOL is given. It concerns an AC coil surrounding a metal cylinder core, and the coil induces eddy currents in the cylinder (See Fig. 2.5).

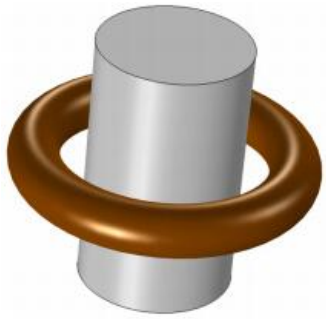

Figure 2.5: An AC coil surrounds a metal cylinder core

The eddy currents induced in the cylinder are shown in the Fig. 2.6. The homogenized multi-turn coil is used. The induced currents on the cylinder are due to the choice of the parameter. The field lines represents for the magnetic flux density. The red solid round represents for the current in the coil. The dark blue in the cylinder is the non-uniform induced current, and in the edge more eddy current is induced. Also, the eddy current has opposite direction with the current in the coil.

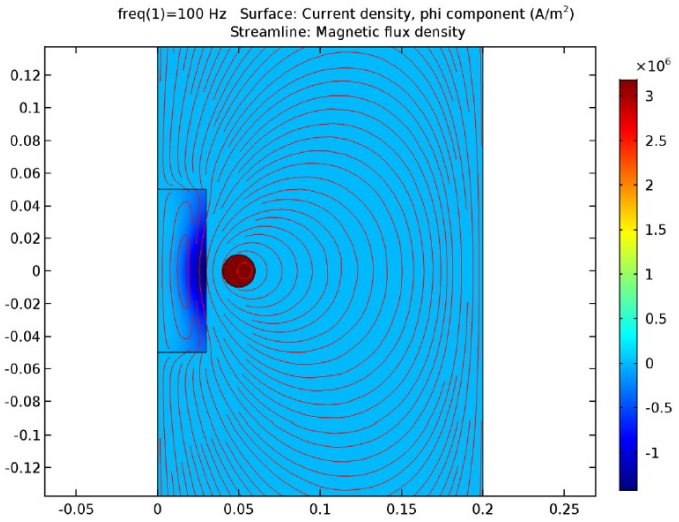

Figure 2.6: Eddy currents induced in the cylindrical conductor

In the spindle of the actuator, the AC current coil generates eddy currents in the spindle, which is like this example. This example gives the researcher a insight of the eddy current distribution in the spindle. Further, the eddy current opposes to the current in the coil, therefore it generates the opposite flux to the flux generated by the coil.

2.4. EDDY CURRENT EFFECT IN THE ACTUATOR

Interest in eddy current in iron masses has kept pace with the development of electromagnetic devices generally [12]. If the new actuator model is described in terms of permeances which are only dependent on the position of the poles, then the model can be used for linear systems in which the electrical currents flow at well-known fixed places [3]. However, if an alternating current flows in the coil, the eddy current effects can occur in the spindle, housing, and poles. The eddy current effect in the spindle is studied for the following reasons:

- The central spindle plays a very important role in the housing because all magnetic fluxes go through the spindle.
- The modelling approach is concerned. The purpose is to know about eddy current and find approach to simulate it, therefore in the first place the spindle is concerned.
- The opposite flux generated by eddy current will reduce the flux generated by the main coil in the spindle.

Since the eddy current effect is important in the actuator, then how the actuator is influenced by the eddy current is illustrated. The input impedance of the new actuator is measured in the case that the actuator is blocked (See Fig. 2.7(a)). If there is no eddy current effect in the spindle, then the input impedance L and R would be constant values.

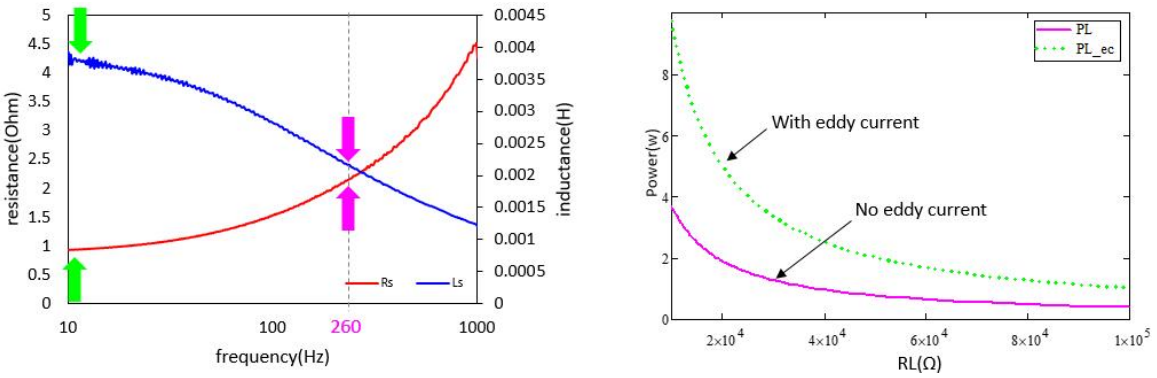

Figure 2.7: (a)Measured input impedance of the blocked actuator (b)Calculated output power of the blocked actuator

Fig. 2.7(a) shows the measured input impedance of the actuator. The L_s decreases while the R_s increases because of the eddy current effect occurring in the spindle. Further, this effect influences the output power(the power of the load) of the actuator. The impedance components are picked up respectively at 10Hz and 260Hz. The output power of the actuator is calculated in the two cases. Fig. 2.7(b) shows the calculated output power in two situations; the PL_ec shows it varies with the assumption of no eddy current effect, while the PL shows the it varies when the eddy current is in at 260Hz. Because 260Hz is the operation frequency of the new actuator in Philips. When the load RL is between 40k-60kΩ, which is the soft load of the toothbrush actuator; one can see that with eddy current in the actuator, the calculated output power is larger than the other one. It is concluded that the eddy current affects the output power in the actuator.

2.5. SUMMARY

- The toothbrush model is a multi-domain model. There are the power source model, the electronics model, the actuator model, the mechanics model, and the load model. In this report, the actuator model is the research object.
- The actuator is an interface between electrical domain and mechanical domain. Next, the toothbrush actuator is a permanent magnet motor. The magnetic cogging effect is used for the realization of the spring function. The simulation model is built for the actuator. It consists of a winding part, a flux generation part, and a torque generation part.
- The skin effect occurs in the conductor as the electrical frequency increases. The induced eddy currents are generated if solid ferromagnetic cores are excited with an AC flux. The induced eddy current has the skin effect, and from the surface to the inner of the lamination, the current decreases. δ is the depth where the eddy current reduced to $1/e$ of the current in the surface, which is called skin depth.
- In the spindle of the actuator, the AC coil generates eddy currents in the spindle. The eddy current opposes to the current in the coil, therefore it generates the opposite flux to the flux generated by the coil.
- Eddy currents can occur in the housing, spindle, and poles in the actuator. The thesis studies the eddy current effect in the spindle, because it plays a very important role in the actuator. Further, the eddy current influences the calculated output power in the actuator.

3

TRANSFORMER RING AND ANALYTICAL CALCULATION

To simplify the complex actuator system, the transformer rings are made to represent the different effects such as eddy current and hysteresis. If the transformer ring model works for the ring, then the model can be applied to the toothbrush system too. In this Chapter, first, the transformer ring will be introduced, including the geometry description, the measurement of the conductivity, and the effective length calculation; second, the analytical calculation is treated, which delivers the 1-dimensional expressions for magnetic flux density and the eddy current density in the ring core. Based on that, the researcher can develop the optimization assumptions for the eddy current model.

3.1. TRANSFORMER RING

The exteriorof the transformer ring is like Fig. 3.1. The has a rectangular cross section. The core can be made of different materials according to different uses or test purposes. Copper coils are wound over the ring uniformly, besides there is an isolation layer between the coils and the core. To reduce the effect of ohm loss of the primary winding, the thick wire is used.

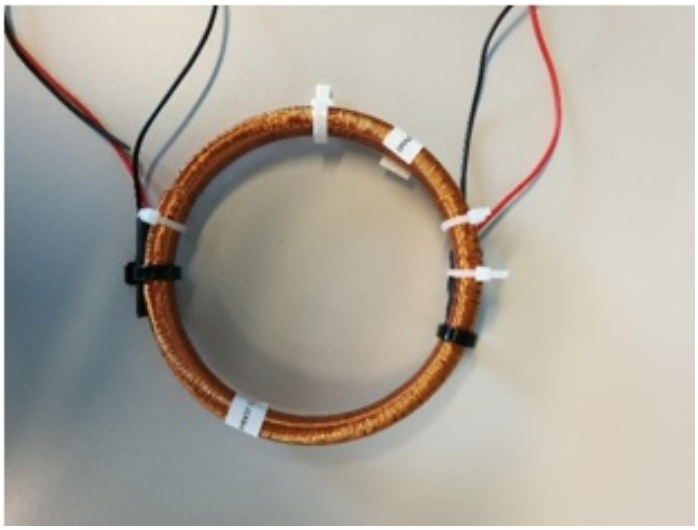

Figure 3.1: Transformer ring with brass metal core; the outside copper coil is primary winding; two wires in left represent for primary side while the other two represent for secondary side.

In the lamellae ring, at high frequency, hysteresis loss is larger than the eddy current loss, which can be used to test hysteresis loss [13]. The brass and alumina are not magnetic materials, they could be used to test the eddy current loss with ignorance of other effects. In the spindle ring, the core of the ring is made of the magnetic material that used for the toothbrush actuator. The hysteresis and saturation effects cannot be ignored in this iron material. Therefore, it is used to test the eddy current model with a BH-curve.

In this Chapter, the eddy current effect in the brass ring is investigated. An analytical model is discussed. The transformer ring is selected for the reasons as the following items:

- The toroidal transformer rings have no air gaps. The coils can uniformly wound around the ring core, and this structure leads to a small leakage.

- Brass is good conductive material but not magnetic material, so the material is linear with $\mu_r = 1$. Therefore nonlinear effects can be ignored. Only the eddy current loss is considered.

- The transformer ring has a rectangular cross section rather than circular cross section, because it would be difficult for the workshop to realize a toroidal ring with a round cross section.

In this section, first the geometry of the ring is described. Second, the conductivity measurement is discussed. Third, the effective length of the ring is calculated.

3.1.1. GEOMETRY DESCRIPTION

First, a pure ring is made. The geometry is shown in Fig. 3.2 and Fig. 3.3.

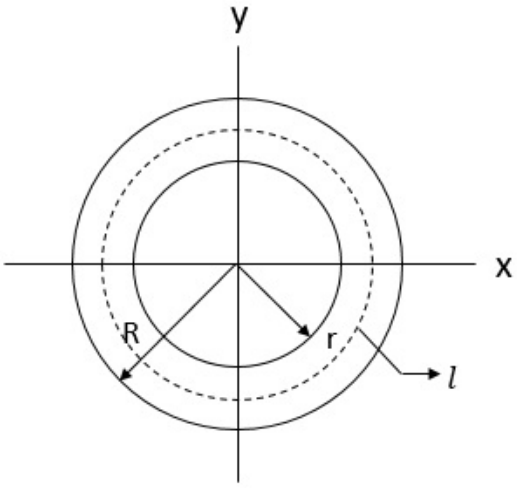

Figure 3.2: The top view for ring, R is the outer radius and r is the inner radius.

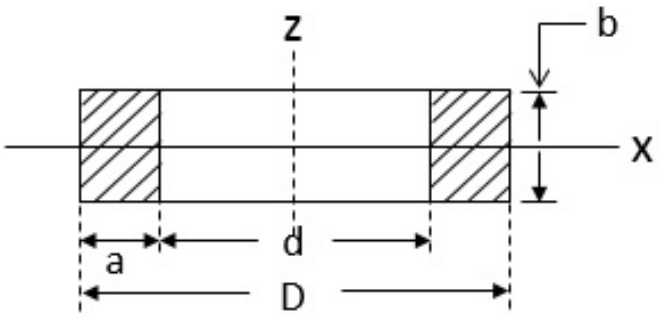

Figure 3.3: Rectangular cross section of toroidal core

D and d are the outer and inner diameters respectively. a is the difference between R and r, b is the height of the core.

The measured parameters in Fig. 3.2 and Fig. 3.3, are shown in the following Table 3.1.

Table 3.1: Measured geometry parameters of ring

Ring core	D(mm)	d(mm)	R(mm)	r(mm)	b(mm)	a(mm)
Brass	110.04	99.87775	55	50	10	5
Alumina	109.9875	99.9675	55	50	10	5

Two layers of copper coils are uniformly wound over the core with an isolation inside. The first layer winding inside is the secondary winding, and it is open circuit. The second layer winding is primary winding, which is connected to the input power. The Table 3.2 gives the information of the coils:

Table 3.2: Parameters of coils around the ring

Ring core	Turns of primary winding n_p	Turns of secondary winding n_s	Diameter of n_p (mm)	Diameter of n_s (mm)
Brass	500	500	0.56	0.25
Alumina	500	500	0.56	0.25

3.1.2. CONDUCTIVITY MEASUREMENT

It is not easy to know the conductivity of the metal cores because, in the cores, any mixture or impurities can influence the conductivity. Therefore, the conductivity of the core is to be measured and then compare with the data sheet.

- Resistivity data sheet

  In the Poly-technisch book [14], a table is found for the information of conductivity with metal and alloys. For metal alumina, the resistivity is $27 \cdot 10^{-9} [\Omega \cdot m]$, while for the alloys, see Table 3.3

Table 3.3: Resistivity of metal from data sheet

Alloys	Composition[mass%]	Resistivity[$\Omega\dot{m}$] $\cdot 10^{-6}$
Alumel	2%Al, 2%Mn, 95%Ni 1%Si	0.30
Brass	90%Cu, 10%Sn	0.14
Messing	55-70%Cu, 30-45%Zn	0.066

The data sheet gives the information about the resistivity of alloys. However, to get the accurate value of resistivity, the four point measurement method is used.

- Four point measurement

  It is difficult to measure the conductivity of the metal core in a normal way. In this case, the four point measurement approach is used to measure the conductivity of the core. Fig. 3.4 shows the draft circuit about four point measurement in the brass ring.

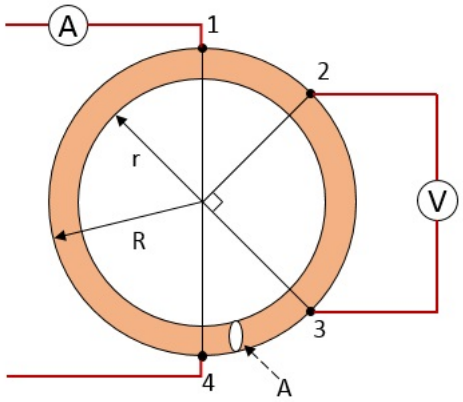

Figure 3.4: Four point measurement illustration

We first define,

R_o : resistance of whole ring

A : area of the cross section

L_r: effective length of the ring

σ : conductivity of the ring

ρ : resistivity of the ring

We use four clamps to clamp four points in the ring, and then the current is input into point 1 and 4. Next, we measure the cross voltage between point 2 and 3. The ring can be regarded as two halves of the ring paralleling to each other. The resistance of one-half is $R_o/2$. It can be seen that the other one-half is divided into three parts, point 1 to 2, 2 to 3, 3 to 4. The Fig. 3.4 can be transferred to the equivalent circuit Fig. 3.5.

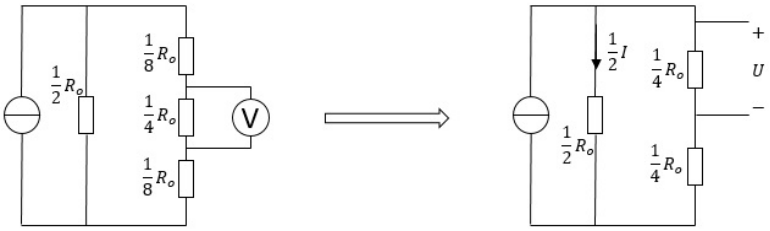

Figure 3.5: Equivalent circuit of four point measurement

In the circuit, $R_o/4$ is the measured part. Assume the voltage across this part is U, and the current through it is $I/2$. The resistance of the whole ring would be:

$$R_o = 8U/I \tag{3.1}$$

Table 3.4: Measured U and I

U(mV)	0.118	0.17	0.228
I(mA)	2000	2994	4003

The measured U and I are shown in the Table 3.4. After calculating the resistances and taking the average value, the R_o becomes:

$$R_o = 4.71 \times 10^{-4}\Omega \tag{3.2}$$

The resistivity and the conductivity of the metal core in the brass ring are:

$$\sigma_b = \frac{L}{R_o \cdot A} = 1.5 \times 10^7 S/m \tag{3.3}$$

$$\rho_b = \frac{1}{\sigma_b} = 0.067 \times 10^{-6}\Omega \cdot m \tag{3.4}$$

The same measurement is done with the alumina ring, and the results are:

$$\sigma_a = 2.61 \times 10^7 S/m \tag{3.5}$$

$$\rho_a = \frac{1}{\sigma_a} = 0.0383 \times 10^{-6}\Omega \cdot m \tag{3.6}$$

The conductivity and resistivity are very close to data sheet for the brass ring and the alumina ring. But due to the fact that the σ_b and σ_a need to be as precise as possible, so we go to the multi-meter manual to check and calibrate the accurate value.

After more accurate calibration, we can derive that for the brass ring

$$\sigma_b = 1.55 \cdot 10^7 S/m \tag{3.7}$$

$$\rho_b = 0.0645 \cdot 10^{-6}\Omega \cdot m \tag{3.8}$$

For the alumina ring

$$\sigma_a = 2.79 \cdot 10^7 S/m \tag{3.9}$$

$$\rho_a = 0.0358 \cdot 10^{-6}\Omega \cdot m \tag{3.10}$$

The conductivity of the metal core is used in the analytical calculation of the eddy current density and magnetic flux density in the ring.

3.1.3. EFFECTIVE LENGTH CALCULATION

The effective length is used to determine the effective magnetic flux path in the core. As for the effective length of the ring, it is not reasonable to use average length directly. Some analysis should be done to ensure the effective length.

As defined before, the resistance of the ring is R_o. Then we assume the micro circle to be R_Ω. R is the outer radius, r is inner radius, and the height of cross section is b. From the center of the circle to any point of the core, the radius is R_r. The thickness of this micro circle is dR_r. In every piece, the resistance is dR_Ω.

$$dR_\Omega = \frac{2\pi R_r}{\sigma \cdot b \cdot dR_r} \tag{3.11}$$

$$dG_\Omega = \frac{\sigma \cdot b \cdot dR_r}{2\pi R_r} \tag{3.12}$$

Do the integral to dG_Ω

$$G_\Omega = \int_r^R dG_\Omega = \int_r^R \frac{\sigma \cdot b \cdot dR_r}{2\pi R_r} = \frac{\sigma b}{2\pi} \cdot \ln \frac{R}{r} \tag{3.13}$$

Then for the precise value of whole resistance in the ring:

$$R_\Omega = \frac{2\pi}{\sigma \cdot b \ln \frac{R}{r}} \tag{3.14}$$

If we estimate the whole resistance of the ring core, then we just assume the effective length of the ring is the following l_{est}:

$$l_{est} = \pi(R + r) \tag{3.15}$$

For the estimation value of R_{est}

$$R_{est} = \frac{\pi(R + r)}{\sigma \cdot b(R - r)} \tag{3.16}$$

Next, we compare the estimation value R_{est} with the precise value R_Ω. If these two values are close to each other, then we can conclude that the estimation value is reasonable and can be apply to analytical model. We take the ratio of the two values.

$$\frac{R_{est}}{R_\Omega} = \frac{1}{2} \cdot \frac{R + r}{R - r} \cdot \ln(\frac{r + \Delta R}{r}) = (\frac{1}{2} + \frac{r}{\Delta R}) \cdot \ln(1 + \frac{\Delta}{r}) \tag{3.17}$$

$$\tag{3.18}$$

and

$$\Delta = R - r \tag{3.19}$$

Because

$$\frac{\Delta R}{r} = \delta = \frac{1}{10} \tag{3.20}$$

Then Eqn.3.17 goes to

$$\frac{R_{est}}{R_\Omega} = (\frac{1}{2} + \frac{1}{\delta}) \cdot \ln(1 + \delta) = 1.00076 \approx 1 \tag{3.21}$$

Therefore the estimation value is nearly the same with the accurate value of R_Ω. In this case, the average length is the same with effective length. The effective length is:

$$l_r = \pi(R + r) \tag{3.22}$$

The effective length of the ring is applied to the analytical calculation model. The length of magnetic flux path in the core is assumed to be l_r.

3.2. ANALYTICAL MODEL

In the previous section, an introduction of the transformer ring is treated. In this section, the eddy current in the ring is to be discussed. First, how the eddy current effect occurs and where the eddy current is distributed are analyzed. Second, a mathematical model is derived. The mathematical model is to express the eddy current and the magnetic flux density in the ring.

3.2.1. INDUCED EDDY CURRENT IN TOROID

In 1820, the Denmark scientist H. C Oersted found the phenomena that the current can generate flux. If the current flows through a metal conductor, then a closed circle magnetic flux is produced in the space around the current. The flux direction is perpendicular to the current flow. This principle can be extended. Imagine that there is a conductive wire with enough length, and then wind the wire around a hollow cylindrical solenoid, as the Fig. 3.6 shows. Every round piece of current would generate flux, the total magnetic flux through the solenoid would be the sum of every piece of flux.

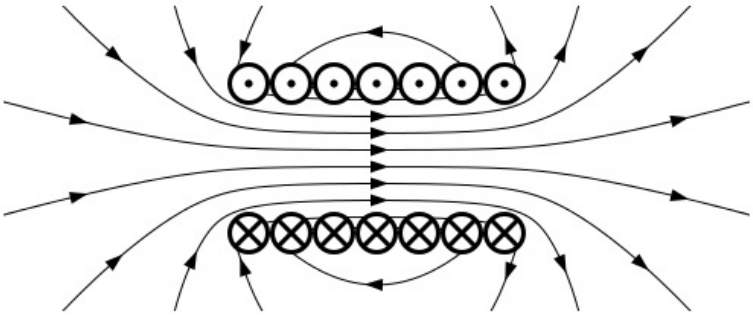

Figure 3.6: Current and flux in the cylindrical solenoid. Dots and crosses represent the current flowing outside paper and inside paper respectively around the solenoid. The lines with arrows are the magnetic flux generated by current.

Based on this principle, three schematic diagrams in the following show how the primary current and induced eddy current distribute in the ring.

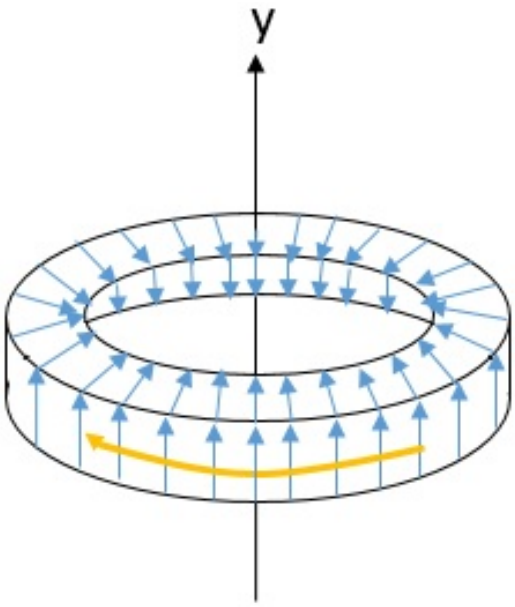

Figure 3.7: The oblique view of the ring

Fig. 3.7 shows the oblique view of the ring. Y-direction is perpendicular to the top view of the ring. The blue lines with arrows show the current direction in the primary winding. The primary current is along the surface of the core, and every piece of current is perpendicular to the round edge. The yellow curve with an arrow shows the direction of the magnetic flux generated by the primary current. The flux direction is parallel with the top view, and perpendicular to the y-direction. The path of this generated flux in the core would be a closed circle, along with the direction of the ring.

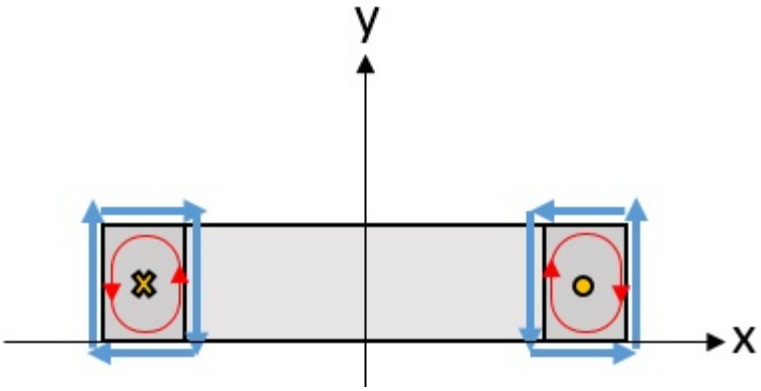

Figure 3.8: The cut view of the ring

Fig. 3.8 shows the cut view of the transformer ring. The blue arrows represent the same primary current as Fig. 3.7 shows. The yellow cross in the left and the yellow dot in the right represent the direction of magnetic flux generated by the primary current. The dot means that the flux is perpendicular outside the paper, while the cross means that the flux is perpendicular inside the paper. The red circle represents the eddy current induced in the core, and the arrows are pointing at the eddy current direction.

The primary winding carrying an AC will generate a changing magnetic field in the core, and because of this alternating field, the eddy current is induced in the core.

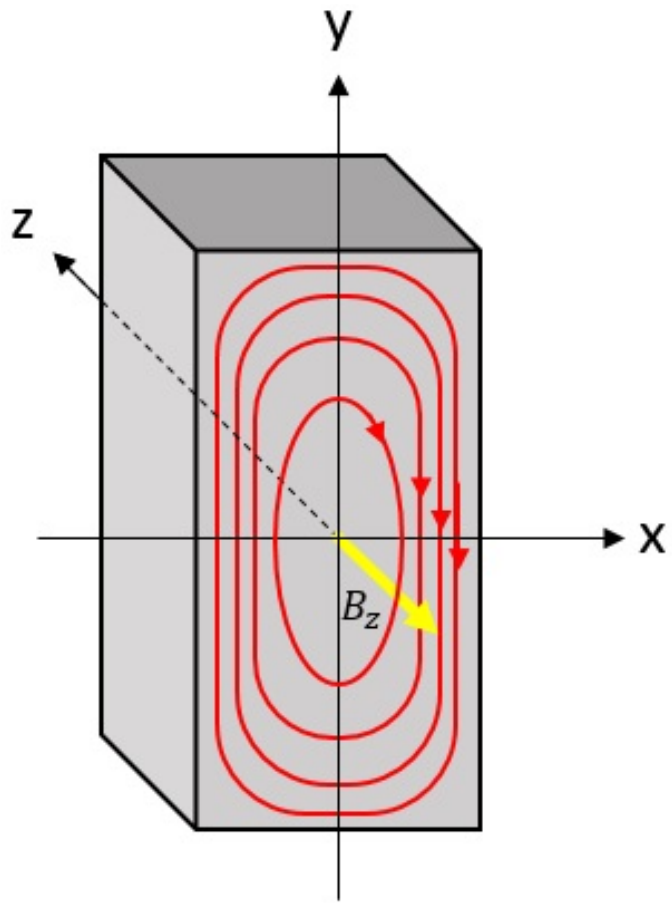

Figure 3.9: The eddy current in the cross section of the ring

In Fig. 3.9, z axis is perpendicular to x-y plane. Four loops are used to describe the induced eddy currents in the cross section. The arrows in the loops point at the current direction; the density of the loop represents the current density. It is clearly visible that the eddy current density is different in x and y axis, because the eddy current always tends to go through the nearest path. Fig. 3.9 also shows the geometry of cross section; the rectangle has different lengths in two directions. This situation leads to different current density in x and y direction.

3.2.2. ANALYSIS BASED ON MAXWELL'S EQUATIONS

By Lenz' law, the magnetic field formed by eddy current will oppose its cause. Therefore, the origin flux generated by the primary current is going to be reduced in the center. To define the expression for the eddy current density, as well as the total flux in the core, Maxwell's equations are discussed.

Maxwell's equations, written in terms of the total fields and currents within the magnetic material, describe the electromagnetic behavior of the material [15]. The following conditions are appropriate to these equations when applied to ideal conductors:

- The free charge term is zero, $\rho = 0$.
- Eddy current density is given by Ohm's law,

$$\overline{J}(t) = \sigma \overline{E}(t) \tag{3.23}$$

- Displacement current is negligible in comparison with conduction current.

- The material is isotropic.

We assume a homogeneous B-field is driven through z-axis, and it varies sinusoidally with an angular frequency ω. The eddy currents in the cross section of the ring are in x and y direction. One can write the following set of equations to express the relationships between total flux density, eddy current density and electrical field:

$$\nabla \times \overline{E} = -\frac{d\overline{B}}{dt} \tag{3.24}$$

$$\nabla \times \overline{H} = \overline{J} \tag{3.25}$$

$$\overline{J} = \sigma \cdot \overline{E} \tag{3.26}$$

It can be seen in Fig. 3.9 that the eddy current is a 2-dimensional effect. Therefore, in the first place, a 2-dimensional calculation is treated.

The Nabla operator and the eletrical field are written as the following equations:

$$\nabla = \frac{\partial}{\partial x}\hat{i} + \frac{\partial}{\partial y}\hat{j} + \frac{\partial}{\partial z}\hat{k} \tag{3.27}$$

$$\overline{E} = E_x\hat{i} + E_y\hat{j} \tag{3.28}$$

The electrical field in z-direction is zero. We can derive the curl of the electrical field:

$$\nabla \times \overline{E} = \begin{vmatrix} \hat{i} & \hat{j} & \hat{k} \\ \frac{\partial}{\partial x} & \frac{\partial}{\partial y} & \frac{\partial}{\partial z} \\ E_x & E_y & 0 \end{vmatrix} = (\frac{\partial E_y}{\partial x} + \frac{\partial E_x}{\partial y})\hat{k} \tag{3.29}$$

The magnetic flux density $\overline{B}$ is in z-direction.

$$\overline{B} = B_z\hat{k} \tag{3.30}$$

The (3.25) can be written as:

$$\frac{1}{\mu}\nabla \times \overline{B} = \begin{vmatrix} \hat{i} & \hat{j} & \hat{k} \\ \frac{\partial}{\partial x} & \frac{\partial}{\partial y} & \frac{\partial}{\partial z} \\ 0 & 0 & B_z \end{vmatrix} = \frac{\partial B_z}{\partial y}\hat{i} - \frac{\partial B_z}{\partial x}\hat{j} \tag{3.31}$$

The current density is written as:

$$\overline{J} = J_x\hat{i} + J_y\hat{j} \tag{3.32}$$

If we combine the (3.29) and (3.30), (3.31) and (3.32), then we can derive the following five equations:

$$\frac{dE_y}{dx} - \frac{dE_x}{dy} = -\frac{d\overline{B}}{dt} = -j\omega B_z \tag{3.33}$$

(3.33) is transferred from time domain to frequency domain:

$$-\frac{d\overline{B}}{dt} \Longleftrightarrow -j\omega B_z \tag{3.34}$$

$$\frac{dB_z}{dy} = \mu J_x \tag{3.35}$$

$$\frac{dB_z}{dx} = -\mu J_y \tag{3.36}$$

$$J_x = \sigma E_x \tag{3.37}$$

$$J_y = \sigma E_y \tag{3.38}$$

The solution of the above five equations is obtained:

$$\frac{d^2B_z}{dx^2} - \frac{d^2B_z}{dy^2} = -j\omega\sigma\mu B_z \tag{3.39}$$

In the ring core, the total magnetic flux consists of the flux generated by the primary winding and the flux generated by the eddy current.

When

B_z is the total flux

B_e is the flux generated by the primary winding

B_i is the flux generated by the eddy currents

If B_p is the amplitude of the magnetic flux generated by the primary winding, then B_e would be:

$$B_e = B_p e^{j\omega t} \tag{3.40}$$

The total flux B_z is

$$B_z = B_e + B_i \tag{3.41}$$

Therefore the (3.39) becomes

$$\frac{d^2(B_e + B_i)}{dx^2} - \frac{d^2(B_e + B_i)}{dy^2} = -j\omega\sigma\mu(B_e + B_i) \tag{3.42}$$

B_e is homogeneous in the core, therefore the second derivatives of x and y are both zeros. Then the (3.42) becomes

$$\frac{d^2B_i}{dx^2} - \frac{d^2B_i}{dy^2} = -j\omega\sigma\mu B_i - j\omega\sigma\mu B_e \tag{3.43}$$

(3.43) is a second order partial differential equation. Normally, it is hard to use analytical approach to solve this equation. In this case, we transfer to the 1-dimensional model. We assume that the length of y-direction is unlimited, and eddy currents flow in y-direction. Therefore, the solutions of the Maxwell's equations can be described as:

$$\frac{dE_y}{dx} = -j\omega \cdot B_z \tag{3.44}$$

$$-\frac{dB_z}{dx} = \mu \cdot J_y \tag{3.45}$$

$$J_y = \sigma \cdot E_y \tag{3.46}$$

The combination of above three equations will lead to a differential equation for the flux density.

$$\frac{d^2B_z}{dx^2} - j\omega\mu\sigma \cdot B_z = 0 \tag{3.47}$$

It can be seen in (3.47), the total B-field varies with position in x-axis. To find the expression for B-field, some boundary conditions are defined in the ring. The boundary conditions are based on the relation between primary current, eddy current and the flux density in the ring.

In Fig. 3.8, the flux goes in from left and comes out from right side, consider the closed magnetic flux loop, which enclose the primary current as well as the eddy current in the core. Use Ampere's circuital law, from left core center to right side core center:

$$\oint_C Hdl = nI + \int JdA \tag{3.48}$$

In (3.48) the left term is the integral of magnetic flux density in its path. The term nI represents the ampere turns of the primary winding. The second term in the right represents for the eddy current enclosed.

If we consider the surface of the ring core, the boundary condition becomes:

$$\oint_C Hdl = nI \tag{3.49}$$

If we assume that the flux generated by the primary winding homogeneously distributes in the ring core. The effective path of the flux will be the effective length l_r. In the boundary, the maximum values of the H-field and B-field are the following results:

$$H_{max} = \frac{nI}{l_r} \tag{3.50}$$

$$B_{max} = \frac{\mu_0 nI}{l_r} \tag{3.51}$$

It is concluded that the flux distribution in the core decreases from boundary to inside in one direction and in the center the flux becomes the minimum, because of the reduction of the magnetic flux generated by eddy current.

3.2.3. MATHEMATICAL MODEL

From (3.47), we already know the expression for the total flux density in the core. It is described by a second order differential equation:

$$\frac{d^2B(x,\omega)}{dx^2} = j\omega\mu\sigma B(x,\omega) \tag{3.52}$$

Factors p and q are introduced to express the function of $B(x,\omega)$. The differential equation is solved by finding a proper general solution for it. (3.53) is the general solution:

$$B(x,\omega) = pe^{(1+j)\frac{x}{\delta}} + qe^{-(1+j)\frac{x}{\delta}} \tag{3.53}$$

δ represents the skin depth of the eddy current. It is described by electrical frequency, magnetic permeability and conductivity of core:

$$\delta = \sqrt{\frac{2}{\omega\mu\sigma}} \tag{3.54}$$

Then we demonstrate the Eqn. 3.53:

$$\frac{d^2B(x,\omega)}{dx^2} = p\frac{(1+j)^2}{\delta^2}e^{(1+j)\frac{x}{\delta}} + q\frac{(1+j)^2}{\delta^2}e^{-(1+j)\frac{x}{\delta}} \tag{3.55}$$

Further, if we substitute the expression for δ, then the equation becomes:

$$\frac{d^2B(x,\omega)}{dx^2} = j\omega\mu\sigma(pe^{(1+j)\frac{x}{\delta}} + qe^{-(1+j)\frac{x}{\delta}}) = j\omega\mu\sigma B \tag{3.56}$$

Therefore, the general solution for B is applicable.

In the core, the distribution of the eddy current is symmetrical. There is a condition to express the eddy current density.

$$J_{y[x=0]} = 0 \Rightarrow p = q \tag{3.57}$$

From above equations, the expression for total flux density distribution is found. It can be written as:

$$B(x,\omega) = p(e^{(1+j)\frac{x}{\delta}} + e^{-(1+j)\frac{x}{\delta}}) \tag{3.58}$$

When $x = \frac{1}{2}a$ or $-\frac{1}{2}a$, $B = B_{max}$,

$$B_{max}(\omega) = p(e^{(1+j)\frac{a}{2\delta}} + e^{-(1+j)\frac{a}{2\delta}}) \tag{3.59}$$

$$p = \frac{B_{max}(\omega)}{e^{(1+j)\frac{a}{2\delta}} + e^{-(1+j)\frac{a}{2\delta}}} \tag{3.60}$$

If we substitute p in (3.53), it would become:

$$B(x,\omega) = \frac{\mu nI}{l_r}\frac{e^{(1+j)\frac{x}{\delta}} + e^{-(1+j)\frac{x}{\delta}}}{e^{(1+j)\frac{a}{2\delta}} + e^{-(1+j)\frac{a}{2\delta}}} \tag{3.61}$$

Finally the expression for eddy current distribution in the cross section of the ring core is derived, in the 1-dimensional case.

$$J_y(x,\omega) = \frac{\mu nI}{l_r}\frac{1+j}{\delta}\frac{e^{(1+j)\frac{x}{\delta}} - e^{-(1+j)\frac{x}{\delta}}}{e^{(1+j)\frac{a}{2\delta}} + e^{-(1+j)\frac{a}{2\delta}}} \tag{3.62}$$

To make (3.61) and (3.62) more visible and easier to analyze, Mathcad is used to plot figures for these two equations. Since they are complex equations which can not be plotted directly, we find the modulus of the results.

Fig. 3.10 shows the modulus of magnetic flux distribution in the cross section of the ring in 1-dimensional case. The x-axis goes from $x = -\frac{1}{2}a$ to $x = \frac{1}{2}a$, and it is the width of the cross section. B is related to the electrical frequency of primary current and the x-axis position. The figure describes the B-field at five frequency levels. When the frequency is 100Hz, the total flux is nearly constant in x-axis, which means a very small eddy current effect occurs in the ring core. When the frequency is 1000Hz, there is an obvious reduction in the B-field, which means the eddy current effect becomes visible. When the frequency increases to 50kHz, the eddy current becomes more and more visible. In the center area between around $x = -\frac{1}{4}a$ and $x = \frac{1}{4}a$, there is an obvious reduction of the flux magnitude which is generated by the eddy current effect. The more eddy current effect occurs, the more reduction of the flux.

Fig. 3.11 shows the modulus of the eddy current distribution in the cross section of the ring in 1-dimensional case. The x-axis goes from $x = -\frac{1}{2}a$ to $x = \frac{1}{2}a$, and it is the width of the cross section. See the (3.62), if the primary current I is a fixed value, then J_y is related to the electrical frequency of the primary current and x-axis position. The figure describes current densities at five frequency levels. It can be seen that when the frequency increases from 100Hz to 50kHz, the eddy current density increases from a small value to approximately $3.8 \times 10^6 A/m^2$. There is a clear tendency that the eddy current distribution changes from approximate linear

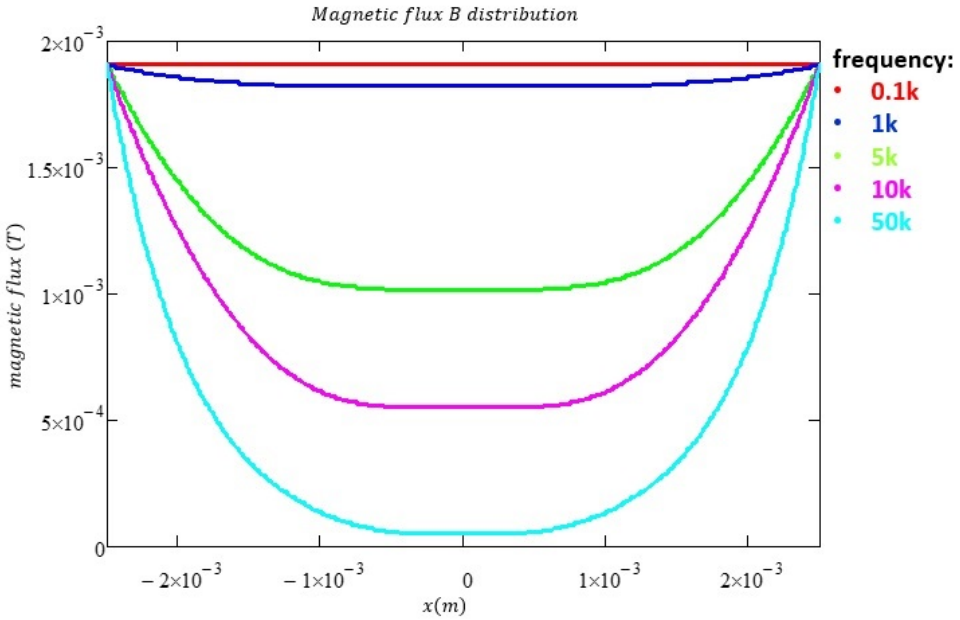

Figure 3.10: Magnetic flux distribution, $|B(x,\omega)|$

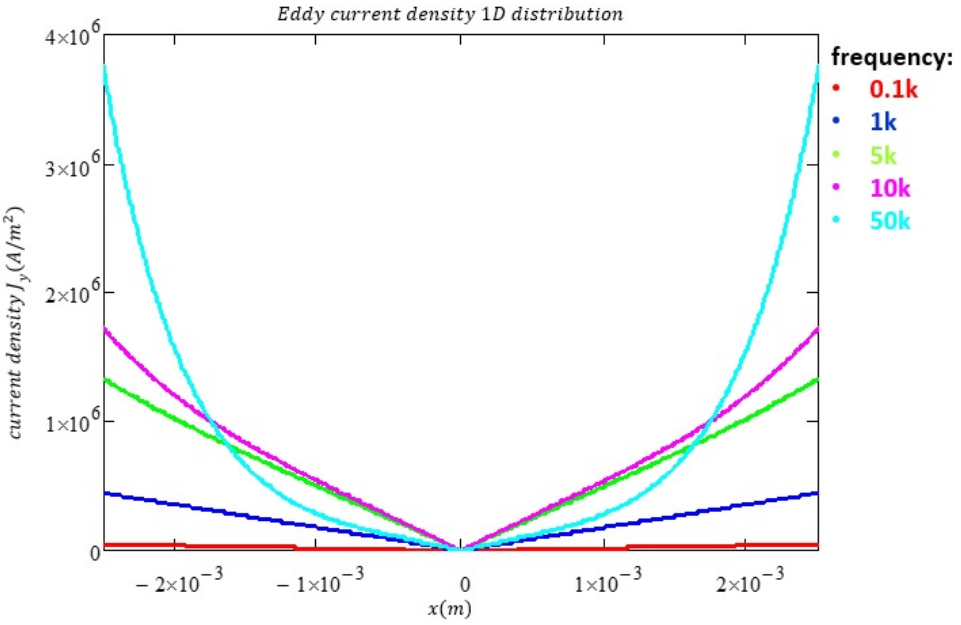

Figure 3.11: Eddy current density distribution $|J_y(x,\omega)|$

distribution to a certain curved distribution, which can be approximated by a polynomial function. Also, it is shown that as the frequency is higher, the eddy currents concentrate more in the edge of the core. From this figure, it is concluded that if the frequency is very high, then the eddy current will be very distributed in the edge of the core; therefore, the eddy current effect can be regarded as a short circuit winding.

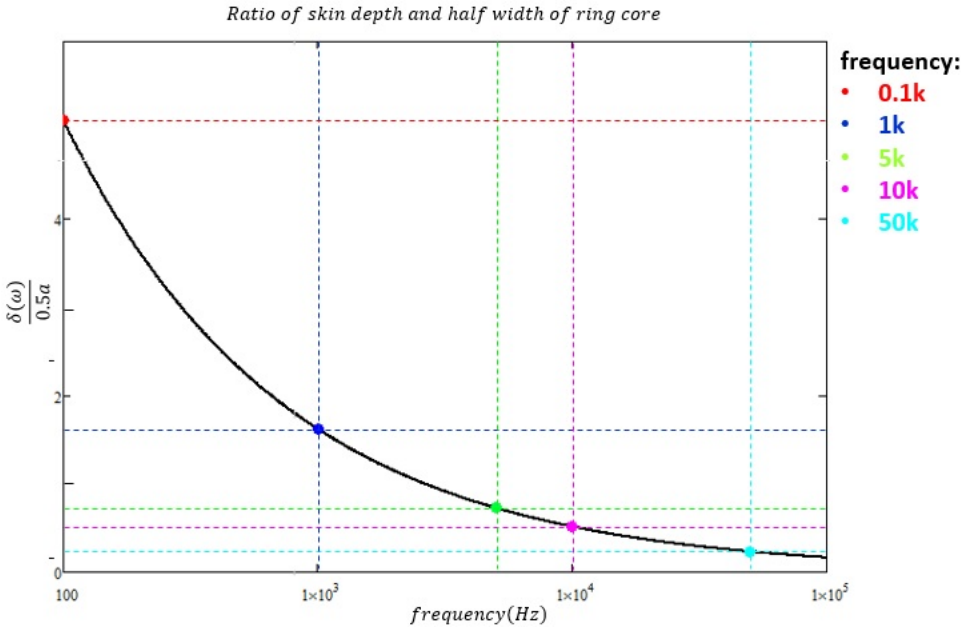

Figure 3.12: Variation of skin depth with frequency

Even though Fig. 3.10 and Fig. 3.11 can give a clear tendency with the magnetic flux and the eddy current density distribution, they can not show that in what frequency the eddy current effect begins to occur. For example, when the frequency is 100Hz, it seems that the eddy current density is small, but it still has some value. So there is also another picture needed to show that in what frequency range the eddy current effect begins to occur.

In Chapter 2, the concept of skin depth is introduced. It is the position where the eddy currents decrease to 1/e compared to the surface value. In this case, we define the position of skin depth is p_{sd}. It is the ratio of skin depth and the half width of the ring core (because core is symmetrical):

$$p_{sd} = \frac{\delta(\omega)}{0.5a} \tag{3.63}$$

The ratio is plot in Fig. 3.12, in which the black curve represents the ratio varies with frequency in logarithm. The five points stand for the positions of skin depth at different levels. From the Fig. 3.12 and Fig. 3.11, we can see that at 100Hz there is no eddy current effect since the skin depth is far beyond the core; at 1000Hz the eddy current effect begins to become obvious because skin depth is smaller than the core width. Clearly when the frequency goes to 50kHz, most of the currents distribute in the skin depth.

The outcomes and analysis in this section help us to know that the eddy current density distribution and magnetic flux density distribution in the cross section. The mathematical expressions are derived. Based on this, the researcher can build the simpler assumptions with the current density distribution, and this will help the researcher to improve the eddy current model.

3.3. SUMMARY

- To simplify the complex actuator system, a transformer ring model is built. Without air gaps, the flux leakage in the ring can be neglected. The ring cores can be made from varies materials based on different research objects. In this Chapter, the analytical analysis is based on the brass ring. In the brass ring, the researcher can get rid of the hysteresis and saturation effects, and the only eddy current effect is considered.

- The geometry of the ring core, as well as the parameters of the windings are treated. The conductivity of the metal core is an important parameter. But the material of the metal core can be alloyed, then it is hard to decide the conductivity of it. In this case, the four point measurement approach is proposed to measure the conductivity of the ring core. Also, the effective length of the ring is calculated, which can be used to decide the effective magnetic flux path.

- An analytical model is discussed. The researcher studies on the induced eddy current in the ring. Based on Maxwell's equations, first a 2-dimensional calculation is conducted, however, it is hard to find the analytical solution of it. The 1-dimensional calculation finally delivers the expressions for eddy current density distribution and the magnetic flux density distribution in the core. From the plots, it is concluded that at low frequencies, the eddy current distribution is linear, while at high frequencies, the distribution can be polynomial; also at high frequencies, the magnetic flux density is reduced in the center of the core. These outcomes help the researcher to develop simpler assumptions to improve the eddy current model.

4

IMPROVEMENT OF EDDY CURRENT MODEL

There is a conclusion in Chapter 3 that when the electrical frequency is very high, the eddy current can be regarded as a short circuit winding, with the thickness of skin depth δ. This concept is used in the eddy current model. This model is called Present Model. However, this concept or assumption still has two problems: 1, the distribution of the eddy current is not good; 2, the relationship between the effective flux and the eddy current is not found. Therefore in this Chapter, three optimization steps are proposed to overcome these two problems. All the calculation and model is based on the brass ring.

4.1. THE TRANSFORMER RING CIRCUIT

The eddy current effect is represented by a short circuit winding in the ring. One can imagine this winding in the core, just close to the surface. Then the equivalent circuit of the transformer ring will become Fig. 4.1.

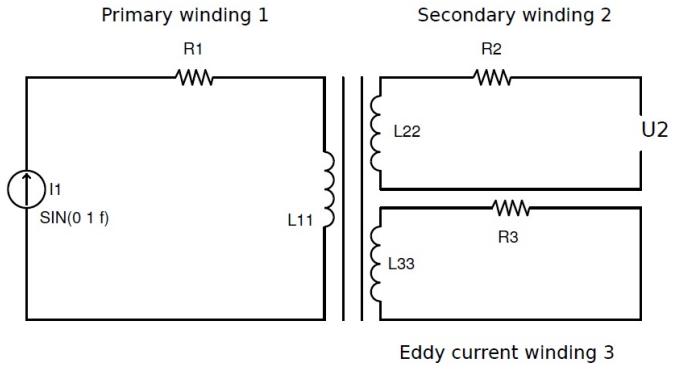

Figure 4.1: Equivalent circuit diagram of the transformer ring

Fig. 4.1 shows the equivalent circuit for the transformer ring; I_1 is the input current in the primary winding, and U_2 is the induced voltage in the secondary winding. The eddy current winding is the short circuit winding 3, which is coupling with the primary and secondary coils. In the circuit diagram, the parameters include the resistance of each winding, the self-inductance of each winding, and the mutual inductance between every two coils. The cross section of the transformer ring is as the following picture:

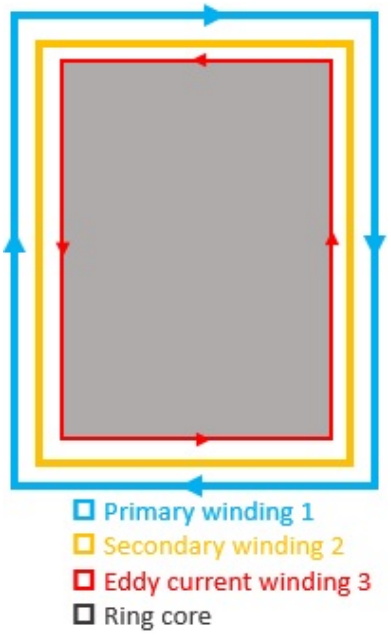

Figure 4.2: The cross section of the ring, with primary, secondary and eddy current representative coils

Fig. 4.2 shows the cross section of core. The gray section represents the ring core; the yellow rectangle represents the secondary winding, which actually is an open circuit winding; the blue rectangle is the primary winding with the input current; the red rectangle stands for the eddy current winding. In this diagram, the primary winding generates flux, and this flux goes through the areas that are enclosed by secondary winding and the eddy current winding. Also, the flux generated by winding 2 or winding 3 will go through the areas that are enclosed by other two coils. In an N coils system, the flux through a winding i consists of the flux generated in the winding itself, and the coupled fluxes of the other winding [16]. We can write this as follows.

$$\phi_i = \sum_{j=1}^{N} \phi_{ij} \tag{4.1}$$

In our case, the transformer ring is a 3 coils system. i=1,2,3 and j=1,2,3. Therefore, the equation becomes:

$$\phi_1 = \phi_{11} + \phi_{12} + \phi_{13} \tag{4.2}$$
$$\phi_2 = \phi_{21} + \phi_{22} + \phi_{23} \tag{4.3}$$
$$\phi_3 = \phi_{31} + \phi_{32} + \phi_{33} \tag{4.4}$$

They can also be written as:

$$\phi_1 = \Lambda_{11}\mathscr{F}_1 + \Lambda_{12}\mathscr{F}_2 + \Lambda_{13}\mathscr{F}_3 \tag{4.5}$$
$$\phi_2 = \Lambda_{21}\mathscr{F}_1 + \Lambda_{22}\mathscr{F}_2 + \Lambda_{23}\mathscr{F}_3 \tag{4.6}$$
$$\phi_3 = \Lambda_{31}\mathscr{F}_1 + \Lambda_{32}\mathscr{F}_2 + \Lambda_{33}\mathscr{F}_3 \tag{4.7}$$

$\mathscr{F}_i$ is the ampere turns of winding i
Λ_{ii} is the self permeance of winding i
Λ_{ij} is the mutual permeance between winding i and j
The permeance means the property of allowing the magnetic flux. In the magnetic circuit, the permeance is the reciprocal of the magnetic reluctance, which can be written as:

$$\Lambda = \frac{1}{R_c} = \frac{\mu_0 \mu_r A}{l_r} \tag{4.8}$$

l_r is the magnetic flux path

A is the area of the flux going through

According to Faraday's law, we can write the induced voltages across the coils caused by time varying currents.

$$u_1 = n_1^2 \Lambda_{11} \frac{dI_1}{dt} + n_1 n_2 \Lambda_{12} \frac{dI_2}{dt} + n_1 n_3 \Lambda_{13} \frac{dI_3}{dt} \tag{4.9}$$

$$u_2 = n_2 n_1 \Lambda_{21} \frac{dI_1}{dt} + n_2^2 \Lambda_{22} \frac{dI_2}{dt} + n_2 n_3 \Lambda_{23} \frac{dI_3}{dt} \tag{4.10}$$

$$u_3 = n_3 n_1 \Lambda_{31} \frac{dI_1}{dt} + n_3 n_2 \Lambda_{32} \frac{dI_2}{dt} + n_3^2 \Lambda_{33} \frac{dI_3}{dt} \tag{4.11}$$

As well one can use self-inductance, mutual inductance and resistance to describe the transformer ring circuit:

$$U_1 = L_{11} \frac{dI_1}{dt} + L_{12} \frac{dI_2}{dt} + L_{13} \frac{dI_3}{dt} + I_1 R_1 \tag{4.12}$$

$$U_2 = L_{21} \frac{dI_1}{dt} + L_{22} \frac{dI_2}{dt} + L_{23} \frac{dI_3}{dt} + I_2 R_2 \tag{4.13}$$

$$U_3 = L_{31} \frac{dI_1}{dt} + L_{32} \frac{dI_2}{dt} + L_{33} \frac{dI_3}{dt} + I_3 R_3 \tag{4.14}$$

From above, we can write down the inductance matrix L.

$$L = \begin{bmatrix} L_{11} & L_{12} & L_{13} \\ L_{21} & L_{22} & L_{23} \\ L_{31} & L_{32} & L_{33} \end{bmatrix} \tag{4.15}$$

or

$$L = \begin{bmatrix} n_1^2 \Lambda_{11} & n_1 n_2 \Lambda_{12} & n_1 n_3 \Lambda_{13} \\ n_2 n_1 \Lambda_{21} & n_2^2 \Lambda_{22} & n_2 n_3 \Lambda_{33} \\ n_3 n_1 \Lambda_{31} & n_3^2 \Lambda_{32} & n_3^2 \Lambda_{33} \end{bmatrix} \tag{4.16}$$

μ_r=1. The coupling factor from winding i to winding j is defined as the ratio of the coupled flux and generated flux:

$$k_{ij} = \frac{\phi_{ij}}{\phi_{jj}} = \frac{\Lambda_{ij}}{\Lambda_{jj}} = \frac{A_i}{A_j},\ i = 1,2,3;\ j = 1,2,3 \tag{4.17}$$

If $A_i > A_j$, then k_{ij}=1.

ϕ_{jj} is the flux generated in the winding j itself

ϕ_{ij} is the flux generated by winding j but enclosed by winding i

The coupling factor k_{ij} is also the ratio between the area A_i enclosed by winding i and the area A_j enclosed by winding j. If we define A_1, A_2 and A_3 for the three windings, then we can see that in Fig. 4.2:

$$A_1 > A_2 > A_3 \tag{4.18}$$

The flux generated by winding 3 will be totally enclosed by winding 1 and 2, and the flux generated by winding 2 will be totally enclosed by winding 1. In this case,

$$\Lambda_{22} = \Lambda_{12} = \Lambda_{21} \tag{4.19}$$

$$\Lambda_{33} = \Lambda_{32} = \Lambda_{23} = \Lambda_{13} = \Lambda_{31} \tag{4.20}$$

The transformer ring circuit analysis gives the expressions for the inductance and resistance of the circuit. These parameters are calculated and will be applied into the simulation model.

4.2. PARAMETERS CALCULATION

In this section, the parameters of the transformer ring circuit will be calculated. The winding 1 and winding 2 are real coils; one can know the current distribution as well as the coils distribution precisely. Therefore, the inductance and resistance for winding 1 and winding 2 can be calculated. However, as for the eddy current winding 3, the problem is how to calculate the inductance and resistance. An assumption comes from the conclusion in Chapter 3, that when the electrical frequency is very high, the eddy current will almost concentrate on the surface of the core. In Fig. 4.1 and Fig. 4.2, we already assume that the eddy current effect is a short circuit winding mounted over the core. From (3.54) in Chapter 3, if the frequency goes to 100kHz, the skin depth of the eddy current will be:

$$\delta(f = 100k) = 0.404mm \tag{4.21}$$

Therefore, we assume that the all the eddy current flowing in the thickness of skin depth, then the δ is the thickness of the eddy current winding.

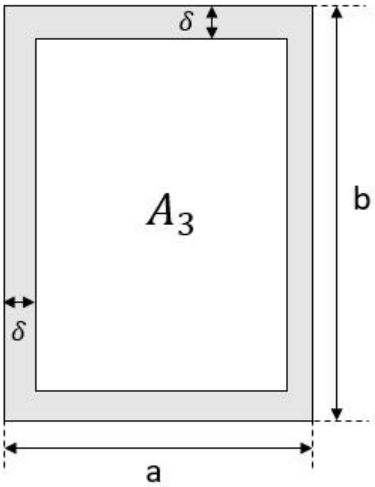

Figure 4.3: The cross section of the ring core

Fig. 4.3 shows the cross section of the ring core. a and b are the width and height of the cross section respectively. The gray section is the thickness of the eddy current winding. In this figure, the eddy current winding can enclose the flux that goes through the area A_3.

To derive the winding 1 area A_1 and winding 2 area A_2, we use the caliper to measure the width and height of the outside cross section of the ring.

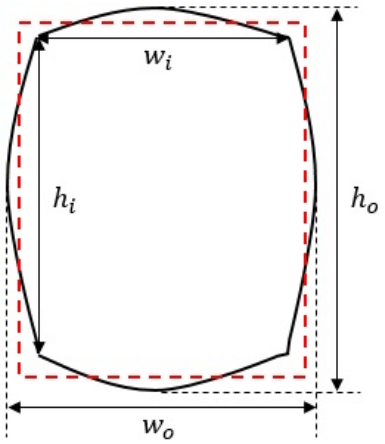

Figure 4.4: Measure the geometry of the outside cross section of the ring

In Fig. 4.4, it is in the perspective of the outside cross section of the ring; the black curve represents the outside primary winding. The coil bends slightly as it is wound around the core. The outside width w_o and height h_o, and inside width w_i and height h_i are measured. Then the averages of w_o and w_i, h_o and h_i are taken to decide the average width w_a and height h_a of the ring, which are illustrated by the red dot rectangle. The results are:

Table 4.1: Measured results of Fig. 4.4

$w_o(mm)$	$h_o(mm)$	$w_i(mm)$	$h_i(mm)$	$w_a(mm)$	$h_a(mm)$
8.4	12.7	8.0	12.2	8.2	12.4

The thickness of the primary winding is 0.56mm, and for the secondary winding it is 0.25mm. Then one can derive the area that is enclosed by winding 1 in the cross section of the ring:

$$A_1 = (w_a - 0.56mm) \cdot (h_a - 0.56mm) = 90.457mm^2 \tag{4.22}$$

For the secondary winding, it is next to the primary winding. Similarly, one can also derive the area that is enclosed by winding 2 in the cross section:

$$A_2 = (w_a - 2 \times 0.56mm - 0.25mm) \cdot (h_a - 2 \times 0.56mm - 0.25mm) = 75.33mm^2 \tag{4.23}$$

We also write down the A_3:

$$A_3 = (a - \delta) \cdot (b - \delta) = 44.1mm^2 \tag{4.24}$$

Next, one can substitute the results of areas into the (4.8) to derive matrix for permeance of the transformer ring circuit.

$$\Lambda = \begin{bmatrix} \Lambda_{11} & \Lambda_{12} & \Lambda_{13} \\ \Lambda_{21} & \Lambda_{22} & \Lambda_{23} \\ \Lambda_{31} & \Lambda_{32} & \Lambda_{33} \end{bmatrix} = \begin{bmatrix} 0.345 & 0.287 & 0.168 \\ 0.287 & 0.287 & 0.168 \\ 0.168 & 0.168 & 0.168 \end{bmatrix} \times 10^{-9} \tag{4.25}$$

The number of turns for winding 1 and 2 are both 500 turns. But for winding 3, the number of turns is 1. Therefore, one can substitute the n_1, n_2 and n_3 into the matrix for inductance of the transformer ring:

$$L = \begin{bmatrix} 8.51 \cdot 10^{-5} & 7.17 \cdot 10^{-5} & 1.68 \cdot 10^{-10} \\ 7.17 \cdot 10^{-5} & 7.17 \cdot 10^{-5} & 1.68 \cdot 10^{-10} \\ 1.68 \cdot 10^{-10} & 1.68 \cdot 10^{-10} & 1.68 \cdot 10^{-10} \end{bmatrix} H \tag{4.26}$$

Next, we need to find the resistance of each winding in the circuit. R_1 and R_2 can be calculated or measured with a multimeter. The details about that will not be introduced. For the eddy current winding resistance, it will be:

$$R_3 = \frac{l}{\sigma A} = \frac{2(a+b-2\delta)}{\sigma l_r \delta} = 1.37 \cdot 10^{-5} \Omega \tag{4.27}$$

The results:

$$R_1 = 1.34\Omega \tag{4.28}$$

$$R_2 = 6.33\Omega \tag{4.29}$$

$$R_3 = 1.37 \times 10^{-5} \Omega \tag{4.30}$$

The parameters of inductance matrix and resistance of each winding will be input into the simulation model of the transformer ring. In this section, the derivation of the parameters of the eddy current winding is based on the the assumption, that the eddy current equally distributes in the thickness of δ. This is defined as Present Model (P-Model).

4.3. IMPEDANCE ANALYSIS

4.3.1. EDDY CURRENT IMPEDANCE LADDER

The impedance analysis of the transformer ring circuit is treated in this section. The eddy current effect can be represented by a series of R/L sections.

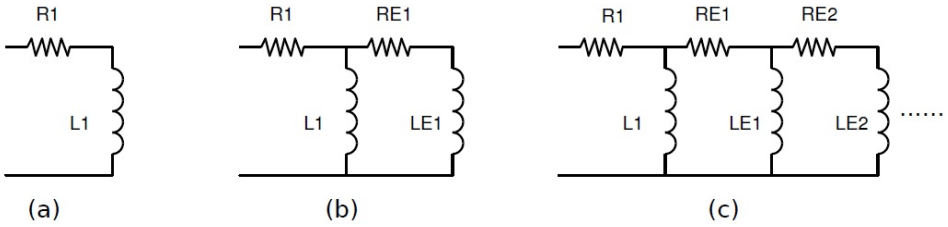

Figure 4.5: Eddy current effect L-R ladder

In Fig. 4.5, the first term (a) shows the impedance of the primary winding. In reality, the eddy currents would be described by a lot of R/L sections [17] (see Fig. 4.5(c)). But with more sections, the circuit could be more complex to express and calculate. Therefore, the eddy current effect in the circuit is described by adding one R/L section to the primary winding (see Fig. 4.5(b)). To explain this phenomenon, the impedance of three cases is plot respectively. In Fig. 4.6, the red line shows the impedance of the primary winding, just as the Fig. 4.5(a); the blue line shows the impedance of the primary winding with one R/L section, just as the Fig. 4.5(b); the green line shows the impedance of the primary winding with two R/L sectionss.

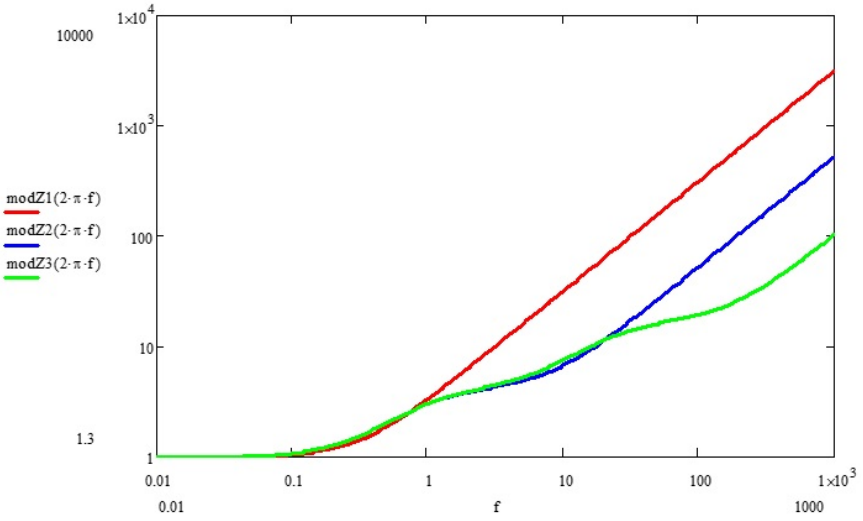

Figure 4.6: Eddy current effect R/L sections

From Fig. 4.6, it can be seen that when R/L section is added to the primary winding, the impedance at some frequency will begin to split to a lower value; when R/L sections are added, then the impedance will split again at another frequency value. That is because when the frequency reaches a certain value, the the influence of the new added L-R ladder begins to be dominant. The split frequency value would be:

$$f_c = \frac{R}{2\pi L} \tag{4.31}$$

R and L are inductance and resistance of the new added section.

we can know that for a primary winding with a number of R/L sections, the split points are dependent on the values of the L and R of every ladder. If the values are not saturation values, the impedance curve can merge together. From Fig. 4.6 we can also know that, when there is eddy current effect, the impedance of the circuit can split, compared to the impedance without eddy current effect. In this case, we use a short circuit winding to describe this effect, that is, adding a R/L section to the primary winding, obviously the split frequency value can be extended. It is concluded that the eddy current model with one R/L section can be good enough for a certain range of the frequency. This analysis can explain why we use a short circuit winding to describe the eddy current effect.

4.3.2. PRIMARY AND SECONDARY WINDING IMPEDANCE

In this part, the impedance of the primary winding and secondary winding is measured respectively. First, from the measurement we can see the influence of the eddy currents in the circuit; second, we can compare the measurement results with the calculation results at the starting frequency, since we expect that they should be the same.

The impedance of the primary winding and secondary winding can be measured directly by the impedance analyzer. First, if we assume that there is no eddy current effect in the circuit, then the circuit becomes Fig. 4.7.

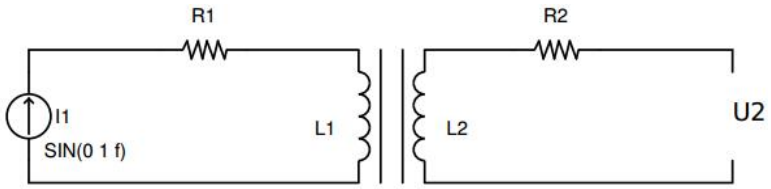

Figure 4.7: Equivalent circuit without the eddy current

In the circuit, the secondary winding is open circuit, therefore the impedance of the transformer ring would be the impedance of the primary winding L11 and R1. So the primary impedance would be constant values with the assumption that no eddy currents are in the ring. But if we measure the impedance of the primary winding in reality, the result is as the Fig. 4.8.

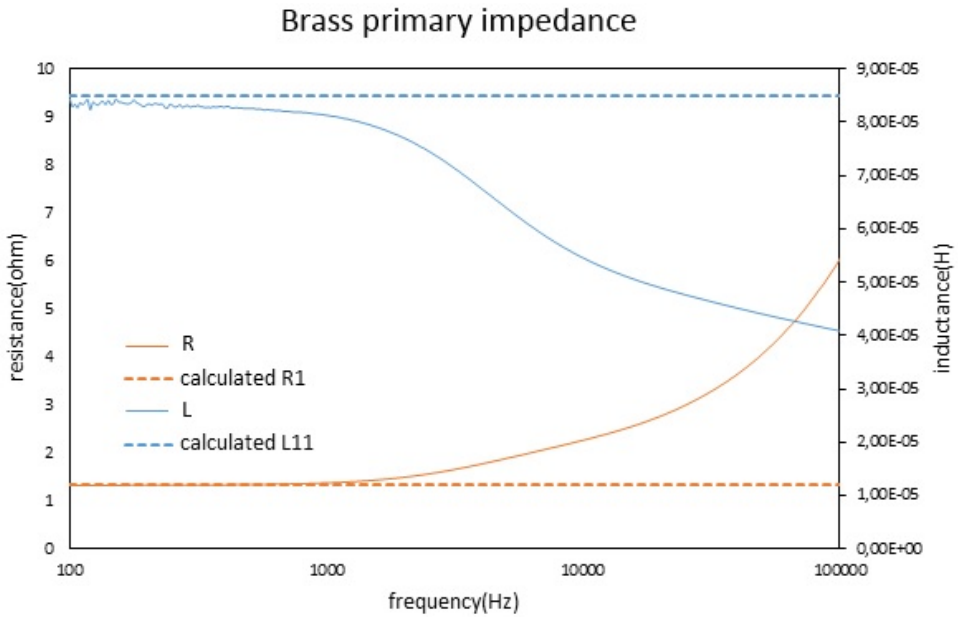

Figure 4.8: Brass primary winding impedance measurement, and comparison with the constant values

In Fig. 4.8, the solid lines show the measurement results of L and R of the primary winding; the dot lines are the constant values of L11 and R1. It can be seen that from the beginning, the measured L and R are equal to L11 and R1. That is because the influence of the eddy current effect can be neglected at the moment. At f=1000Hz, the inductance begins to decrease while resistance begins to increase, and this is caused by eddy current effect in the core. When the eddy current effect becomes obvious, the total flux will be reduced; so at the moment, the magnetic flux permeance would be reduced. If the frequency goes to higher, then the resistance goes up; because the primary side sees more eddy current L-R ladders.

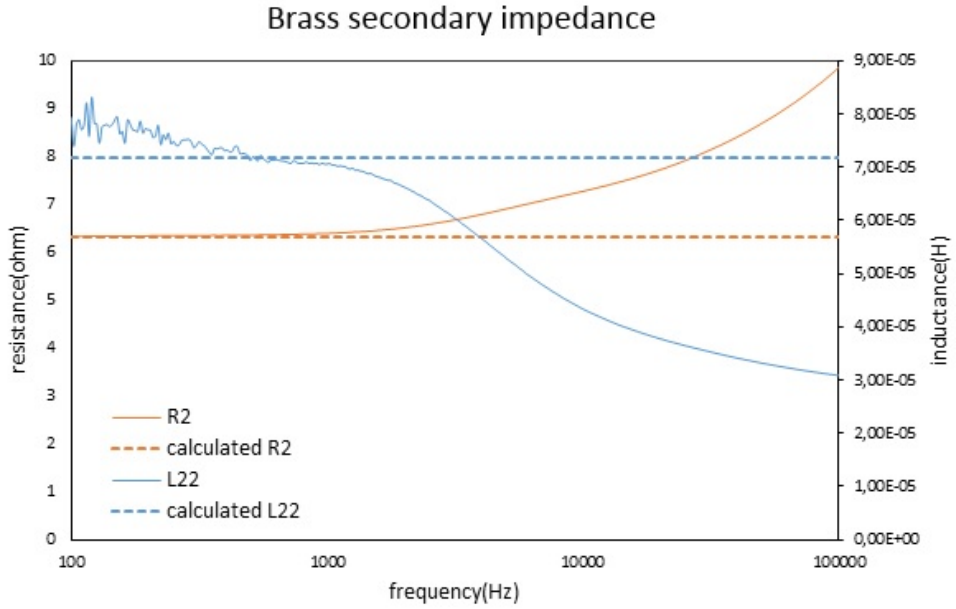

Figure 4.9: Brass secondary winding impedance measurement under frequency sweep, and comparison with the calculated impedance

Fig. 4.9 gives the same kind of information as Fig. 4.8, but it shows the measured impedance of the secondary winding. Detailed explanations will not repeat. The noise from the measurement in inductance is not known yet. If we concentrate on the starting points, the measured L and R are equal to the L22 and R2. This can show that the calculation of L22 and R2 is good.

4.3.3. TRANSFER IMPEDANCE MEASUREMENT

The transfer impedance of the circuit can also show the eddy current effect. This part begins with the calculation of transfer impedance without the eddy current effect. If there is no eddy currents in the circuit, then the circuit diagram will be:

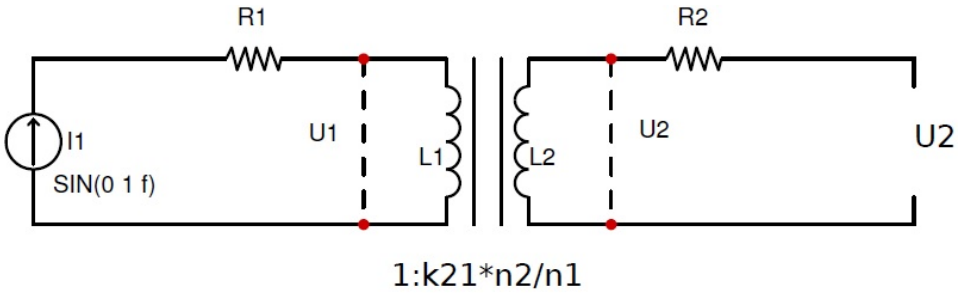

Figure 4.10: Equivalent circuit without the eddy current to calculate transfer impedance

In Fig. 4.10, the transfer impedance Z_{21} is calculated.

$$Z_{21} = \frac{U_2}{I_1} \tag{4.32}$$

$$U_2 = U_1 \cdot \frac{n_2}{n_1} \cdot k_{21} \tag{4.33}$$

$$\frac{U_1}{I_1} = j\omega L_1 \tag{4.34}$$

We already know that the self inductance L1

$$L_1 = n_1^2 \Lambda_{11} \tag{4.35}$$

$$L_1 \cdot \frac{n_2}{n_1} \cdot k_{21} = n_1^2 \Lambda_{11} \frac{n_2}{n_1} k_{21} = n_1 n_2 \Lambda_{11} k_{21} = L_{21} \tag{4.36}$$

If we substitute these results into (4.32), the the transfer impedance would be:

$$Z_{21} = j\omega L_{21} \tag{4.37}$$

Therefore, in the transfer impedance measurement, we expect the starting values of the inductance is L_{21}, and of the resistance is 0.

The transfer impedance measurement needs the primary current I_1 and the secondary voltage U_2. However, from the impedance analyzer, the transfer impedance L-R can not be derived directly. But the bode plot from U_2 to I_1 is derived. The impedance quantities can be found from the bode plot. Fig. 4.11 shows the measurement circuit.

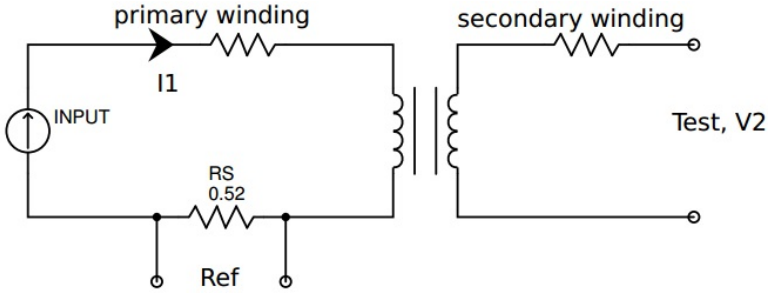

Figure 4.11: Circuit for transfer impedance measurement

In the circuit, the Ref probe measures the voltage across the reference resistance R_s, and the $Test$ probe measures the secondary winding voltage. The appliance in the test set-up provides a gain and a phase value.

In the HP Analyzer gain and phase is defined as:

$$gain = 20log_{10}\frac{U_{Test}}{U_{Ref}} \tag{4.38}$$

$$\theta = phase(degree) \tag{4.39}$$

The relations between these parameters are:

$$U_{Ref} = R_s I_1 \tag{4.40}$$

$$U_{Test} = U_2 \tag{4.41}$$

$$\tag{4.42}$$

The transfer impedance is:

$$Z_{tsf} = \frac{U_2}{I_1} = 10^{\frac{1}{20}gain} R_s \tag{4.43}$$

Then components of transfer impedance Z_{tsf} can be derived:

$$R_{tsf} = |Z_{tsf}| cos\theta \tag{4.44}$$

$$L_{tsf} = \frac{|Z_{tsf}| sin\theta}{2\pi f} \tag{4.45}$$

Fig. 4.12 shows the measured transfer impedance L and R.

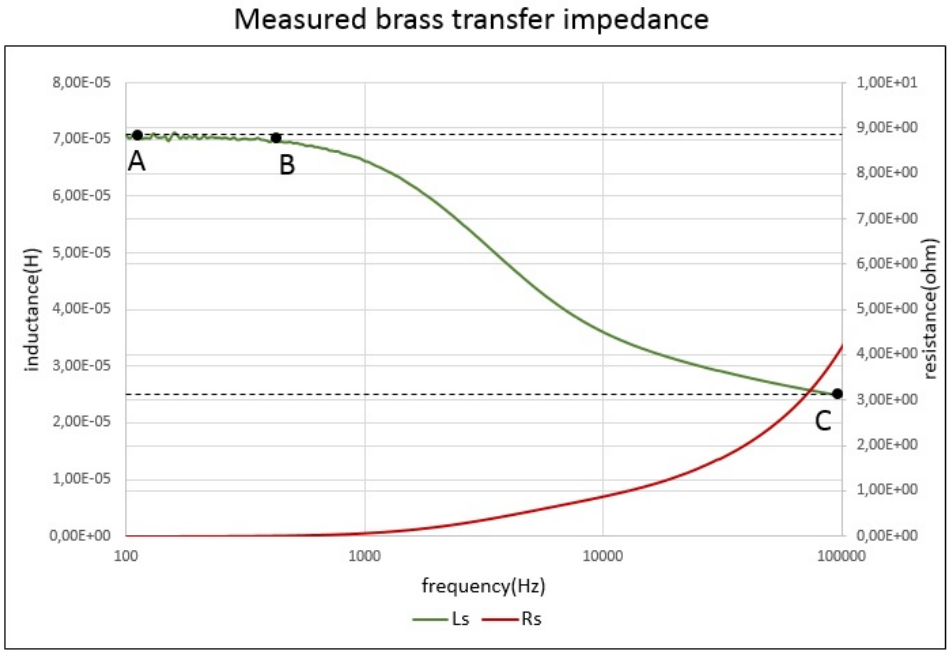

Figure 4.12: Brass ring measured transfer impedance

Fig. 4.12 shows the measured transfer impedance components L_s and R_s. At the starting point A, the values of the inductance and the resistance are constant; the value of inductance is the same as L_{21} and the value of resistance is 0. These results correspond to the expectation. At the point B, the inductance begins to decrease and the resistance begins to increase, because the eddy current effect becomes obvious. At point C, where the frequency is very high, the inductance tends to be smooth. This is due to the fact that total flux is highly reduced by the flux generated by the eddy current, currently the eddy current focus on the edge of the core. Thus, only the flux through the thickness of the secondary winding is enclosed. One can see that the ratio of the inductance value of point A and point C would be the same as $A_2/(A_2 - A_3)$, and this confirm the explanation.

From the transfer impedance, the eddy current effect can also be illustrated. Also, the resistance at very low frequency is 0, therefore one can more clearly see the appearance of the eddy current effect.

4.4. SIMULATION OF THE PRESENT MODEL

The transformer ring circuit model is built in LTspice. Previously, the calculation for the relating parameters is finished, and the results will be adapted to the simulation model. After that, the simulation result for the transfer impedance is compared with the measured result.

4.4.1. LTSPICE MODEL

In Fig. 4.13, the top block is the primary winding circuit with sine wave AC current input; the middle block is the secondary open circuit winding; the bottom block is eddy current representative short circuit winding. The left three circuit blocks give the magneto motive force of each winding; the right three blocks compute the total flux of each winding.

Until now, the parameters of the Present Model in the section 4.2 already have been derived. The impedance of the primary winding and the secondary winding has been verified in the section 4.3. As for the eddy current winding, in the Present Model, it is defined as a

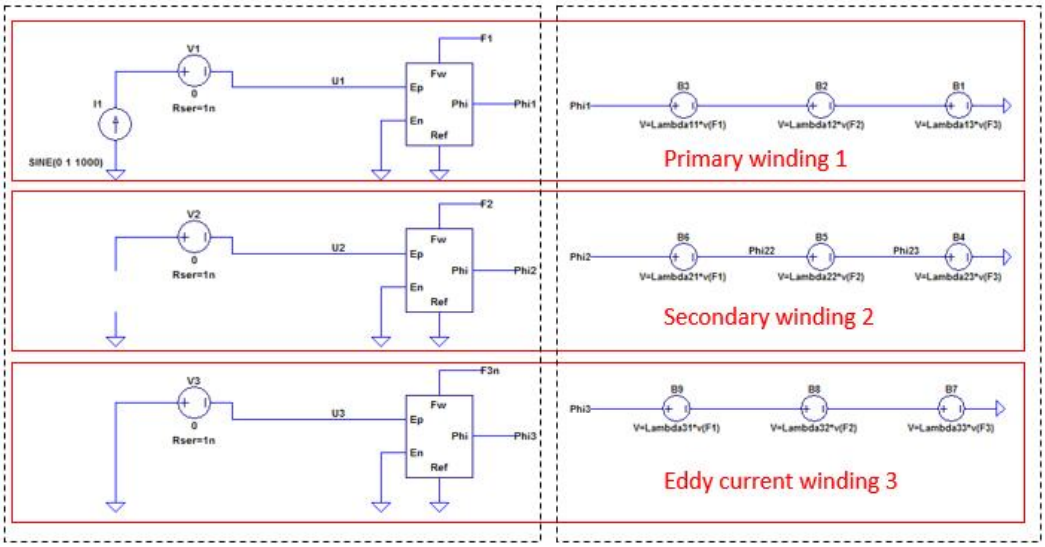

Figure 4.13: The transformer ring circuit model in LTspice

short circuit winding with thickness of δ. Therefore, the number of turns of each winding, and the parameters of the (4.25), (4.28), (4.29), and (4.30) will be put into the simulation.

4.4.2. SIMULATION RESULTS

In this part, the simulation is based on parameters of the Present Model. Fig. 4.14 shows the eddy current distribution and flux density distribution of the Present Model: The assumption is that the eddy current is equally distributed in the thickness of δ, and the magnetic flux generated by the eddy current goes through the core; the eddy current encloses the flux.

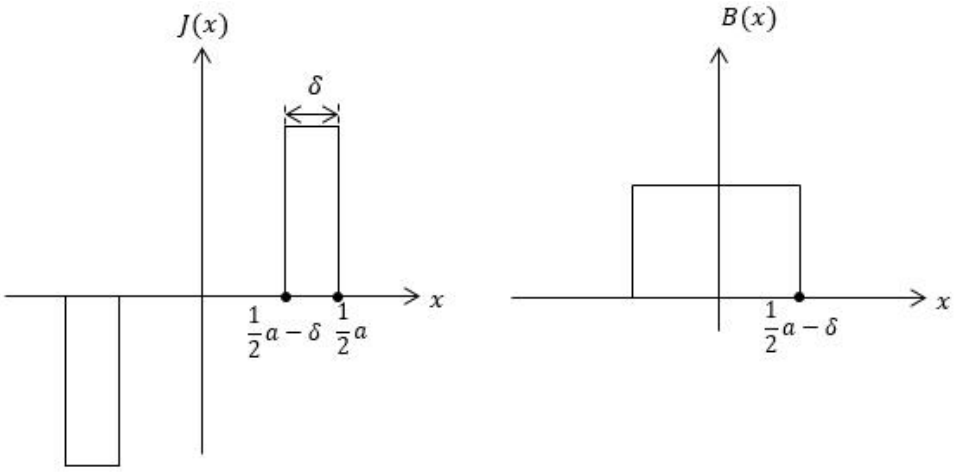

Figure 4.14: Present Model diagrams for eddy current distribution and magnetic flux distribution

Simulation method: In LTspice, the primary winding is set up to use small signal analysis, just the same as the measurement mode. Also, the bode plot is derived directly from the simulation. Then the same transformation method is used in Section 4.3.3. The impedance components L_s and R_s are shown in Fig. 4.15.

In Fig. 4.15, the dash lines are the measured transfer impedance, while the solid lines are the simulation transfer impedance. At the low frequencies, the measured impedance and the simulation impedance are at the same levels. However, they are splitting just before 1000Hz,

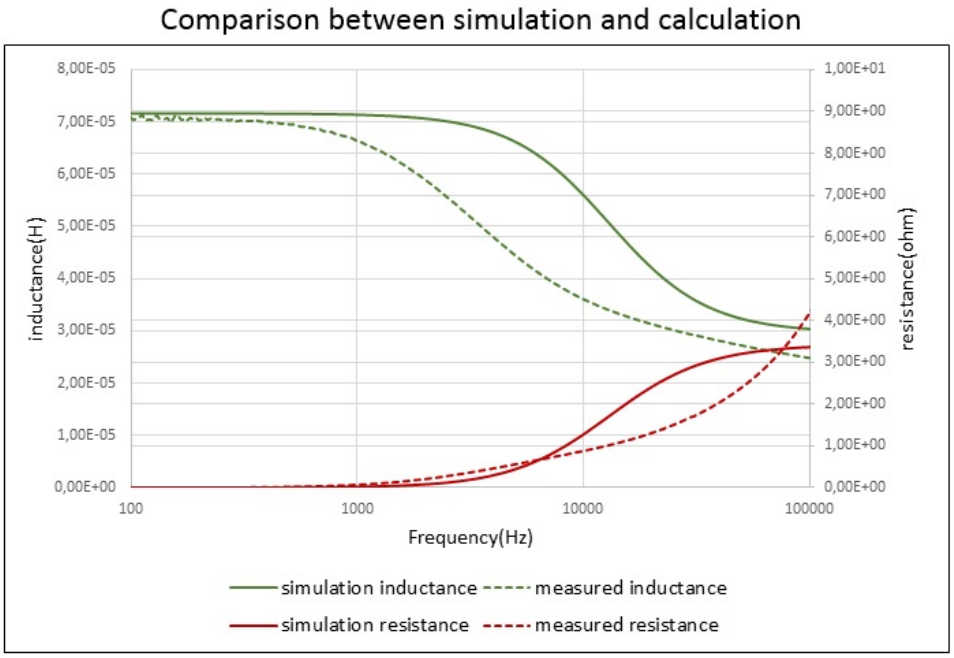

Figure 4.15: Transfer impedance simulation result, compared with measurement

where the measured inductance goes down. This phenomenon shows that the eddy current effect appears much later in the simulation model than in the measurement. But the measured resistance and simulation resistance correspond to each other until 10000Hz. When the frequency goes to 100000Hz, the simulation impedance will try to correspond to the measured impedance. That is because in the Present Model, the eddy current is regarded as a winding around the core, which is an imagination of a high-frequency case.

It is clear to see a big deviation of these two results that for the simulation model: the eddy current effect occurs later than measurement. That is because there are two problems of the Present Model:

- The distribution of the eddy current is not correctly described. The eddy current distributes in the core everywhere, and can vary with frequencies.
- The relationship between the eddy current and the effective magnetic flux through the core is not found.

To solve these two problems, several steps for optimization are taken in the next section.

4.5. IMPROVEMENT FOR EDDY CURRENT MODEL

In the LTspice model, for the eddy current representative winding, L and R are the most important two factors. While based on the Present Model, the simulation result is far from what we need. The Present Model can be improved on two aspects: Find a reasonable eddy current distribution; find the relationship between the eddy current and the effective magnetic flux through the core.

In LTspice, it is difficult to simulate the real distribution of the eddy current in the core, since the distribution varies with frequency. Therefore, as for the improvements for the model, the applicable frequency range should be discussed first. In this section, there will be a survey of the eddy current distribution as well as the relationship between the current and the effective flux. Based on this survey, some assumptions are proposed in several steps, and further to optimize the Present Model.

- Present Model: the eddy current is equally distributed in the thickness of δ, and the magnetic flux generated by the eddy current goes through the core; the eddy current encloses all the flux. Problems of this model: the eddy current distribution is not described correctly, since the eddy current can distribute everywhere in the core and vary with frequencies; the relationship between the eddy current and the effective flux is not found.

- Optimization 1: the eddy current is equally distributed in the thickness of δ; the effective flux through the core is explored. Problem of this model: the eddy current distribution is not true.

- Optimization 2: the eddy current is linear distributed in the core; the effective flux through the core is explored. Problem of this model: the linear distribution of eddy current is applicable to the low and middle frequency ranges; for higher frequency, this is not applicable.

- Optimization 3: the eddy current is polynomial distributed in the core; the effective flux through the core is explored. If the simulation result of Opt2 is good, then it can be extended to higher frequencies.

4.5.1. OPTIMIZATION STEP1

Two problems are proposed for the Present Model. In this Opt1, one problem is explored: find a proper relationship between the eddy current and the effective magnetic flux in the core.

We assume that the eddy current is a constant current source, and the amplitude of total current is I. The eddy current is equally distributed in a certain thickness δ. A new method is created to find the effective flux enclosed by the eddy currrent.

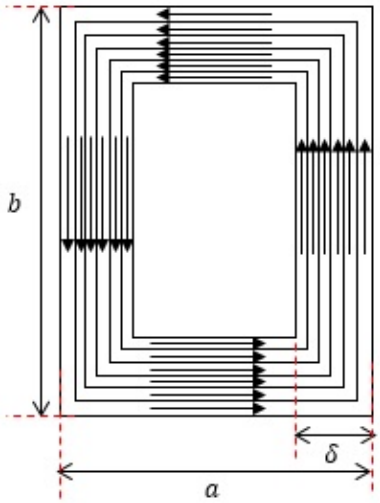

Figure 4.16: Eddy current distribution and current tubes schematic diagram

Fig. 4.16 is the sketch for the assumption, with the eddy current flows in the representative winding. The thickness of the eddy current region is δ. It is regarded as N number of current tubes connecting in series together. Each current tube has the same thickness δ/N. In every current tube, the current is the same which is I/N. This current-tube theory is to help us to find the effective flux in the core. Because the eddy current winding has a certain thickness, there will be flux through the eddy current. Also, for every current piece, the contribution to the magnetic flux is different. That is the reason that why the eddy current winding is

divided into N number of current tubes. In this case, the Fig. 4.17 shows the relationship between current density and one dimension (x-axis), and the magnetic flux distribution in the core.

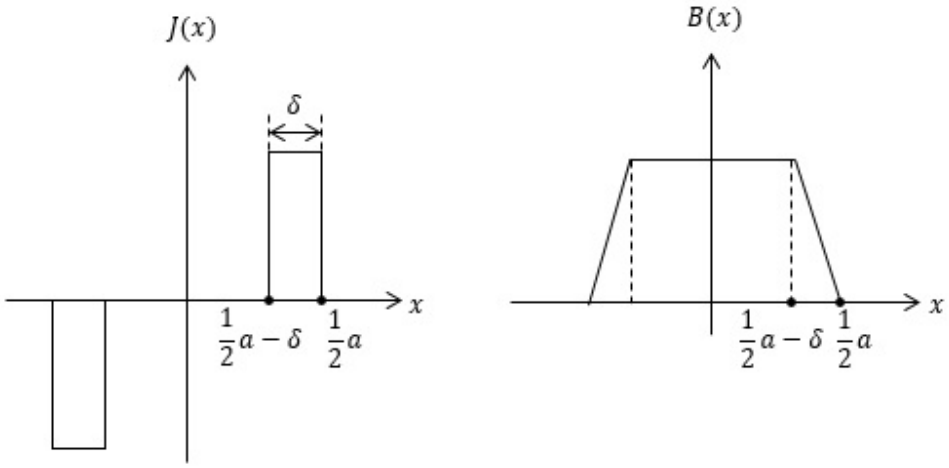

Figure 4.17: Eddy current distribution in one dimension, magnetic flux distribution in one dimension in the ring core

The eddy current density distribution and magnetic flux density distribution is shown in Fig. 4.17. It is 1-dimensional occasion. In x-axis of the cross section, from the negative terminal, the total eddy current flows in the negative direction and increases from x=-a/2 to x=δ-a/2. Therefore the flux density distribution increases linearly at the same range. Then the flux density becomes constant until x=a/2-δ, going down to zero at x=a/2. From this, we know that the flux through every current tube is different.

Next, we will find the effective flux through the core. Further, we discuss the analytical derivation of the expressions for the impedance. In fact, for the impedance of the primary and secondary winding, it has been derived previously, and the optimization steps will not discuss it. However, in the optimization steps, the eddy current distribution will be analyzed and discussed. Therefore, for every step, the impedance of the eddy current winding will be calculated for every time.

In Fig. 4.17, one can find the function between $J(x)$ and I:

$$I = l_r \int_{\frac{a}{2}-\delta}^{\frac{a}{2}} J(x)dx = J\delta l_r \tag{4.46}$$

l_r is the effective magnetic flux path, J is the eddy current density.

First, the inductance of the eddy current winding is to be found. The effective flux enclosed by the eddy current winding and inductance of the winding can be described as:

$$\phi_e = \Lambda \cdot n_3 I \tag{4.47}$$

$$L_{33} = \Lambda \cdot n_3^2 \tag{4.48}$$

The cross section of the core is divided into 5 zones, see Fig. 4.18. In zone 2, 3, 4, and 5, there is eddy current flowing in it. Since the plane is symmetrical, we consider the zone 1, zone 2 and zone 3.

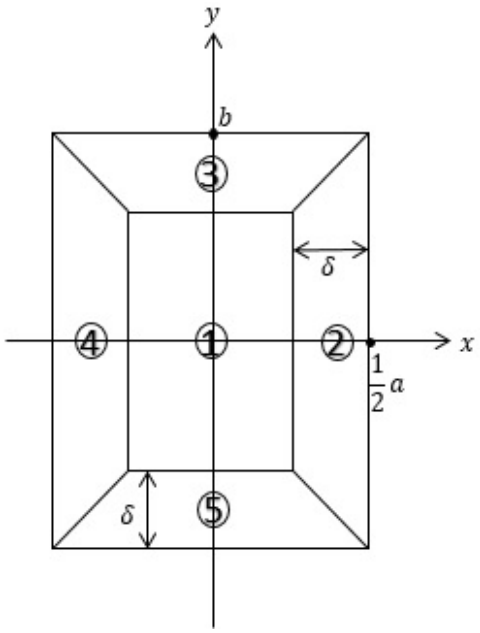

Figure 4.18: 5 zones in the cross section of the core

In every zone, the magnetic flux density is described as:

$$zone1 : B = \frac{\mu I}{l_r} \tag{4.49}$$

$$zone2 : B(x) = \frac{\frac{1}{2} - x}{\delta} \frac{\mu I}{l_r} \tag{4.50}$$

$$zone3 : B(y) = \frac{\frac{1}{2} - y}{\delta} \frac{\mu I}{l_r} \tag{4.51}$$

l_r is the effective magnetic flux path.

For simplicity we only discuss the flux density in x-axis, since the quantities for the tube can also be described by x.

According to previous analysis, the eddy current zone is formed by N current tubes. For every tube the thickness is dx,

$$\frac{\delta}{N} = dx \tag{4.52}$$

For example one picks up a current tube in x-axis. It is the i-th current tube in N number tubes. Also the flux seen by this tube is $\Delta\phi_i$. The thickness of the current tube is dx. See the Fig. 4.19

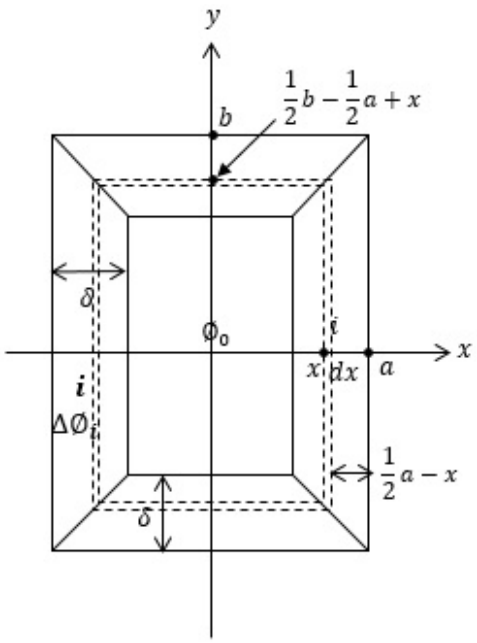

Figure 4.19: The i-th current tubes definition and specific data of it

The specific dimensions of the current tube i is defined as Fig. 4.19. The tube i is where the dashed lines enclosed. The flux seen by it would be $\Delta\phi_i$. Thus the total flux generated by eddy current I and enclosed by all the current tubes is as the following equation:

$$\phi_t = N\phi_0 + (N-1)\Delta\phi_1 + (N-2)\Delta\phi_2 + ... + (N-i+1)\Delta\phi_i + ... + 1\cdot\Delta\phi_N \tag{4.53}$$

ϕ_0 is the magnetic flux enclosed by the most inner current tube. The number of of tubes is N. Each tube will enclose the flux through this area. Thus the total flux through zone 1 is $N\phi_0$.

However, in our case to get the self-permeance of the virtual winding, the effective flux should be used. There are N number of tubes, and the total flux enclosed by them is ϕ_t. Therefore, if we merge the N tubes to only 1 tube, then the effective flux through this winding would be:

$$\phi_e = \frac{\phi_t}{N} \tag{4.54}$$

$$\phi_e = \phi_0 + \frac{N-1}{N}\Delta\phi_1 + \frac{N-2}{N}\Delta\phi_2 + ... + \frac{N-i+1}{N}\Delta\phi_i + ... + \frac{1}{N}\Delta\phi_N \tag{4.55}$$

Next, we make a description of the i-th current tube. By doing the integral of the $\Delta\phi_i$, we can find the total flux ϕ_t.

- Self-inductance L_{33} calculation For the length of current tube i,

$$c(x) = 2(2x + b - a + 2x) = 8x + 2(b-a) \tag{4.56}$$

For $\Delta\phi_i$,

$$\Delta\phi_i = d\phi_i = B(x)\cdot dA \tag{4.57}$$

$$dA = c(x)dx \tag{4.58}$$

Different current tubes weight differently in the zone. In Fig. 4.17, we can see that from tube 1 to tube N, the flux density decreases. Therefore, for the weight factor of tube i, it would be:

$$w_f = \frac{N-i}{N} = \frac{\frac{a}{2}-x}{\delta} \tag{4.59}$$

Since the eddy current density is equally distributed in the eddy current winding, for the total current from current tube i to x=a/2, it would be:

$$I_i = l_r \int_x^{\frac{a}{2}} J(x)dx \tag{4.60}$$

Thus, the weight factor can also be written as:

$$w_f = \frac{l_r \int_x^{\frac{a}{2}} J(x)dx}{I} \tag{4.61}$$

Then we can go to the calculation for the self-inductance of the eddy current winding. For the flux in zone 1:

$$\phi_0 = \frac{\mu I}{l}(b-2\delta)(a-2\delta) \tag{4.62}$$

For the flux in current tube i:

$$\Delta\phi_i = \frac{2\mu I}{\delta l_r}(\frac{a}{2}-x)(2x+b-a+2x)dx \tag{4.63}$$

Considering the contribution of $\Delta\phi_i$,

$$\frac{\frac{a}{2}-x}{\delta}\Delta\phi_i = \frac{2\mu I}{\delta^2 l_r}(\frac{a}{2}-x)(2x+b-a+2x)^2(4x+b-a)dx \tag{4.64}$$

Then the effective flux through all current tubes or the eddy current winding is:

$$\phi_e = \phi_0 + \int_{\frac{a}{2}-\delta}^{\frac{a}{2}} \frac{\frac{a}{2}-x}{\delta}\Delta\phi_i \tag{4.65}$$

$$\phi_e = \phi_0 + \frac{2\mu I}{\delta^2 l_r}(\frac{a}{2}-x)(2x+b-a+2x)^2(4x+b-a)dx \tag{4.66}$$

For the eddy current winding, the number of turns is 1. The effective flux can also be describe by ampere turns,

$$\phi_e = \Lambda_{33} n_{33} I \tag{4.67}$$

$$L_{33} = n_{33}^2 \Lambda_{33} \tag{4.68}$$

$$n_{33} = 1 \tag{4.69}$$

Finally the self-inductance for virtual eddy current winding under this optimization is derived:

$$L_{33} = \frac{\mu}{l_r}(2\delta^2 - \frac{4}{3}a\delta - \frac{4}{3}b\delta + ab) \tag{4.70}$$

- Mutual-inductance L_{13} calculation:

  Next, the mutual inductance L_{13} between winding 1 and winding 3, and the mutual inductance L_{23} between winding 2 and winding 3 are going to be discussed. L_{13} and L_{23} represent the magnetic flux generated by eddy current winding 3 seen by winding 1 and winding 2 respectively. Therefore in this case, $L_{13} = L_{23}$. Also, $L_{13} = L_{31}$. For simplicity, only L_{13} will now be calculated since the other two parameters would be the same.

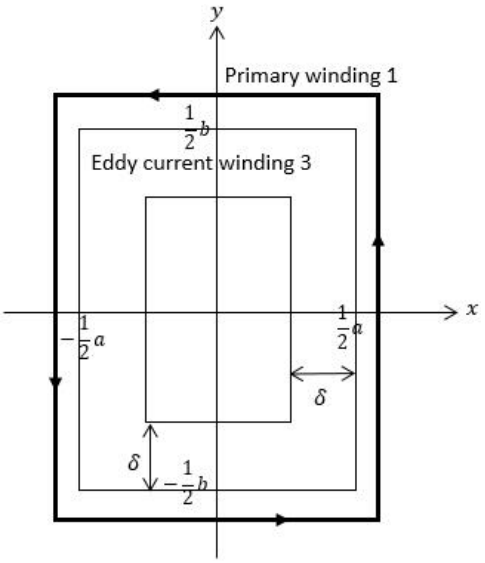

Figure 4.20: Sketch to describe the situation that flux generated by winding 3 and enclosed by winding 1

In this situation, the magnetic flux density distribution enclosed by winding 1 is the same as Fig. 4.17. Since the winding 1 is only a winding which can not be regarded as number of current tubes, the total flux enclosed by winding 1 is integral with $B(x)$ in x-axis. So the weight factor will not be considered. According to the right picture of Fig. 4.17, the function $B(x)$ varies with x is defined.

$$B(x) = \begin{cases} \dfrac{\mu I}{l_r}, x \in (-\dfrac{a}{2} + \delta, \dfrac{a}{2} - \delta) \\ \dfrac{\mu I}{\delta l_r}(\dfrac{a}{2} - x), x \in (\dfrac{a}{2} - \delta, \dfrac{a}{2}) \\ \dfrac{\mu I}{\delta l_r}(\dfrac{a}{2} + x), x \in (-\dfrac{a}{2}, -\dfrac{a}{2} + \delta) \end{cases} \tag{4.71}$$

The calculation method is the same with the calculation process of L_{33}, the derivation of dA, $\Delta\phi_i$, and ϕ_0 are the same. But for the effective magnetic flux through winding 1, it would be:

$$\phi_{effective} = \phi_0 + \int_{\frac{a}{2}-\delta}^{\frac{a}{2}} \Delta\phi_i \tag{4.72}$$

The difference is that the weight factor is not considered anymore. Finally, the relationship between the effective flux and the mutual-inductance becomes:

$$\phi_{effective} = \Lambda_{13} n_{33} I \tag{4.73}$$

$$L_{13} = n_{33}^2 \Lambda_{13} \tag{4.74}$$

$$n_{33} = 1 \tag{4.75}$$

And the L_{13} can be solved,

$$L_{13} = \frac{\mu}{l_r}(\frac{4}{3}\delta^2 - a\delta - b\delta + ab) \tag{4.76}$$

Finally, we derived the self-inductance of the eddy current winding, and the mutual inductance between the eddy current winding and the other two coils. After that, the resistance of the eddy current winding will be discussed.

Next we discuss the calculation for resistance of the eddy current winding R_3. First, we assume that N turns of the current tubes connect in series together.

- Resistance of one current tube inside dx.

  Before, we defined that the number of current tubes in dx is 1. But here we introduce a new concept n(x). n(x) is the number of current tubes in dx. This concept does not influence the calculation result. Then the number of current tubes in the dx is:

  $$n_{ct} = l_r n(x) dx \tag{4.77}$$

  The length of each current tube is:

  $$c(x) = 4x + 4\frac{b}{a}x = 4x(1 + b/a) \tag{4.78}$$

  In the current piece dx, the width of every current tube is:

  $$w_{ct}(x) = \frac{dx}{n_{ct}} = \frac{1}{n(x) l_r} \tag{4.79}$$

  Then the current flow cross section for one current tube is:

  $$A_{ct}(x) = w_{ct} \cdot l_r = \frac{1}{n(x)} \tag{4.80}$$

  Therefore the resistance of every current tube can be derived:

  $$R_{ct}(x) = 4\sigma^{-1} n(x)(1 + b/a)x \tag{4.81}$$

- Total resistance of all current tubes in series.

  For every piece dx, the resistance contribution in it is:

  $$dR = n(x) l_r dx \cdot R_{ct}(x) \tag{4.82}$$

  Then for the total resistance in series of the eddy current:

  $$dR = 4\sigma^{-1} n(x)^2 l_r (1 + b/a)x \cdot dx \tag{4.83}$$

  $$R_N = \int_0^{\frac{a}{2}} 4\sigma^{-1} l_r (1 + b/a) n(x)^2 x dx \tag{4.84}$$

  $$R_N = 4\sigma^{-1} l_r (1 + b/a) \int_0^{\frac{a}{2}} n(x)^2 x dx \tag{4.85}$$

- For one turn eddy current winding 3:

  In fact, the number of turns of the eddy current winding 1. Therefore, we need to find the effective resistance for one turn of the eddy current winding. In Fig. 4.21, the coil is N turns, the current input is i and voltage cross is u. If this N-turn coil melt together, the current input changes to Ni, voltage becomes $\frac{1}{N}u$. Therefore, for the N-turn coil:

$$\frac{u}{i} = R \tag{4.86}$$

  For one turn,

$$\frac{\frac{1}{N}u}{Ni} = \frac{1}{N^2}R \tag{4.87}$$

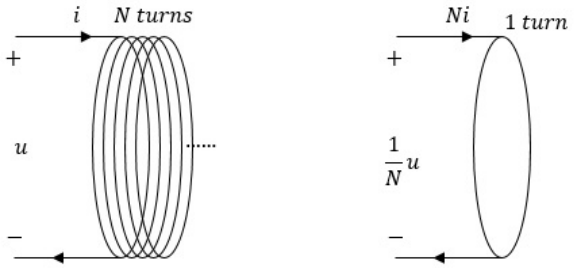

Figure 4.21: sketch to show resistances of N turns coil and one turn coil

  Thus, for one turn, the R_N will become R_1:

$$R_1 = 4\sigma^{-1} l_r (1 + b/a) \int_0^{\frac{a}{2}} (\frac{n(x)}{N})^2 x dx \tag{4.88}$$

  Then we need to find the relationship between $n(x)$ and N. We already know that the current density is $J(x)$, if one assume that the current in every current tube is ∂I, then the current flows in dx is:

$$n(x) \cdot l_r dx \partial I = J(x) \cdot l_r dx \tag{4.89}$$

$$J = n(x)\partial I \tag{4.90}$$

  For ∂I, it is:

$$\partial I = \frac{I}{N} \tag{4.91}$$

  Then the relation between $n(x)$ and N is found:

$$\frac{n}{N} = \frac{J}{I} \tag{4.92}$$

  n is constant because J is constant.

  Finally the equation of R_1 is solved:

$$R_3 = (1 + \frac{b}{a}) \cdot \frac{a^2 l_r}{2\delta^2 \sigma} \tag{4.93}$$

Till now, the solutions for impedance of the eddy current winding have been derived. These parameters can be adapted into the simulation model and then compared with the measurement results. However, one can see that the L_{33}, L_{13} and R_3 are all functions of δ, and δ is a function of frequency. In this case, if one wants to apply the optimization 1 into the simulation model, firstly a proper thickness of the virtual winding should be fixed.

4.5.2. OPTIMIZATION STEP2

In optimization 1, the current tube theory is adapted and effective flux through the core as well as the eddy current is calculated. However, there still remains a problem. The eddy current distribution is not discussed yet. Previously, the eddy current is equally distributed in the edge of the core, which is not true. Because the eddy current distributes in the core everywhere. When the frequency is at low and middle values, the distribution is more or less linear. Therefore, in this section, the eddy current is assumed to have a linear distribution in the ring core.

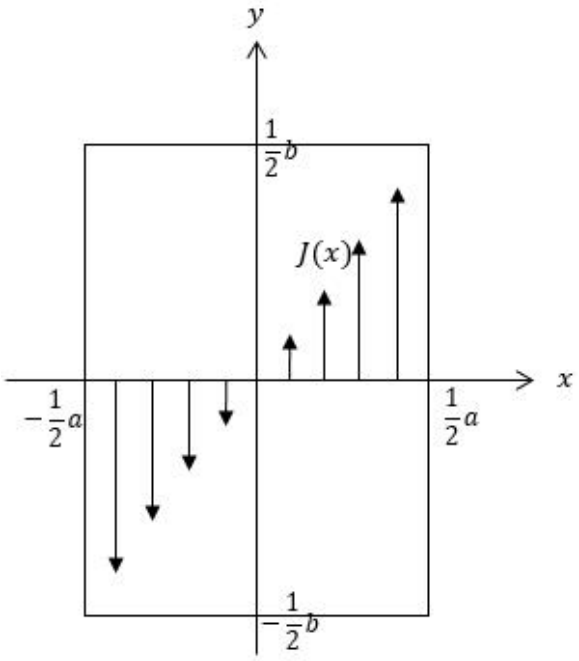

Figure 4.22: The assumption: eddy current distributes linearly in the core

Fig. 4.22 shows the eddy current is linear in x-axis. Since the cross section has two dimensions, it is the same case with the y-axis. For simplicity, the y-direction will not be discussed here. To work out the eddy current winding impedance, the same current tube theory is used as the previous part, that eddy current is formed by N number of current tubes connecting in series together. The expressions for the current density and the total eddy current would be:

$$J(x) = kx \tag{4.94}$$

$$I = l_r \cdot \int_0^{\frac{a}{2}} kx dx = \frac{1}{8} k a^2 l_r \tag{4.95}$$

From $x = -a/2$ to $x = a/2$, the current in x-aixs varies.

$$I(x) = \int_{-\frac{a}{2}}^{x} J(x) dx = \frac{1}{2} k x^2 - \frac{1}{8} k a^2 \tag{4.96}$$

Also the function of the magnetic flux density $B(x)$ and the diagram for it are to be found:

$$\mu J(x) = -\frac{dB(x)}{dx} \tag{4.97}$$

$$B(x) = B_0 - \mu \int_0^2 J(x) dx = B_0 - \frac{1}{2} k \mu x^2 \tag{4.98}$$

When $x = \frac{1}{2}a$, $B = 0$,

$$B_0 = \frac{1}{8}\mu k a^2 B(x) = \frac{1}{8}\mu k a^2 - \frac{1}{2}k\mu x^2 \tag{4.99}$$

It is clear that $B(x)$ has a parabola distribution in 1-dimensional case.

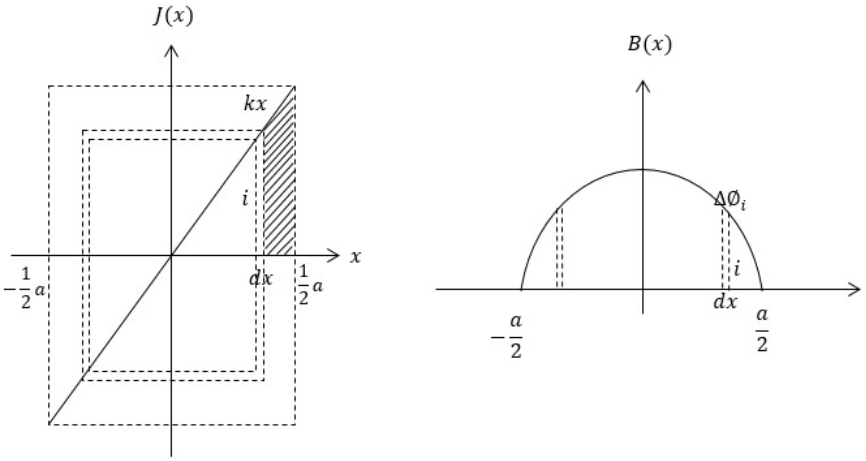

Figure 4.23: Eddy current distribution in one dimension, magnetic flux distribution in one dimension in ring core, when eddy current density is linear

In Fig. 4.23, the current tube with the number i is chosen, which is the same method and idea as optimization step1. Therefore in this part some detailed calculation and explanation is omitted. The contribution of each current tube is different. If the current density is linearly distributed, the weight factor of i-th current tube is the ratio between the current in the shadow area and the total current I. The flux in the center is very important, because it is enclosed by the majority of the current tubes. The current tubes in the center are less important, because they enclose less flux. Therefore, the closer to the center, the more contribution of the flux has.

$$w_f = \frac{1}{2}\frac{(\frac{1}{2}a - x)(kx + \frac{1}{2}ak)}{\frac{1}{8}ka^2} = \frac{1}{2}(\frac{1}{2}a - x)(kx + \frac{1}{2}ak) \tag{4.100}$$

The cross section area of each current tube is:

$$\Delta A = \frac{8b}{a}xdx \tag{4.101}$$

In dx, the magnetic flux through each current tube is:

$$\Delta\phi_i = B(x)\Delta A \tag{4.102}$$

The effective flux through the core can be derived from the integral to the contribution of each current tube:

$$\phi_e = \int_0^{\frac{a}{2}} \Delta\phi_i \cdot w_f \tag{4.103}$$

$$\phi_e = \int_0^{\frac{a}{2}} \frac{\mu bk}{2a}(ka^2 - 4kx^2)(\frac{1}{4}a^2 - x^2)xdx \tag{4.104}$$

To get the self-inductance of the virtual winding in the linear eddy current distribution,

$$\phi_e = \Lambda_{33} I \tag{4.105}$$

The permeance of winding 3 becomes:

$$\Lambda_{33} = \frac{\mu}{3l_r} ab \tag{4.106}$$

As for mutual inductance L_{13} and resistance R_3, they have the same calculation ideas as optimization 1. Here only the final results are shown.

Mutual inductance:

$$\Lambda_{13} = \frac{\mu}{2l_r} ab \tag{4.107}$$

$$\Lambda_{13} = \Lambda_{23} = \Lambda_{31} = \Lambda_{32} \tag{4.108}$$

$$R_3 = (1 + \frac{b}{a}) \cdot \frac{4}{\sigma l_r} \tag{4.109}$$

Until now, the calculation of the optimization 2 is finished. The impedance of the eddy current winding is derived through the calculation. The two problems of the Present Model have been solved in the optimization 2. However, the optimization 2 can be applied to the low and middle the frequency ranges. At high frequencies, the eddy current density is not linear anymore. Therefore, we want to extend to a higher frequency range.

4.6. OPTIMIZATION STEP3

In optimization 3, a further step is discussed for the eddy current density distribution at high frequencies. This step is to extend the optimization 2 to higher frequencies. From the Fig. 3.11 in Chapter 3, we already know that the current distribution would be polynomial at a high frequency. Optimization 3 will be based on the solutions of eddy current and magnetic flux density in Chapter 3. The plot curves and calculation will be conducted in Mathcad directly. In this step, the same analysis process and current tube theory as the optimization 1 and 2 are used. According to (3.62) in Chapter 3, the analytical solution for current density in the core in one dimension is derived:

$$J(x,\omega) = \frac{\mu n I}{l_r} \frac{1+j}{\delta} \frac{e^{(1+j)\frac{x}{\delta}} - e^{-(1+j)\frac{x}{\delta}}}{e^{(1+j)\frac{a}{2\delta}} + e^{-(1+j)\frac{a}{2\delta}}} \tag{4.110}$$

Now we define the eddy current flow in the surface of the core is I:

$$I = \int_0^{\frac{a}{2}} J(x,\omega) dx \tag{4.111}$$

No matter in the present model, or optimization 1 or 2 model, the magnetic flux density $B(x)$ is built based on the current source is eddy current. Thus here use the same situation.

$$B(x) = \mu_0 \int_x^{\frac{a}{2}} J(x,\omega) dx \tag{4.112}$$

For a piece dx, there is a current tube and the flux density in this tube would be:

$$dA(x) = \frac{8b}{a} x dx \tag{4.113}$$

$$d\phi(x) = \frac{8b}{a} \mu_0 \int_x^{\frac{a}{2}} J(x,\omega) dx \tag{4.114}$$

Similarly, the contribution of each current tube, which is weight factor is defined:

$$w_f = \int_0^x \frac{I - \int_0^x J(x,\omega)dx}{I} \tag{4.115}$$

Therefore the effective magnetic flux in the core is:

$$\phi_e(x) = \int_0^{\frac{a}{2}} d\phi_x \cdot \frac{I - \int_0^x J(x,\omega)dx}{I} \tag{4.116}$$

Since the eddy current winding is one turn, $n_3 = 1$.

$$L_{33} = \frac{|\phi_e|}{I} \tag{4.117}$$

The mutual inductance and resistance would be:

$$L_{13} = \int_0^{\frac{a}{2}} \frac{\mu 8b}{al_r} x \frac{I - \int_0^x J(x,\omega)dx}{I} \tag{4.118}$$

$$R_3 = 4\sigma^{-1} l_r (1 + \frac{b}{a}) \cdot \int_0^{\frac{a}{2}} (\frac{J(x,\omega)}{Il_r})^2 x dx \tag{4.119}$$

The eddy current winding resistance, the self-inductance and the mutual inductance have been derived. These parameters will also be adapted into the simulation model, and then the simulation result would be compared to the other optimization steps.

In above solutions, the eddy current density is a function of x and frequency. It is still a function of frequency after doing integral to dx. Therefore, the solutions for L_{33}, L_{13} and R_3 are all function of frequency. If one wants to apply the optimization 3 into the simulation model, then a frequency should be chosen. Since the purpose of the optimization 3 is to extend the frequency to higher values, we expect that the simulation results can behave well at high frequencies.

4.7. SIMULATION RESULTS

In this section, the simulation results of transfer impedance from Present Model, opt1, opt2 and opt3 will be compared with the measured results.

According to the bottom legend of Fig. 4.24, the dashed lines are the measured impedance results, the green one is L_s and the red one is R_s. The $presentL_s$ and $presentR_s$ are the simulation results from the Present Model. The other two group lines $opt1$ and $opt2$ are the simulation results of opt1 and opt2. Therefore, to apply opt1, an arbitrary choice for the δ should be fixed. Because in opt1, the eddy current is equally distributed in the edge of the core, which is a very high frequency case. So if the frequency is 100kHz, then the skin depth δ is around 0.4mm. We expect that the simulation results will behave well at high frequency values. If we see the results in Fig. 4.24, the inductance of opt1 corresponds to the measured inductance; the resistance of opt1 corresponds to the measured resistance from low frequencies to high frequencies. The opt2 is based on the assumption that the eddy current has a linear distribution. Therefore, we expect that the simulation results of the opt2 can behave well at low frequencies and middle frequencies. In Fig. 4.24, we see that at low frequencies, the simulation results are quite same with the measurement results. However, the inductance of opt2 begins to split at around 1000Hz, which is not what we expected. It means that the eddy current effect in the simulation model occurs later than in the measurement. But the resistance of opt2 corresponds with the measured result at both low and middle frequencies. It can be seen that compared with the Present Model, the opt1 and opt2 have already been improved and become closer to the measurement results.

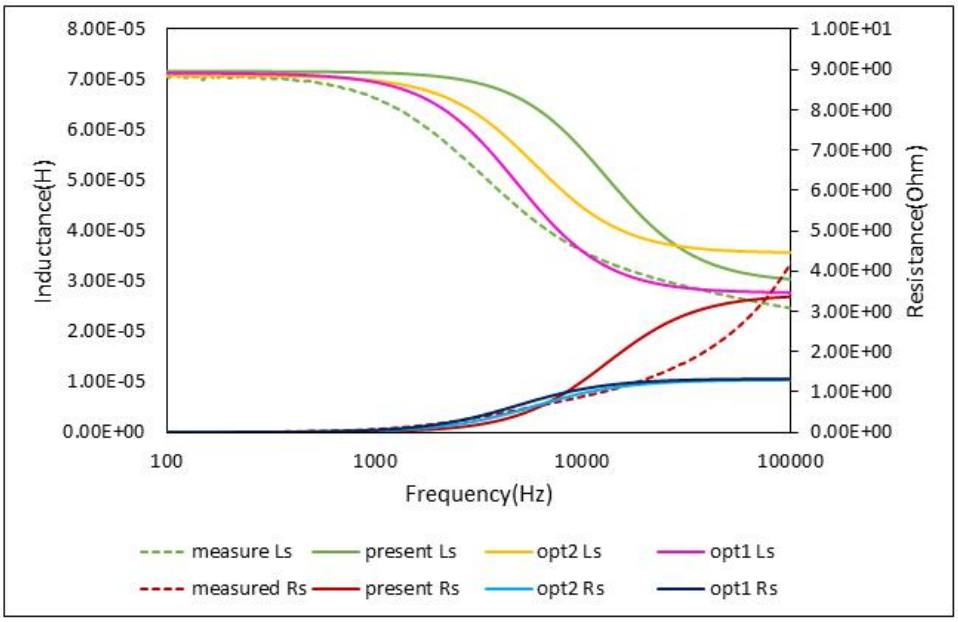

Figure 4.24: Transfer impedance simulation results of optimization1 and 2, compare with measurement and the Present Model

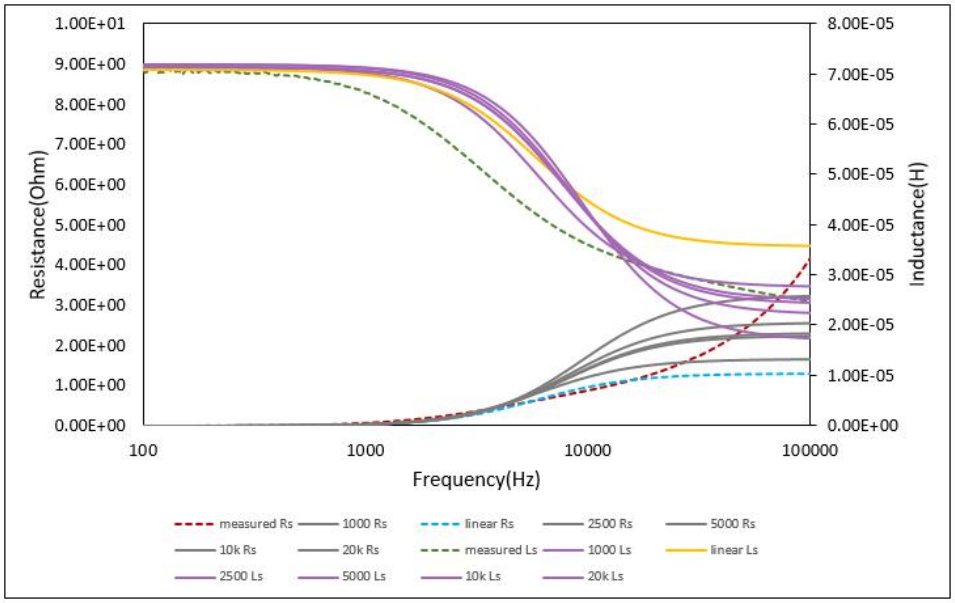

Figure 4.25: Transfer impedance simulation results of optimization2 and 3, compare with measurement

Fig. 4.25 shows the simulation results of opt3, compared with the opt2 and the measured results. As concluded in opt3, the solutions are all functions of frequency. Therefore, the arbitrary choices of frequency should be fixed first: 1KHz, , 2.5kHz, 5kHz, 10kHz, 20kHz, from middle frequency values to high frequency values.

In Fig. 4.25, one can see the legend to check the representatives of these lines. Actually, the expectation of opt3 is that with a certain arbitrary choice of the frequency, the simulation results can correspond to the measured results at high frequency levels. However, in Fig. 4.24, the opt2 did not reach to the expectation in middle frequencies. Therefore one can expect that in opt3, the simulation results will not reach to the expectation either. It can be seen that from low frequencies to middle frequencies, the inductances and resistances of opt3 are corresponding to each other. At high frequencies, they split, because the permeances of the magnetic flux are different. Higher the frequency, lower the magnetic flux permeance of the real winding. Thus, the L_{12} will be lower with higher frequencies. These phenomenon can be seen in the figure. However, since the simulation result of opt2 is not applicable for lower frequencies, the simulation result of opt3 will not be meaningful.

4.8. SUMMARY

- The transformer ring equivalent circuit is a 3-winding transformer circuit, with the primary winding, the secondary winding, and the eddy current winding. Through the magnetic circuit analysis and using the Faraday's law in the circuit, the inductance matrix and the resistances of the three coils are derived.

- The eddy current effect can be regarded as L-R ladders in the circuit. The more R/L sections are considered, the more accurate of the eddy current model. After the verification, one R/L section is good enough to represent the eddy current effect.

- For the eddy current winding's impedance, there is a first assumption that the eddy current is distributed equally at the edge of the core, just like a short circuit winding. This is the Present Model. In the Present Model, there are two problems: the effective flux through the core is not found; the eddy current distribution is not true.

- As for the impedance of the primary winding and the secondary winding, the calculated results are compared with the measurement results. With the comparison, one can conclude that the calculation of the impedance of the real coils are good.

- The transfer impedance of the circuit is measured. By comparing the transfer impedance between the measurement and the simulations, the simulation model can be verified. There is a big deviation between the simulation result of Present Model and the measured result, therefore, three optimization steps are proposed to improve the eddy current model.

- The optimization 1 finds the relationship between the effective flux and the eddy current density. A current-tube approach is used for it. The optimization 2 not only finds the effective flux, but also finds a more correct eddy current density distribution. It is that the current density has a linear distribution. We expect that the simulation of the optimization 2 can correspond to the measurement at low and middle frequencies. However, in the simulation results of optimization 2, the eddy current effect shifts compared to the measurement results. This leads to a difference between them at middle frequencies. The reason for that is not understood yet. The purpose of optimization 3 is that if the optimization 2 works well, then the optimization 3 can extend the frequency

range to high values. But the fact is that the optimization 2 does not works at middle frequencies, then the optimization 3 will not be meaningful.

5

TEST OF THE EDDY CURRENT MODEL IN SPINDLE MATERIAL RING

In this Chapter, the metal core of the transformer ring is replaced by the magnetic material that applied in the toothbrush actuator's spindle. This transformer ring is called spindle ring. According to the Fig. 1.3, firstly, the eddy current model is studied in the brass ring. If the eddy current model is applicable for the brass ring, then it will be tested in the spindle ring. In Chapter 4, the eddy current model has been improved, although there is still a difference that can not be explained. In this Chapter, the eddy current model is to be tested in the spindle ring. However, in the spindle ring, except for the eddy current effect, there is also a nonlinear effect. If the researcher wants to study the eddy current model separately, the BH-curve is to be measured. After that, the parameters related to the nonlinear effect are applied to the transformer ring circuit.

In this Chapter, first, the BH-curve of the spindle material is measured; second, the non-linear effect model in the transformer ring circuit is introduced; third, the impedance of the coils in the spindle ring is calculated; finally, the simulation results will be shown.

5.1. THE NON-LINEAR EFFECT

5.1.1. BH CURVE MEASUREMENT OF THE SPINDLE RING

The purpose of measuring the BH curve of the spindle ring is to know the nonlinear property of this material. Further, one can derive the coefficients about the nonlinear property, and apply then to the nonlinear model. This is to get rid of the effects of the saturation and hysteresis effects.

The magnetic hysteresis loop shows the behaviour of a ferromagnetic core graphically as the relationship between B and H is non-linear [18]. The principle of BH curve measurement is based on Faraday's law.

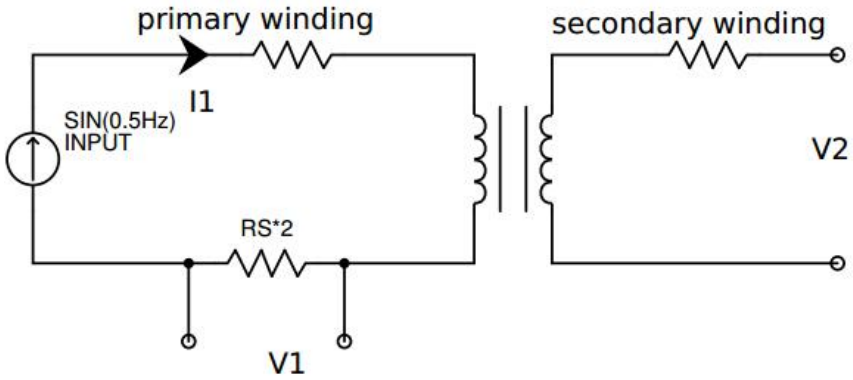

Figure 5.1: BH curve measurement circuit sketch

Fig. 5.1 shows the BH curve measurement circuit for the spindle ring. A current source with 0.5Hz sinusoidal signal is input. By changing the different amplitudes the different BH curves are measured. 0.5Hz is a low frequency value that can make sure that a clear BH curve can be derived. There is an internal resistor Rs and an amplifier with the factor of 2 in the circuit. V1 and V2 are the measured quantities.

The primary and secondary coils of the ring have the same number of turns N=500. These two coils are tightly close to each other; the fluxes going through two coils are the same. I_1 is the input primary current. In the measurement setup, the input magnetic field generated by the primary winding is H(t):

$$I_1(t) = \frac{V_1(t)}{2Rs} \tag{5.1}$$

$$H(t) = \frac{NI_1(t)}{l_r} \tag{5.2}$$

According to the Faraday's Law, the induced secondary voltage is:

$$V(t) = N\frac{d\phi}{dt} \tag{5.3}$$

If the cross section area of ring is A, the flux density can be calculated as:

$$B(t) = \frac{1}{NA}\int V dt \tag{5.4}$$

Based on the calculation, the BH curve can be plot. The spindle material has saturation effect, when the magnetic field reaches to a big value, the magnetic flux can become saturation. But at a low field, only hysteresis effect is in, saturation will not occur. Therefore, by picking up several levels of input current amplitudes, one can get different BH curves. The amplitudes of input current are arbitrary choices: 0.5A, 1A, 2A, 6A.

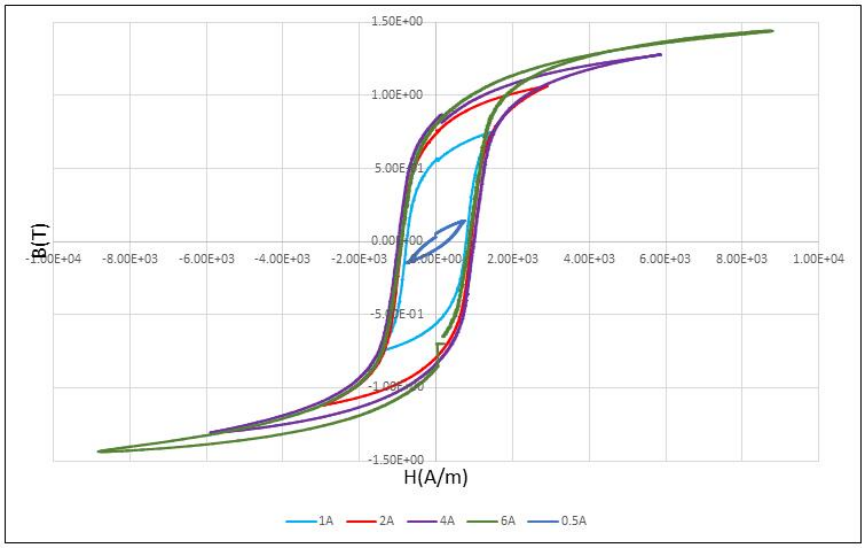

Figure 5.2: BH curve measurement results at different input current amplitudes

Fig. 5.2 shows BH curve measurement results at 0.5A, 1A, 2A, 6A current levels. Generally, the BH curve follows the path as the AC flowing through the primary winding. When the amplitude of the primary current is 0.5A, the magnetizing current is so small that the maximum external field is small. The magnetization in the core is not completely switched on. One can imagine that with lower and lower input current, the nonlinear effect can be neglected. When the primary current level increases from 1A to 6A, the saturation effect becomes more and more obvious. The saturation point of flux density is lower than 1.5T, which shows this spindle material is not a good ferromagnetic material. As the vector H goes back to zero, the flux density is at Br(positive residual point), which is around 0.6T-0.7T. At a certain magnetic flux density the field becomes zero, B(-Hc)=0. Hc is called coercive field intensity or coercive force, and in the figure Hc is around 920 A/m.

5.1.2. THE NON-LINEAR MODEL

After the BH curve measurement, we need to apply the BH curve to the transformer ring circuit. The connection between the measurement and the application is nonlinear simulation model. How to find the coefficients of the non-linearity will be introduced in the next section. In this section, the nonlinear model in the transformer ring circuit as well as in the actuator is introduced. The nonlinear model is already built by Philips, but we need to study it. Because we want to know the drawbacks of the model, and to know the parameters needed for the model.

Now, an arbitrary transformer with a piece of nonlinear part is described. In Fig. 5.3, the piece of material with the nonlinear behavior can be represented by a circuit component. This piece can receive a flux ϕ_c from winding 1 and winding 2 of the transformer. The magneto motive force of winding 1 is $\mathscr{F}_1$, and of winding 2 is $\mathscr{F}_2$.

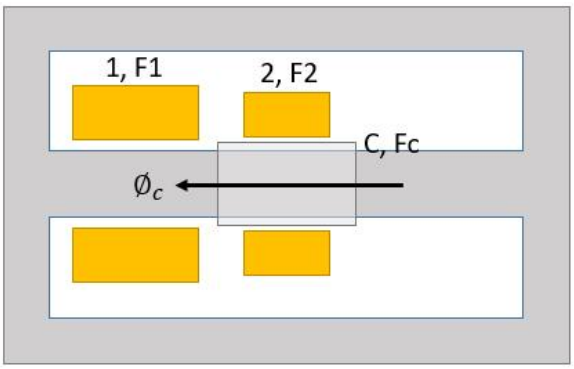

Figure 5.3: Explanation for extra winding C in a two winding system

The nonlinear part is represented by an additional winding $\mathscr{F}_c$ in the model [19]. In a finite element model, this winding is defined, together with a constant magnetic reluctance Rm_c. This is the reluctance that the spindle piece would have for a certain predefined constant permeability. A finite element model is then based on a magnetic system with an additional winding $\mathscr{F}_c$ around the spindle piece with constant magnetic properties. The calculation, which is therefore done on a linear system, determines all permeances and mutual permeances. These permeances are transferred into the transformer circuit model. It is now possible to make the source dependent on the flux ϕ_c. In such a way, the nonlinear behavior of the metal piece becomes applicable. If the B-field and H-field of this piece is determined by the Fig. 5.4, we can write the equations:

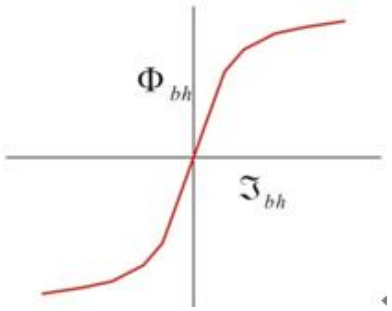

Figure 5.4: Relationship between flux and ampere turn in the system

$$\mathscr{F}_{bh} = -\mathscr{F}_c + Rm_c \cdot \phi_c \tag{5.5}$$

$$\phi_{bh} = \phi_c \tag{5.6}$$

The source of the extra winding C will be:

$$\mathscr{F}_c = (Rm_c - \frac{\mathscr{F}_{bh}}{\phi_{bh}}) \cdot \phi_c \tag{5.7}$$

In the spindle transformer ring, Rm_c represents the reluctance of the ring. The ring has length of l_r and cross section of A, the above equation can be also written as:

$$\mathscr{F}_c = (\frac{1}{\mu_c} - \frac{H_{bh}}{B_{bh}}) \cdot \frac{l_r}{A} \cdot \phi_c \tag{5.8}$$

While the term $\frac{B_{bh}}{H_{bh}}$ represents the BH-curve of the material. In this term, B-field is the function of H-field. In the (5.8), however, the H-field as a function of the B-field is required. Therefore, we need to find the H field when the B-field is an input. To achieve this, we can use a feedback loop with a very high open loop gain. The idea is:

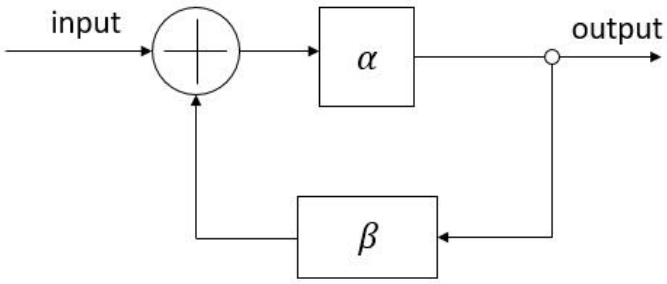

Figure 5.5: The feedback loop idea

Fig. 5.5 shows the feedback loop to transfer from B-H function to H-B function. In the loop, characteristic β represents the non-linear property.

$$V_{out} = \alpha(V_{in} - \beta V_{out}) \tag{5.9}$$

When α is very large,

$$\frac{V_{out}}{V_{in}} = \frac{\alpha}{1+\alpha\beta} \approx \frac{1}{\beta} \tag{5.10}$$

$$V_{in} = \beta V_{out} \tag{5.11}$$

Which is corresponding to the relation:

$$B = \mu H \tag{5.12}$$

This loop inverses the transfer β into $1/\beta$. By this the term $\frac{B_{bh}}{H_{bh}}$, which we make available, can be transferred into $\frac{H_{bh}}{B_{bh}}$, which is needed.

The block in Fig. 5.6 is the BH curve model in LTspice. In this model, B3 and H3 would be the measured BH curve quantities; Phi3 is the total flux through the extra representative winding; F3bh is the magneto motive force of the extra representative winding. Actually this block consists of several sub blocks. These sub blocks can realize the equations from (5.5) to (5.8), the function of the feedback loop, and the function of hysteresis and saturation effects. Therefore, a group of related parameters are needed for the BH curve block. To duplicate the measured BH curve in the model, except for the length of the ring l_r and the cross section A, a fitting curve equation is also to be found.

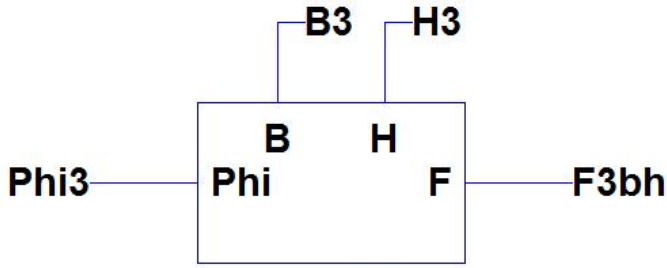

Figure 5.6: BH curve model representative block in LTspice

5.1.3. FIND THE FITTING CURVE

A mathematical method is used in the model to define the proper equation to describe the BH curve. In the LTspice model, there is an $arctan$ equation to describe BH curve:

$$V = v_0 \cdot atan(am_0 \cdot v(Hhyst)) + v_1 \cdot atan(am_1 \cdot v(Hhyst)) + v_2 \cdot atan(am_2 \cdot v(Hhyst)) + \mu_0 \cdot Hfield \tag{5.13}$$

If the BH curve is divided into 4 parts, and we assume that every part has the same hysteresis and saturation effect. One part in the first quadrant is picked up, and would be described by (5.14). Following that the whole loop can be plot. The (5.14) is combined by three $arctan$ equation components and a term $\mu_0 Hfield$. $Hhyst$ is the width of two times the coercive force H_c. $Hfield$ represents H-field in the BH curve. The unknown parameters are:

$$(v_0\ , v_1\ , v_2) \tag{5.14}$$

$$(am_0\ , am_1\ , am_2) \tag{5.15}$$

These parameters are going to be found from the measured BH curves by using the fitting curve equation. This can be achieved by using the fitting curve function app in Matlab. An example is introduced in detail about finding the parameters. If we pick up a measured BH curve from Fig. 5.2, and it is the curve at the primary current of 2A. See the red curve in Fig. 5.7.

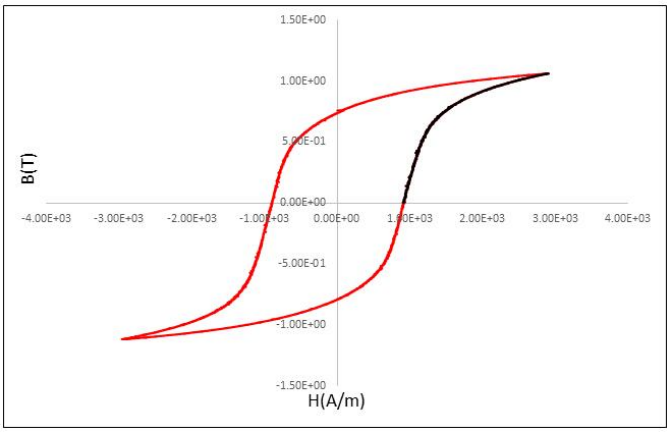

Figure 5.7: Measured BH curve under 2A amplitude level

In Fig. 5.7, the black part is chosen to represent the fitting curve, and the related data is imported to Matlab.

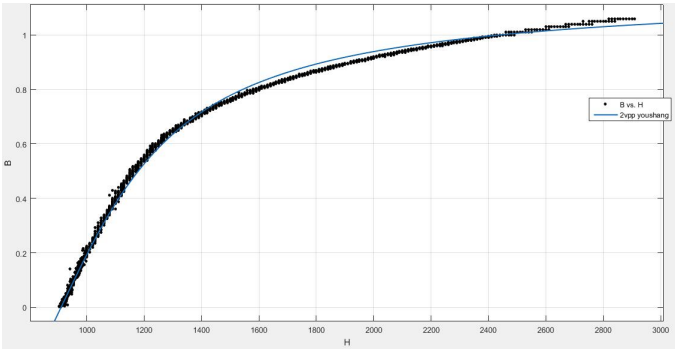

Figure 5.8: Fitting curve for BH loop

In Fig. 5.8, the black dot curve is the exported black part in the first quadrant from Fig. 5.7. According to these data, Matlab gives the fitting curve of it based on (5.14), which is the blue curve. In Matlab the fitting equation is written as:

$$f(x) = v_0 atan(am_0(x-911)) + v_1 atan(am_1(x-911)) + v_2 atan(am_2(x-911)) + \mu_0 x \tag{5.16}$$

In (5.16), $H_c = 911$, and x represents the H-field in the loop, which starts from $(H_c, 0)$. The parameters found are:

$$H_p = 2H_c = 1822 v_0 = 0.5534,\ v_1 = 0.1919,\ v_2 = 0 \tag{5.17}$$

$$am_0 = 0.002848,\ am_1 = 0.002848,\ am_2 = 0.3404 \tag{5.18}$$

These parameters are brought to LTspice model. The simulation result is shown in Fig. 5.9.

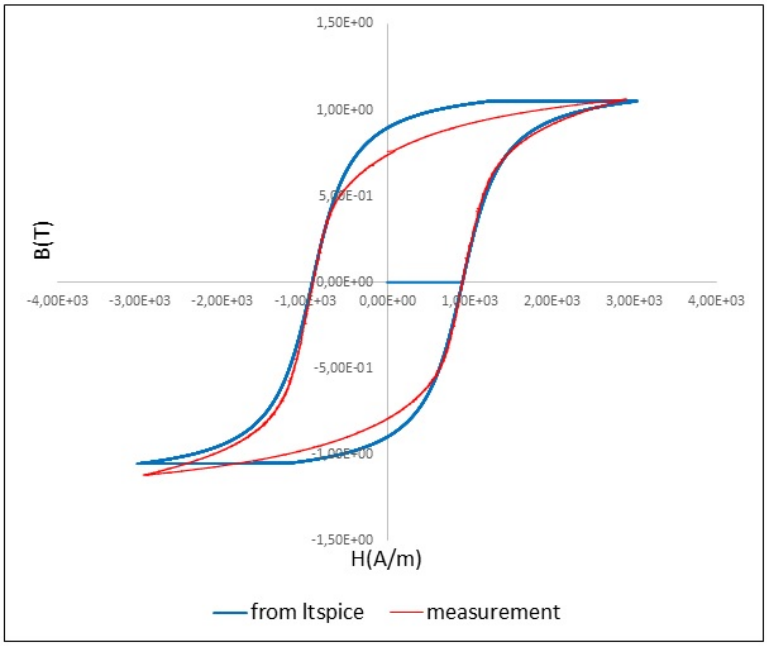

Figure 5.9: Simulation result for BH curve at 2A current input, compared with the measured result

In the Fig. 5.9, the red figure is the BH curve derived from measurement which is at 2A input current source; the blue figure is BH curve derived from simulation at same condition as measurement. It can be seen that two curves correspond to each other well though there still exists some deviation. For the measured loop the top is curve but for the simulation loop the top is flat. This is because the LTspice model itself has some problems and disadvantages that can not be solved till now. The BH curve simulation result is formed by shifting the fitting curve. It does not really find the real path of the BH curve. Therefore, it can be possible that when the BH curve becomes smaller, the deviation between measurement and simulation will become larger.

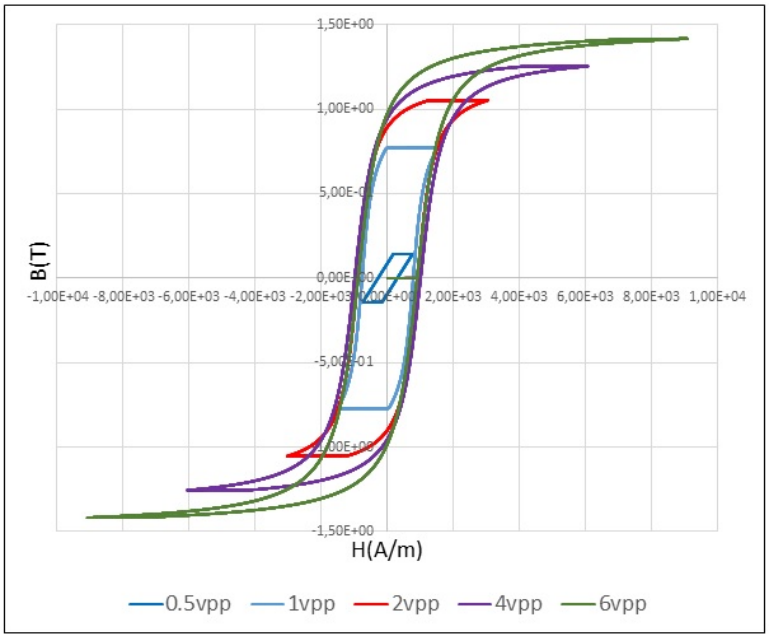

Figure 5.10: BH curve measurement results under different input current amplitudes

Fig .5.10 gives all the simulation results that correspond to Fig. 5.2. It can be concluded that the lower the input current level, the larger the deviation of the simulation model. When current level is 0.5A, the measured BH curve is like an oblique spindle shape while in the simulation result it is parallelogram. Also, the area of the simulation curve is larger than the measured one.

Generally speaking, this BH curve model can simulate the non-linear effect in the transformer ring, and at higher input H-field it behaves well. Therefore, these nonlinear coefficients will be brought into the simulation model to get rid of the nonlinear effect.

5.2. THE INPUT IMPEDANCE MEASUREMENT

The input impedance is measured in this chapter, and by comparing the measured results with simulation results, the simulation model would be verified. The measurement process is the same with the transfer impedance measurement in Chapter 4. Therefore, the details of the measurement will not be discussed in this Chapter, and only the results are shown.

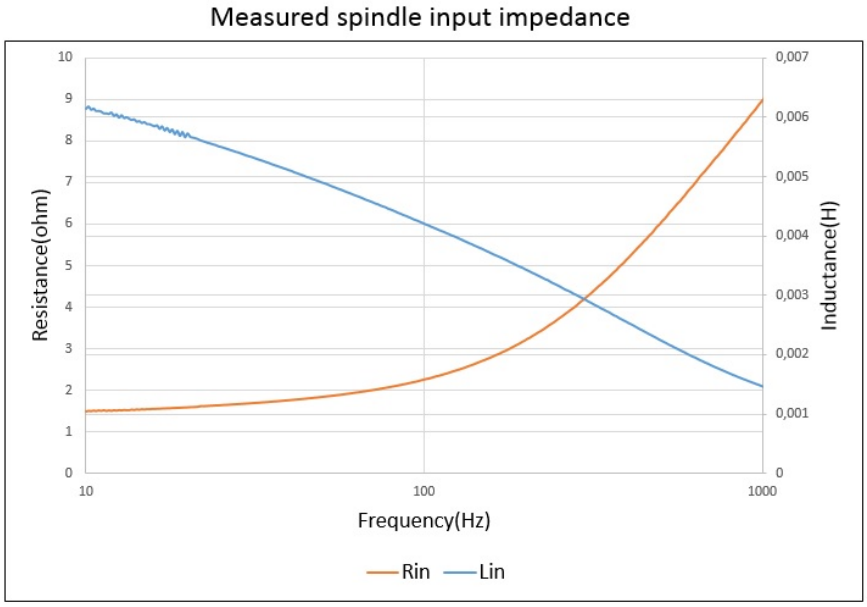

Figure 5.11: Spindle ring measured input impedance

Fig. 5.11 shows the measured input impedance of spindle ring at 1V input voltage. The blue curve is inductance component while the orange curve is the resistance component. The impedance varies with the frequency from 10Hz to 1000Hz. With frequency increases the eddy current effect increases in the circuit, this leads to the decrease of the inductance and increase of resistance. For the inductance, before 10Hz, we can imagine that there is a gentle line of it. Because at very small frequencies, the eddy current effect is not obvious yet.

At the same time, the BH curves at 10Hz, 100Hz, and 1000Hz are measured.

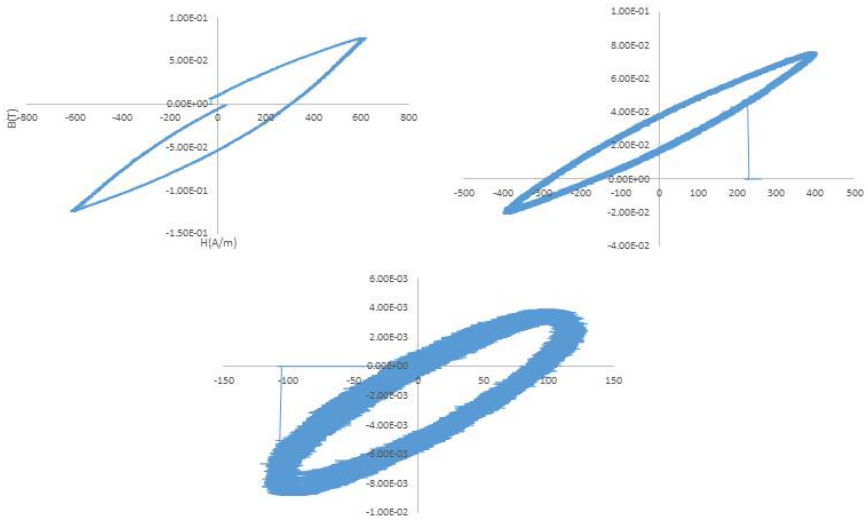

Figure 5.12: Measured BH curves under three frequency levels

Fig. 5.12 shows the BH curves measuring at the same time with input impedance measurement. These BH curves are minor loops. Three loops show three occasions at the frequencies of 10Hz, 100Hz, and 1000Hz. The μ_r calculated in each occasion is 130, 95 and 35. This figure shows that when the frequency sweeps in the circuit, the μ_r changes with the frequency. Also, the input voltage is not big enough to generate high current in the primary winding, so that

the flux in the core is far from saturation. Since the BH curve is very small, we can neglect the nonlinear effect in the spindle ring in the simulation. In this case, we should find a good representative value for μ_r in the model. The spindle ring circuit becomes a linear model.

5.3. PARAMETERS CALCULATION

In this Chapter, there are four coils in the transformer ring. The primary winding, the secondary winding, the eddy current winding, and the BH curve winding. But in the previous section, it is concluded that during the measurement of input impedance, the measured results are minor loops. In this case, the BH curve winding can be removed. Therefore, there are the primary winding, the secondary winding, and the eddy current winding in the circuit, as well as a constant permeability $ur = 125$. After that, we are going to determine the parameters of the three coils, including the inductance matrix and the resistances.

Currently it is a 3-winding transformer ring model, then the matrix for the transformer permeances would be:

$$\Lambda = \begin{bmatrix} \Lambda_{11} & \Lambda_{12} & \Lambda_{13} \\ \Lambda_{21} & \Lambda_{22} & \Lambda_{23} \\ \Lambda_{31} & \Lambda_{32} & \Lambda_{33} \end{bmatrix} \tag{5.19}$$

The resistances of the three coils are:

$$R = \begin{bmatrix} R_1 & R_2 & R_3 \end{bmatrix} \tag{5.20}$$

Except for the material of the metal core, the spindle ring is the same as the brass ring. They have the same geometries, the same number of turns, and the same thicknesses of the real coils. To derive the permeances, in the cross section of the ring, the area that every winding encloses is to be known. For the primary winding and the secondary winding, the areas are A_1 and A_2 respectively. A_1 and A_2 are the same as the brass ring in Chapter 4. Also, we define a A_c, and it is the cross section of the core.

$$\begin{aligned} A_1 &= 90.457 mm^2 \\ A_2 &= 75.33 mm^2 \\ A_3 &= 51.95 mm^2 \end{aligned} \tag{5.21}$$

Then Λ_{11} and Λ_{22} would be:

$$\Lambda_{11} = \frac{\mu_0(A_1 - A_3) + \mu_0\mu_r A_3}{l_r} \tag{5.22}$$

$$\Lambda_{22} = \frac{\mu_0(A_2 - A_3) + \mu_0\mu_r A_3}{l_r} \tag{5.23}$$

Next, we need to determine the eddy current distribution in the spindle ring. Based on that, we can calculate the impedance of the eddy current winding.

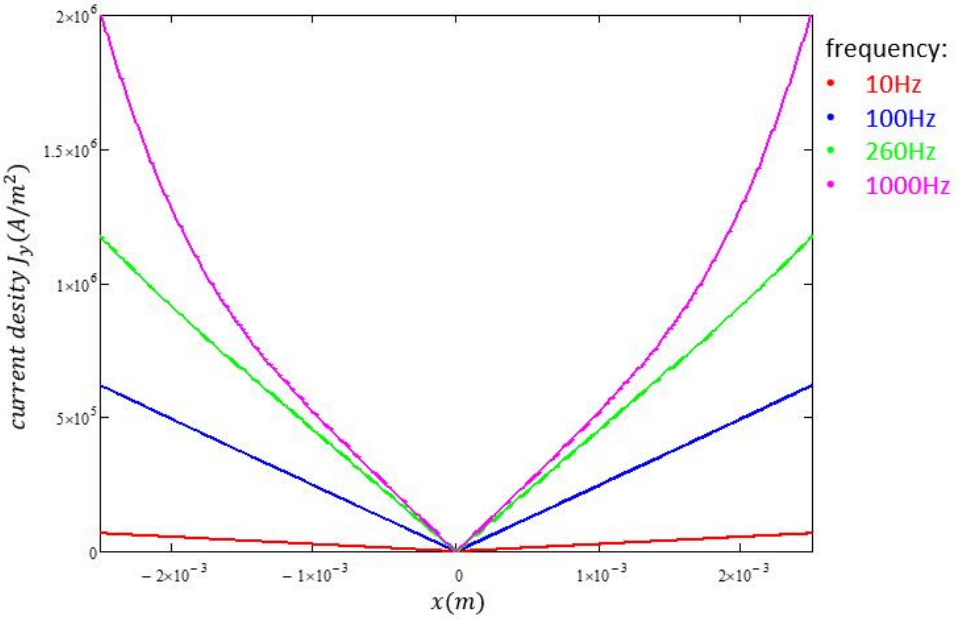

Figure 5.13: Eddy current density distribution in the cross section of the spindle core

Fig. 5.13 depicts the eddy current density distribution in the cross section of the spindle core. The eddy current density varies at four frequency values. 260Hz is the operation frequency of the toothbrush actuator. It can be seen that at 10Hz, 100Hz, and 260Hz, the eddy current has a linear distribution. Therefore, the optimization 2 will be applied to the spindle ring. Because in the optimization 2, the eddy current is linearly distributed, and the problem of the effective flux is considered. Also, the expressions for the eddy current impedance are not functions of frequency. The most important reason is that it derived an obvious improved result compared to the Present Model.

The permeances of the transformer are determined as the following:

$$\Lambda = \begin{bmatrix} 24.7 & 24.65 & 12.4 \\ 24.65 & 24.65 & 12.4 \\ 12.4 & 12.4 & 9 \end{bmatrix} \times 10^{-9} \tag{5.24}$$

The resistances of the transformer are determined as the following:

$$\begin{aligned} R_1 &= 1.32 \\ R_2 &= 5.87 \\ R_3 &= 20u \end{aligned} \tag{5.25}$$

These parameters are imported into the simulation model of the spindle ring. The simulation result of the input impedance of the ring can be derived.

5.4. SIMULATION RESULTS

Fig. 5.14 shows the input impedance of the spindle ring from the simulation model, and compared with the measurement result. The solid curves are simulated input impedance; the red one is the inductive part while the green one is the resistance. The dot curves are the measured input impedance.

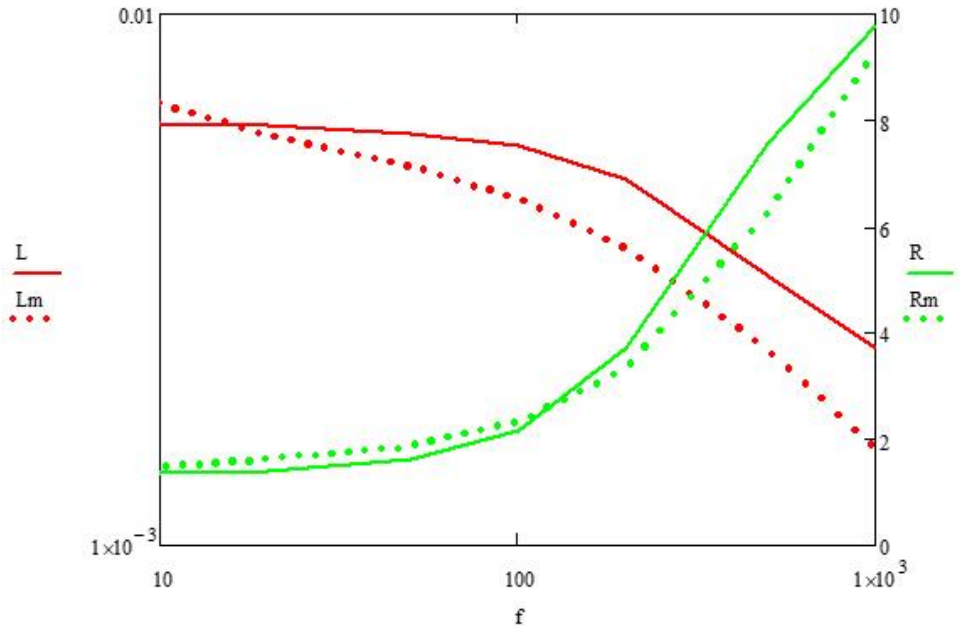

Figure 5.14: Simulation result for the input impedance of the spindle ring

From Fig. 5.14, it can be seen that the measured resistance corresponds to the simulation result. For the inductive part, the simulation result keeps smooth at 10Hz, and shows an obvious decrease at 100Hz; the measured result, however, already shows a decline at 10Hz. It depicts that in the simulation model, the eddy current appears later than that in the measurement. The eddy current effect becomes visible later in the simulation model: this is the same phenomenon as in the brass ring in Chapter 4. But unfortunately, there is still no idea about why this will happen in the model. It should be emphasized that this problem is in the model and highly needed to be solved.

5.5. SUMMARY

- The eddy current model is applied to the spindle ring. In the spindle ring, there is nonlinear effects such as saturation and hysteresis effects. Therefore, the BH curve of the spindle ring is measured. According to the measured data, the fitting curve is found and is adapted to the BH curve simulation model.

- The nonlinear property in the simulation model is finally removed. Because in the input impedance measurement, the BH curve is also measured, and it is very small loop. Therefore, the nonlinear effect is neglected. The transformer ring model is a linear 3-winding transformer circuit with a constant permeability.

- The input impedance is compared between the simulation result and the measurement. From the comparison, it is concluded that in the simulation model, the eddy current appears later than that in the measurement. This is the problem of the eddy current model currently. There is still no idea about the reason for that and how to solve it.

6

APPLICATION OF THE IMPROVED EDDY CURRENT MODEL IN THE ACTUATOR

In this Chapter, the eddy current model will be applied into the spindle of the actuator. In Chapter 4, the eddy current model is improved in the brass ring, and if it works in the brass ring, then it will be brought into the spindle ring. If it works in the spindle ring, then it will be brought back to the actuator. Normally, the operation frequency of the actuator is 260Hz. The number of turns of the coil is 180. The specific details about the geometry and material property of the spindle will be provided by Philips. First, the input impedance is measured; at the same time, there is an approximate estimation about the H-field in the spindle. Since the H-field reaches to the saturation value of the BH curve, therefore the nonlinear model would be adapted in the actuator model. Second, a finite element analysis is done by ANSYS, and with the help of ANSYS the permeances and mutual permeances can be derived. Finally, the actuator permeances are imported to the LTspice simulation model. The simulation result and the measurement are compared.

6.1. INPUT IMPEDANCE MEASUREMENT

The actuator consists of the spindle, the permanent magnets, the coil, and the housing. The material of the spindle is the same as the material of the spindle ring in Chapter 4, and they have the identical properties. Fig. 6.1 shows the actuator for testing. The two wires are the two terminals of the coil around the spindle. The coil will be connected to the impedance analyzer, and input impedance can be measured by the analyzer.

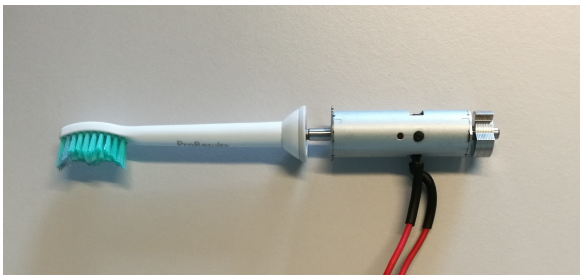

Figure 6.1: The toothbrush actuator that used for testing

When the actuator is connected to the circuit, the actuator begins to vibrates with the varying frequency. However, we investigate the eddy current effect in the spindle. In this case, the actuator can not move during the measurement. Because the vibration of the actuator

will influence the flux permeance in the spindle, and further affects the permeance of the virtual eddy current winding. Therefore, one can use a clamp to block the actuator and keep it stationary during the input impedance measurement. Directly, the BODE plot is shown from the impedance measurement, and quantities of gain and phase are derived. After that, they are transferred to the impedance quantities. The details of the measurement process are not discussed in this Chapter, since they have been introduced before. The input impedance of the blocked actuator from the measurement is as the Fig. 6.2:

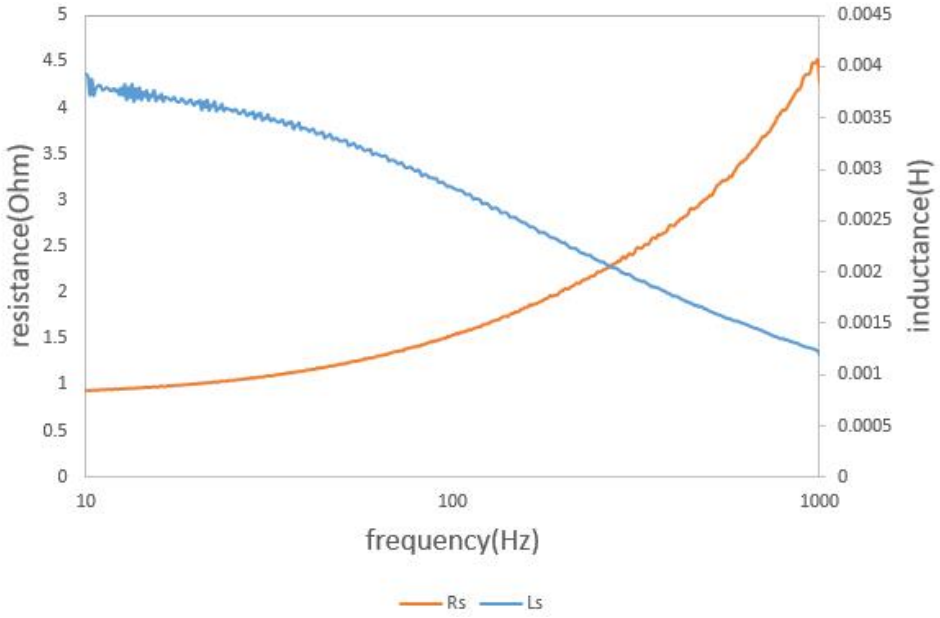

Figure 6.2: The measured input impedance of the blocked actuator

From the measurement, we can know that when the electrical frequency is very low in the circuit, the eddy current effect is not visible yet. At that moment the resistance of the coil is about 0.83Ω and inductive of the coil is around 4mH. The resistance and the inductance vary with the frequency because of the eddy current effect occurs in the spindle. The input voltage is be 1v. Now we do an approximate estimation for the H-field in the spindle. In the measurement circuit, there is a reference resistor Rs connecting in series with the actuator. The current flows in the coil is:

$$I = \frac{U}{R + Rs} = \frac{1}{0.83 + 1.0228} = 0.539A \tag{6.1}$$

The flux generated by the current in the spindle would be:

$$\phi = \Lambda_{CC} nI \tag{6.2}$$

Λ_{CC} is the peremance of the coil
nI is the ampere turns of the coil
The B-field in the spindle would be:

$$B = \frac{\phi}{A_s} \tag{6.3}$$

A_s is the area of the cross section of the spindle.

$$\Lambda_{CC} = 0.1333 \times 10^{-6} \tag{6.4}$$

$$A_s = 4\pi(mm^2) \tag{6.5}$$

$$n = 180 \tag{6.6}$$

Finally the value of B-field is:

$$B = 1.03T \tag{6.7}$$

In Chapter 5, Fig. 5.2 shows the measured BH curves of the spindle material. The calculated B-field is referred to that picture. The estimated B-field has already reached to the saturation value. Therefore, this gives us a conclusion that, in the actuator model, the nonlinear model should be included.

6.2. ANSYS SIMULATION

The testing approach for the actuator is a combination of a finite element analysis, and the comparison between LTspice simulation and measurement. There is already a completed ANSYS model for the toothbrush actuator, and it is a very complex and big model. The purpose of this part is to adapt the eddy current model into the actuator and compare with the measurement. This requires that the distribution of the eddy current is defined in the ANSYS first, and then the simulation is done by the ANSYS. After that, the permeances and mutual permeances of the actuator will be extracted and then be applied to the LTspice.

Both the ANSYS model and the LTspice model for the actuator are complicated, because the permanent magnetic system and the mechanical part are included. But during the measurement, the actuator is blocked and could not move. In this case, in the ANSYS the model needs to achieve the same effect, and only the permeance and mutual permeances of the real winding, the sense winding, and the BH curve winding will be extracted and be used in the LTspice model. In this Chapter, first, the eddy current is defined to have an equal distribution in the spindle; second, the eddy current is defined to have a linear distribution.

6.2.1. EQUAL DISTRIBUTION

In this section, the actuator is tested in the occasion that the eddy current is equally distributed in the spindle.

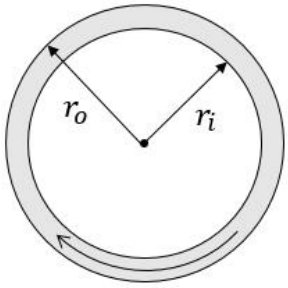

Figure 6.3: Equal distribution of the eddy current in the spindle

Fig. 6.3 depicts the cross section of the spindle. The eddy current is equally distributed in the outer gray section. The arrow points at the direction that the eddy current flows. r_o is the radius of the spindle, and r_i is the radius of the inner circle. If we define the thickness of the eddy current is dskin, it would be:

$$dskin = r_o - r_i \tag{6.8}$$

The dskin would be defined as four arbitrary choices: 0.25mm, 0.5mm, 0.75mm, 1mm. These values are defined in the ANSYS respectively, and after simulation, one can get four groups of the permeances and mutual permeances of the three windings in the actuator. Also, the resistance of the eddy current winding could be calculate by using the following equation:

$$R_{ec} = \frac{l}{\sigma A} = \frac{\pi(r_o + r_i)}{\sigma \cdot dskin \cdot l_{ec}} \tag{6.9}$$

l_{ec} is the length where the eddy current flows.

The four groups of the permeances and the resistance is listed in the Table 6.1:

Table 6.1: Permeances derived from ANSYS simulation and resistance derived from calculation

dskin(mm)	0.25	0.5	0.75	1
Λ_{CC}	0.13330E-06	0.13330E-06	0.13330E-06	0.13330E-06
Λ_{AA}	0.13223E-06	0.13223E-06	0.13223E-06	0.13223E-06
Λ_{EE}	0.12952E-06	0.12485E-06	0.11435E-06	0.10025E-06
Λ_{CA}	0.13007E-06	0.13007E-06	0.13007E-06	0.13007E-06
Λ_{CE}	0.11091E-06	0.96844E-07	0.84187E-07	0.73005E-07
Λ_{AE}	0.11221E-06	0.97987E-07	0.85186E-07	0.73873E-07
$R_{ec}(\Omega)$	1513u	706u	437u	303u

Λ_{CC} is the permeance of the real coil; Λ_{AA} is the permeance of the nonlinear winding; Λ_{EE} is the permeance of the eddy current winding; Λ_{CA}, Λ_{CE} and Λ_{AE} are the mutual permeances between every two windings.

In the Table 6.1, it can be seen that the permeances of the real winding and the nonlinear winding are constant values. Also, the mutual permeance between these two windings is a constant value. That is logical because the actuator is in the situation of blocked. Λ_{CC} and Λ_{AA} are independent of the choice of dskin. Only the permeaces and resistances related to the eddy current winding vary with the dskin. The dskin is larger, the resistance of the eddy current winding is smaller. If we calculate the coupling factor between the real winding and the eddy current winding:

$$k_{CE} = \frac{\Lambda_{CE}}{\sqrt{\Lambda_{CC}\Lambda_{EE}}} \tag{6.10}$$

The coupling factors of the 4 groups are listed in the following:

Table 6.2: The coupling factor K_{CE}

dskin(mm)	0.25	0.5	0.75	1
k_{CE}	0.844	0.751	0.682	0.631

From Table 6.2, we can see that the coupling factor k_{CE} decreases as the dskin goes up. This is logical. The thinner of the eddy current winding, the better coupling between the eddy current and the real winding. Because more flux can go through the eddy current winding.

The parameters in Table 6.1 would be applied to the LTspice model. The simulation result is shown in the next section.

6.2.2. LINEAR DISTRIBUTION

In this section, the actuator is tested in the occasion that the eddy current is linearly distributed in the spindle.

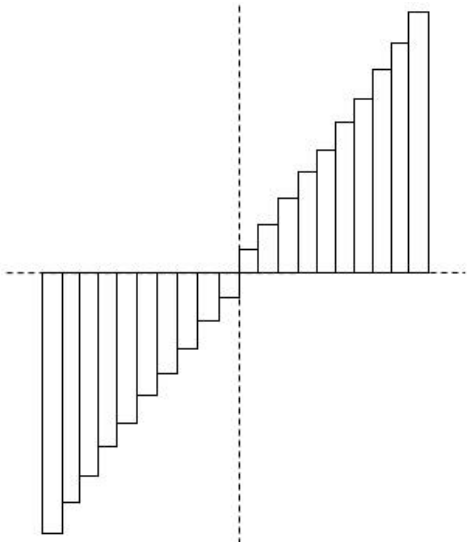

Figure 6.4: Linear distribution of the eddy current in the spindle

In Fig. 6.4, the eddy current is defined by N current paths with the same thickness. From the center of spindle to the edge, the current is linearly increasing in every current . If the current amplitude in the first current path, which is mostly close to the center is k, then the total current in the spindle can be described as:

$$I = k + 2k + 3k + \cdots + Nk = \frac{(1+N)Nk}{2} \tag{6.11}$$

The current amplitude in the tube j is:

$$i_j = kj = \frac{2I}{N(N+1)}j \tag{6.12}$$

In ANSYS, I equals 150A and N equals 10. The value of the total current I does not influence the output permeances and mutual permeances, so it is an arbitrary choice. The radius of the spindle is 2mm, so the thickness of each current path is 0.2mm. 10-current-tube is good enough for the spindle. Then the permeances can be derived from ANSYS. But the resistance of the eddy current winding needs to be calculated by hand. The current tubes are regarded as connecting in series. According to the resistance analysis in Chapter 4. We can directly write the resistance for every current tube:

$$R_{ct}(x) = 2\pi\sigma x n(x) \tag{6.13}$$

n(x) is the number of current tubes in dx. For every piece dx, the resistance contribution in it is:

$$dR = n(x) l_{ec} dx \cdot R_{ct}(x) \tag{6.14}$$

Then for the total resistance of the eddy currents:

$$dR = 2\sigma^{-1} n(x)^2 l_{ec} \pi x \cdot dx \tag{6.15}$$

$$R_N = \sigma^{-1} l_{ec} \pi \int_0^r 2n(x)^2 x dx \tag{6.16}$$

r is the radius of the spindle.

The effective resistance of the eddy currents would be:

$$R_{ec} = \frac{R_N}{N^2} = 100u \tag{6.17}$$

Now a list of the data from ANSYS as well as the calculated result shows in the following table:

Table 6.3: Parameters derived from ANSYS and calculation K_{CE}

Λ_{CC}	0.13330E-06
Λ_{AA}	0.13223E-06
Λ_{EE}	0.75707E-07
Λ_{CA}	0.13007E-06
Λ_{CE}	0.64644E-07
Λ_{AE}	0.65412E-07
k_{CE}	0.643
R_{ec}	100u

The parameters in the Table 6.3 would be applied to the LTspice model. The simulation result is shown in the next section.

6.3. SIMULATION RESULTS

The input impedance of the actuator is the simulation result from the LTspice. The simulation results of the equal distribution and linear distribution are illustrated in the Fig. 6.5. The simulation results are compared with the measurement input impedance.

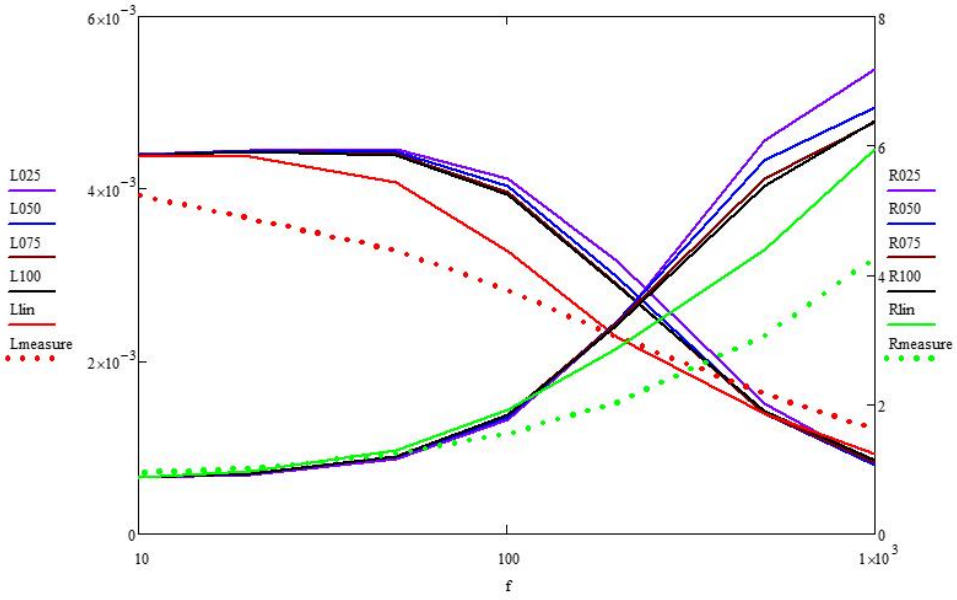

Figure 6.5: Simulation results for the actuator

In the Fig. 6.5, the $L_{measure}$ and $R_{measure}$ are the input impedance from the measurement; the L_{lin} and R_{lin} are the simulated impedance from the linear distribution; the remaining 4

groups are from the equal distribution. It can be seen that in the equal distribution, the 4 groups' simulated impedances are close to each other. This can be true. Because when the dskin goes up, the coupling factor k_{CE} decreases while the eddy current resistance increases. The coupling factor and the resistance can interacts and influence each other. In the linear distribution, the inductance and the resistance become closer to the measured results compared to the equal distribution. It is clear that in the measurement, at the starting frequency, the inductance goes down because there is already an obvious eddy current effect in the spindle. Also, we can see that both in the equal distribution and the linear distribution, the eddy current becomes to be visible later than in the measurement. Therefore, it appears the same phenomenon as simulation results in the brass ring and the spindle ring. The phenomenon is that the eddy current effect in the simulation model shows later than in the measurement.

Till now, the comparison between the measurement and simulation is derived. But how we evaluate the simulation result ? The output power of the actuator is compared. The impedance quantities of the measurement and simulation(linear distribution) are picked up respectively, at the operation frequency f=260Hz. The output power of these two occasions are compared. In this case, we can see the difference of the output power between them. If we consider the spring and mass in the actuator, the the actuator circuit could be simplified as the Fig. 6.6.

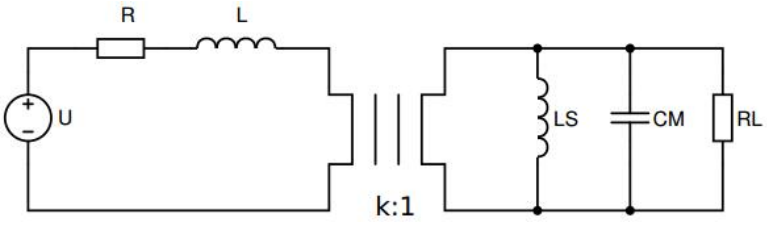

Figure 6.6: The simplified actuator equivalent circuit

The output power of the load R_L can be calculated in the following steps:
The impedance of the circuit:

$$Z(R_L) = R + j\omega L + \frac{1}{\frac{1}{j\omega L k^2} + j\omega\frac{Cm}{k^2} + \frac{1}{R_L k^2}} \tag{6.18}$$

The input current into the circuit would be:

$$I(R_L) = \frac{U}{Z(R_L)} \tag{6.19}$$

The current flows in the load R_L is:

$$I_L(R_L) = \frac{j\omega L k^2 + \frac{1}{j\omega\frac{Cm}{k^2}}}{j\omega L k^2 + \frac{1}{j\omega\frac{Cm}{k^2}} + R_L k^2} \cdot IR_L \tag{6.20}$$

The output power of the load in the actuator is:

$$P_L(R_L) = \frac{1}{2} \cdot (I_L(R_L))^2 \cdot R_L \tag{6.21}$$

The relating parameters from the measurement and the simulation at frequency of 260Hz are listed below:

Table 6.4: The comparison parameters

Data sources	R(Ω)	L(mH)	Ls(H)/(rad/N/m)	Cm(nF)/(kg·m^2)	k
Measurement	2.25	2.082	1.468	202.44	0.024
Simulation	3	2	1.468	202.44	0.024

The Ls and Cm are mechanical quantities. The units of them can be described in two ways. These parameters are brought to the (6.21). The output power of the simulation and measurement can be plot.

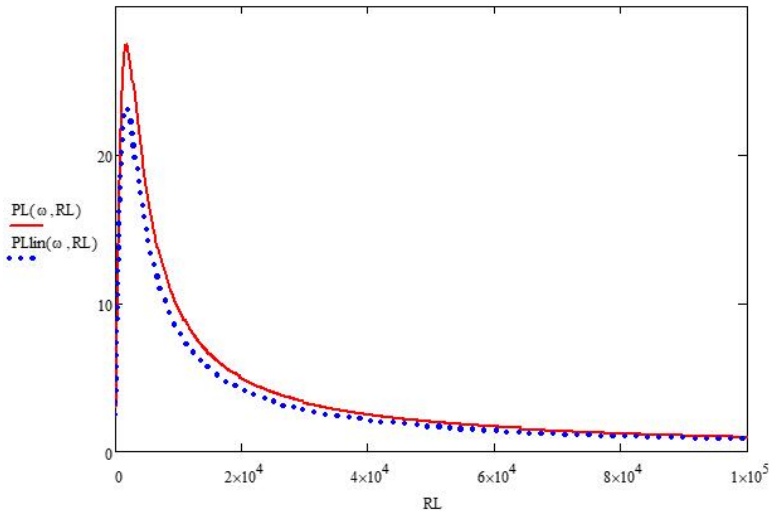

Figure 6.7: The output power comparison between the measurement and the simulation

In Fig. 6.7, PL is the output power of the measurement; PLlin is the output power of the simulation model. The operation frequency is 260Hz. The output power deviates with the resistance of the load. It is shown that for the output power, the difference between the two occasions is not that big.

The deviation of the two results is:

$$dev = \frac{P_L - P_{Llin}}{P_L} \tag{6.22}$$

The deviation of the two results in the Fig. 6.7 is plot in the following:

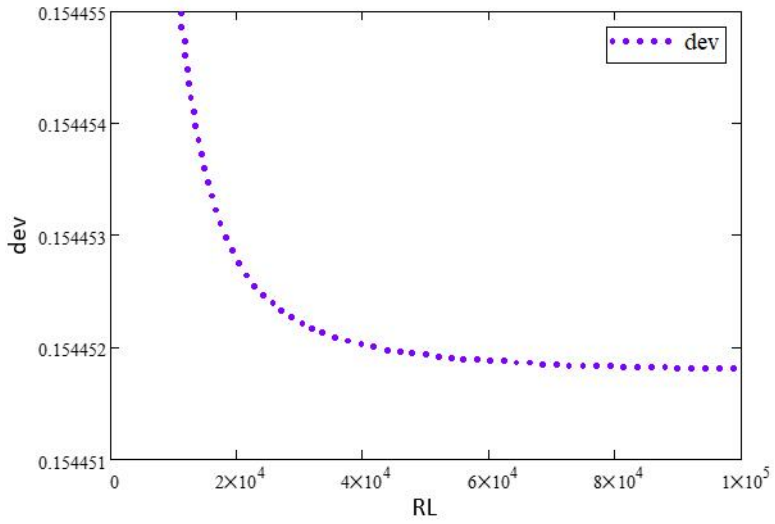

Figure 6.8: The output power deviation between the measurement and the simulation

For the toothbrush, normally the range of the G load ($\frac{1}{R_L}$) is 0-100u. The larger the G load is, the more pressure of the toothbrush is; the smaller the G load is, the softer of the toothbrush is. In our case, G load equals to a soft value 25u. That is, R is 40k. In this point, the deviation between the measurement and the simulation is around 15.4%.

In this way, the optimized eddy current model (linear distribution of the eddy current) is applied to the actuator model. Finally, by comparing output power between the simulation result with the measurement, the eddy current model could be evaluated. The result has been generally reached to the expectation, and it is logical.

6.4. SUMMARY

- The input impedance is measured, and at the same time, the estimation about the H-field in the spindle is done. During the measurement, the flux in the spindle reaches to the saturation value. It concludes that the nonlinear model should be included in the model.

- A finite analysis element is done by ANSYS. In ANSYS, two occasions are defined for the eddy current distribution in the spindle: equal distribution and linear distribution. In every occasion, the permeances are derived from ANSYS. Also, the resistance of eddy current is calculated. These parameters are applied to the LTspice model.

- In the simulation results, it shows that the same phenomenon as simulation simulation results in the brass ring and the spindle ring. The phenomenon is that the eddy current effect in the simulation model appears later than in the measurement.

- The output power of the actuator is compared in the two occasions, at the operation frequency f=260Hz. In this way, the simulation model could be evaluated. Finally, the deviation between the measurement and simulation is around 15.4%. The result has been generally reached to the expectation, and it is logical.

7

CONCLUSION

The thesis deals with the analysis, modelling, optimization and test of the eddy current model that is used for the toothbrush actuator. The objectives of this thesis have been achieved. First, the eddy current effect in the actuator is described; second, a new modelling method to study the eddy current effect is derived; third, the eddy current model has been optimized based on the mathematical analysis; finally, the modelling method and optimized eddy current model are applied to the actuator model. The key points of each chapter made in this thesis are summarized at first. The progress of the work, the limitations of the model, and the further research are presented in the end.

7.1. CONCLUSIONS

- The primary aim of this thesis is to develop a methodology for the optimization of the eddy current modelling method in the toothbrush actuator. To achieve this, the following steps have been completed.

- First the concept of the electromagnetic actuator the eddy current effect in the actuator are introduced. The central spindle plays a very important role in the actuator because all magnetic fluxes go through it. The eddy current generates the opposite flux, which will reduce the total flux in the spindle. This will influence the available output power of the actuator.

- Next the transformer ring topology is presented. The transformer ring has been chosen for studying the modelling approach, because only the eddy current effect is considered in the brass ring. In that way the problems are simplified. If the modelling approach and the optimization steps are feasible in the brass ring, then the approach can be tested into the spindle ring, and further into the actuator. Also, a 1-dimensional eddy current analysis is discussed. The eddy current distribution and the magnetic distribution in the ring are derived.

- Subsequently, the transformer ring circuit is calculated. The Present Model of the transformer ring circuit has two problems. One is the eddy current distribution is not described correctly, the other is the effective flux is not found. To solve these two problems, the eddy current model is improved by three optimization steps.

- Finally, the optimized eddy current model is applied to the spindle ring and the actuator. The result shows the modelling method and the optimization process to be useful. The optimized eddy current model is more accurate and logical.

7.2. LIMITATIONS AND FUTURE WORK

Through the whole thesis, there are still some serious differences between the expectation result and the modelling results. The limitations of the research and further investigations are listed below.

- The most important limitation of the optimized eddy current model is that in the modelling result, the eddy current occurs later than in reality. This does not reach to what we expected at the middle frequency values. Since the analytical calculation on the eddy current, and the optimization steps have been completed, the modelling transfer impedance or input impedance should be correspond to the measured results at both low and middle frequencies.
- The analytical calculation for the eddy current is based on the 1-dimensional case. However, in the cross section of the ring, the eddy current flows in a 2-dimensional case. Therefore, it is recommended to see the eddy current distribution in the ring is to use the finite element analysis. This work can be added in Chapter 4. In the improvement steps, the eddy current flowing in the cross section is assume to be a rectangular path. However, the actual path should be more round at the corner. This is recommended to reconsider.
- For the BH curve model, it has two limitations. The first one is that it can not model the minor BH curve loop; the second is that it has a ceiling for the B-field. If the BH curve model can be optimized, then the nonlinear effects can be better modelling and further the eddy current model can be better evaluated.

BIBLIOGRAPHY

[1] J. A. Ferreira, *Power electromagnetics,* Delft University of Technology (2015), course Notes EE4C05.

[2] Wikipedia, *Electric toothbrush,* https://en.wikipedia.org/w/index.php?title=Electric_toothbrush&oldid=782318788 (2017), [Online; accessed 29-July-2017].

[3] P. J. Bax, *Actuator concept and simulation approach,* (2013), unpublished book.

[4] M. Cacciola and G. Calcagno, *Eddy current modeling in composite materials,* PIERS Online **5**, 591 (2009).

[5] H. Tsuboi and I. Seshima, *Transient eddy current analysis of pulsed eddy current testing by finite element method,* IEEE Trans **40**, 1330 (2004).

[6] K. Preis and O. Biro, *Fem analysis of eddy current losses in nonlinear laminated iron cores,* IEEE Trans **46**, 1412 (2005).

[7] T. Theodoulidis and E. Kriezis, *Impedance evaluation of rectangular coils for eddy current testing of planar media,* NDT and E International **35**, 407 (2002).

[8] W. Yin and A. Peyton, *Sensitivity formulation including velocity effects for electromagnetic induction systems,* IEEE Trans **46**, 1172 (2010).

[9] Y. He and F. Luo, *Defect characterisation based on pulsed eddy current imaging technique,* Sensors and Actuators **A**, 1 (2010).

[10] T. Itaya and K. Ishida, *A new analytical method for calculation of eddy current distribution ad its application to a system of conductor-slab and rectangular coil,* PIERS Online **7**, 766 (2011).

[11] P. J. Bax, *The electromagnetic system of the motor,* (2013), unpublished book.

[12] H. M. McCONELL, *Eddy current phenomena in ferro-magnetic materials,* Carnegie Institute of Technology, Magnetic Amplifiers-Technical Report **14** (1953).

[13] J. Zhang, *Iron loss measurement,* (2016), internship report.

[14] J. Barranger, *Poly-technisch zakboekje* (add later, 1965) add later.

[15] J. Barranger, *Hysteresis and eddy-current losses of a transformer lamination viewed as an application of the poynting theorem* (Lewis research center, 1965) nASA technical note.

[16] P. J. Bax, *Transformer theory and circuit models,* (2013), unpublished book.

[17] P. J. Bax, *Modelling of inductive properties of the line-output transformer; from field-line pictures to equivalent circuit* (Eindhoven University of Technology, 1995).

[18] E. Tutorials, *Magnetic hysteresis,* http://www.electronics-tutorials.ws/electromagnetism/magnetic-hysteresis.html (2017), [Online; accessed 17-August-2017].

[19] P. J. Bax, *Bh curve model,* (2013), unpublished book.